PhD Dissertation

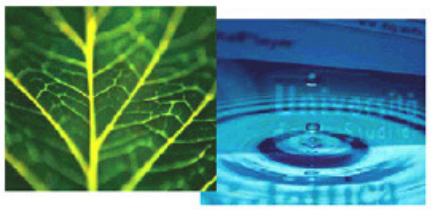

International Doctorate School in Information and Communication Technologies

DISI - University of Trento

Advanced methods for tree species classification and biophysical parameter estimation using crown geometric information in high density LiDAR data

Aravind Harikumar

Advisor:

Dr. Francesca Bovolo

Fondazione Bruno Kessler, Trento

Co-advisor:

Prof. Dr. Lorenzo Bruzzone

University of Trento, Trento

September 2019

Abstract

The ecological, climatic and economic influence of forests makes them an essential natural resource to be studied, preserved, and managed. Forest inventorying using single sensor data has a huge economic advantage over multi-sensor data. Remote sensing of forests using high density multi-return small footprint Light Detection and Ranging (LiDAR) data is becoming a cost-effective method to automatic estimation of forest parameters at the Individual Tree Crown (ITC) level.

Individual tree detection and delineation techniques form the basis for ITC level parameter estimation. However SoA techniques often fail to exploit the huge amount of three dimensional (3D) structural information in the high density LiDAR data to achieve accurate detection and delineation of the 3D crown in dense forests, and thus, the first contribution of the thesis is a technique that detects and delineates both dominant and subdominant trees in dense multilayered forests. The proposed method uses novel two dimensional (2D) and 3D features to achieve this goal.

Species knowledge at individual tree level is relevant for accurate forest parameter estimation. Most state-of-the-art techniques use features that represent the distribution of data points within the crown to achieve species classification. However, the performance of such methods is low when the trees belong to the same taxonomic class (e.g., the conifer class). High density LiDAR data contain a huge amount of fine structural information of individual tree crowns. Thus, the second contribution of the thesis is on novel methods for classifying conifer species using both the branch level and the crown level geometric characteristics.

Accurate localization of trees is fundamental to calibrate the individual tree level inventory data, as it allows to match reference to LiDAR data. An important biophysical parameter for precision forestry applications is the Diameter at Breast Height (DBH). SoA methods locate the stem directly below the tree top, and indirectly estimate DBH using species-specific allometric models. Both approaches tend to be inaccurate and depend on the forest type. Thus, in this thesis, a method for accurate stem localization and direct DBH estimation is proposed. This is the third contribution of the thesis.

Qualitative and quantitative results of the experiments confirm the effectiveness of the proposed methods over the SoA ones.

Keywords: Light Detection and Ranging (LiDAR), Airborne Laser Scanning (ALS), Airborne Laser Scanning (TLS), Forest Parameter Estimation, Forestry, Remote Sensing.

Acknowledgements

First and foremost, I thank my parents for believing in me more than myself. If it was not for their unconditional love, support and prayers, I wouldn't have achieved any of my goals in life. I also thank my brother for supporting me in all respects. A special thanks to both my grandmothers for being the most kind and loving people of my life, in addition to being big fans of my research.

I thank my thesis supervisor Dr. Francesa Bovolo for her constant encouragement and subtle guidance throughout the Ph.D. I greatly appreciate the freedom she has given me to find my own path in research. I appreciate all her contributions in terms of time, ideas, and funding to make my Ph.D. experience productive and stimulating. She has always been very kind to me throughout and I feel extremely lucky to have had her as the PhD supervisor.

I express my gratitude to Prof. Dr. Lorenzo Bruzzone for all the invaluable advices that he gave me during the co-supervision of my Ph.D research. It is undoubtedly his foresight on prospective research directions and timely guidance that allowed me to successfully finish my thesis on time. His passion towards research has always been a motivation for me. I consider it as an honor to be his student.

I thank all my friends for being with me during both happy and challenging times. Thanks to Davide Pirrone for being a good friend and also for all those late night Italian lessons and big small talks. However beautiful it is, life in a foreign country would not have been this happier without my Indian friends Akshara Preethy Byju, Sanchari Thakur and Balanand Santhosh. They made me feel at home every time I missed her. I thank Yady Tatiana Solano Correa for all her support and help, and being a good friend for all these years. At last, but not the least, I thank each and every member of the Remote Sensing Laboratory (RSLab) for being the most wonderful colleagues you were to me.

Aravind Harikumar

The work compiled in this thesis has been fully supported by the research grant from the Fondazione Bruno Kessler, Italy

Dedicated to my mother, father, teachers and God

Contents

List of Tables

List of Figures

List of Abbreviations

DET	Detection Accuracy
CE	Commission Error
OE	Omission Errors
SoA	State of the Art
RADAR	Radio Detection and Ranging
LiDAR	Light Detection and Ranging
2D	Two Dimensional
3D	Three Dimensional
FoV	Field of View
MODIS	Moderate Resolution Imaging Spectroradiometer
ALOS-PALSAR	Advanced Land Observing Satellite Phased Array Type L-band Synthetic Aperture Radar
GLAS	Geoscience Laser Altimeter System
MSS	Multispectral Scanner
LANDSAT	Land Remote-Sensing Satellite
SAR	Synthetic Aperture Radar
COSMO-SkyMed	COnstellation of Small Satellites for the Mediterranean Basin Observation
AVIRIS	Airborne Visible and Infrared Imaging Spectrometer
UAVSAR	Unmanned Aerial Vehicle Synthetic Aperture Radar

LASER	Light Amplification by Stimulated Emission of Radiation
ALS	Airborne Laser Scanning
TLS	Terrestrial Laser Scanning
DBH	Diameter at Breast Height
ITC	Individual Tree Crown
RS	Remote Sensing
1D	One Dimensional
AGLAS	Advanced Geoscience Laser Altimeter System
GEDI	Global Ecosystem Dynamics Investigation LiDAR
GPS	Global Positioning System
IMU	Inertial Measurement Unit
DGPS	Differential Global Positioning System
ABM	Area Based Methods
CHM	Canopy Height Model
RANSAC	RANdom Sample Consensus
NIR	Near Infrared
PCA	Principal Component Analysis
GLCM	Grey Level Co-occurrence Matrix
CSSM	Candidate Segment Surface Model
CSDM	Candidate Segment Density Model
ME	Mean Error
MAE	Mean Absolute Error
MSE	Mean Squared Error
NS	Norway Spruce
EL	European Larch
SP	Swiss Pine
SF	Silver Fir
EGFs	External Crown Geometric Features

IGFs	Internal Crown Geometric Features
EQV	Elementary Quantization Volume
TSI	Tree Independent
TSD	Tree Dependent
PA	Producer Accuracy
UA	User Accuracy
FS	FScore
OA	Overall Accuracy

List of symbols

P_{ret}	Power returned to the receiver
D_r	Receiver antenna/sensor diameter
D_{tar}	Target diameter
R_L	Range
γ	Beam divergence
D	Aperture diameter
P_t	Transmitted power
Δt	Time lag between the transmitted and received pulse
$\Delta\phi$	Phase lag between the transmitted and received pulse
c	Speed of light
λ_{IM}	Wavelength of the intensity modulation signal
f_{IM}	Frequency of the intensity modulation signal
h	Distance of the platform from the target
P	The point cloud set of an individaul tree
N	Total number of LiDAR point associated with a tree
t_j	Tree top of the j^{th} tree
T	Total number of tree tops
S	Total number of subdominant trees in a candidate CHM segment

$p_v = [x_v, y_v, z_v]$	The highest point in P
$p_i = [x_i, y_i, z_i]$	3D Euclidean coordinates of the LiDAR point p_i
d	The shortest distance between a LiDAR point p_i and the stem
l	The length of the arc with radius r
r	The base radius of cylinder
θ	The smallest angle between the p_i and the reference plane L_r
L_r	Reference plane for projecting P to the novel space
d_{min}	The distance to the point in the cloud that is maximally away from the stem in the direction of L_r
d_{max}	The distance to the point in the cloud that is maximally away from the stem in the direction of PC1
B	Total number of branches in an individual tree
c_b	b^{th} branch cluster
S_n	The neighborhood point density of n^{th} LiDAR point
Y_B	The number of nearest neighbors of a LiDAR point in P
λ_1^b	The eigenvalue associated with the PC1 of c_b
λ_2^b	The eigenvalue associated with the PC2 of c_b
λ_3^b	The eigenvalue associated with the PC3 of c_b
L_b	The distance between the b^{th} branch tip and the tree stem computed along the direction of its respective PC1

α_b	The angle between the direction of the PC1 of c_b and the stem
K_b	The mean of the perpendicular distance of LiDAR points in the branch to the corresponding branch line
W_b	The eigenvalue along PC2
S_b	The ratio between eigenvalues λ_2^b and λ_3^b
D_b	number of LiDAR points associated with c_b
H_T	Tree height
α_{hull}	Convex hull parameter
$V_c = [x_c, y_c, z_c]$	Vertex of cone
α	Cone opening angle
V_{hull}	Volume of convex hull formed on the tree point cloud
V_{cone}	Volume of regression cone fitted on the tree point cloud
H_C	Crown height
$F = \{\vec{\mathrm{v}}_\mathrm{i}\}_{i=1}^{N_G}$	Training feature vector set
N_G	Number of training samples
R^f	Feature space formed by f features
$U = \{u_i\}_{i=1}^{N_G}$	Class label vector associated with F
$\vec{\mathrm{w}}$	Weight vector
e	Bias
C	Regularization parameter
ξ_i	Slack variable
M_k	Number of kernels
d_m	Weight associated with a kernel
$K(.,.)$	Positive definite Kernel function
γ	RBF parameter
g_v	Projection of p_v on xy plane
L_t	The line connecting p_v and g_v

r_t	Maximum radius of tree crown
p_e	The farthest point from L_t
A	Cylindrical angular dimension
R	Cylindrical radial dimension
H	Cylindrical height dimension
$\vec{S}_i = [\alpha_i \; r_i \; h_i]$	Cylindrical space vector
R_N	Radial divisions of cylindrical space
A_N	Number of angular sections of cylindrical space
H_N	Number of Height divisions of cylindrical space
r_{max}	Maximum crown radius in a set of trees
h_{max}	Maximum height in a set of trees
$\delta\alpha^{TSI}$	Angular step calculated in tree independent way
δr^{TSI}	Radial step calculated in tree independent way
δh^{TSI}	Height step calculated in tree independent way
$\delta\alpha^{TSD}$	Angular step calculated in tree dependent way
δr^{TSD}	Radial step calculated in tree dependent way
δh^{TSD}	Height step calculated in tree dependent way
V	Total number of height sections in cylindrical volume
$\vec{a}_{EQV_v}$	Attribute vector of U_v
U_v	V^{th} height section in cylindrical space
$a^i_{EQV_v}$	i^{th} element of height section U_v
I_v	Set of indices of EQV in belonging to U_v
V_T	Attribute vector of a tree

ζ	Lagrangian multiplier
$K_{int}(.,.)$	Histogram intersection Kernel function
I_b	Set of indices of LiDAR points in c_b
(s_l, s_w, s_h)	Semi-axis dimensions of ellipsoid fitted on c_b
(v_l, v_b, v_h)	Semi-axis directions of ellipsoid fitted on c_b
α_b	Slope of b^{th} branch
l_b	Length of b^{th} branch
k_b	Compactness of b^{th} branch
p_b	Symmetry of b^{th} branch
d_b	Density of b^{th} branch
$M(.)$	Median operator
p_t^b	Tip point of b^{th} branch
S_p	Stem point set
I_m	Set of indexes of the points that are farthest from the respective branch tip of the B branch clusters
T_r	Threshold distance from stem beyond which the stem points are ignored
$S_c = \{s_i\}$	Set of stem centers along the N_s height sections of a tree
N_s	Height sections of a tree
S_{DBH}	Stem DBH derived from the stem model
η	DBH measurement height from base of the tree

Chapter 1

Introduction

1.1 Background

The ecological, climatic and economic influence of forests makes them an essential natural resource to be studied, preserved, and managed. Forests occupy approximately 30% of the world's land area, and hence are habitats for the major share of the terrestrial biodiversity [1]. Forests also act as huge carbon sinks by sequestering it in their biomass, thus preventing the presence of disproportionately large amount of carbon in the atmosphere which adversely influences the Earth's climate (i.e., release of carbon to the atmosphere warms up the planet). It is estimated that the percentages of above and below ground carbon stored by forests alone are approximately 80% and 40%, respectively [2]. However, forests are also the major source of timber and associated non-timber products which are of huge socio-economic value to the society. Extraction of timber and associated products results in deforestation and forest ecosystem degradation, and has negative consequences on the downstream water flows, terrestrial biodiversity, traditional sources of livelihoods for local people, and global climate. In fact, the share of deforestation and forest degradation account for approximately 17% of carbon emissions, more than the entire global transportation sector and second only to the energy sector [3]. Thus, it is essential to maintain a balance between the procurement of forest resources and the resulting ecological and climatic impacts. Any activity directed at maintaining the balance requires an accurate and periodic inventorying of forests. Accurate inventory data serves the purpose of national forest database generation and policy making at a regional and national scale. On a global scale they are central to the understanding of the terrestrial biosphere [4]. Area level inventorying results in data aggregation at the species and/or spatial level(s) resulting in bias together with an almost certain reduction in both accuracy and precision of the estimates [5]. Hence, inventorying at the individual tree level is a good choice to accurately derive forest information in terms of tree species distribution and associated

parameter estimates such as tree biomass (i.e., carbon stocks) [6; 7] and stem diameter [8]. Accurate tree detection and delineation provide ecologically relevant forest data such as canopy cover [9], above-ground biomass [10], spatial pattern of trees [11], study forest fire behavior [12], disturbance extent mapping [13], and habitat classification [14]. However, error in individual tree level attributes is amplified when using allometric models. Thus, accurate extraction of parameter is critical to estimations at the individual tree level. Precision forestry, which can be defined as the practice of using modern tools and methods to accurately determine characteristics of forests and treatments at stand, sub-stand or individual tree level, also demands accurate fine resolution inventory data for activities such as site/tree specific fertilization treatment and accurate supply chain planning [15].

The inventoried forest data mostly include tree count, tree/crown height, stem diameter, canopy cover, basal area, leaf area index, biomass, and species. In particular, characterization of tree species and their underlying spatial distribution are critical to the execution of sustainable forest management, and understanding regional ecological processes [1]. Forest parameters can be accurately estimated from data acquired from individual trees in forests. Thus, the conventional method of accurate data collection is to directly measure the tree attributes on the field. Although parameter estimation can be very accurately done for small areas by measuring attributes of individual trees, the on-site measurement of parameters for large areas is often impossible and/or very costly in terms of human labour and time. Thus, attribute estimates of large forest areas are economically obtained using statistical techniques [16], where a few field-measured-tree-attribute data, randomly collected on a small forest plots, are considered representative of large areas. Whatsoever, the accuracy of the estimates depends on factors such as, the amount of field collected data, the forest type, the tree count, and the tree species.

Remote sensing is an efficient alternative to economically inventory forest attributes at a range of resolutions, in a synoptic and timely manner. The different remote sensing data acquisition technologies include optical sensors, Radio Detection and Ranging (RADAR) and Light Detection and Ranging (LiDAR). Optical remote sensors capture multi-/hyper-spectral data that contain Two Dimensional (2D) canopy level spatial and spectral information. However, optical sensors fail to collect information on the vertical structure of forest, including that of subdominant trees and under-story vegetation [17]. Instead, LiDAR and RADAR remote sensing can capture Three Dimensional (3D) data of the forest vertical profile and are used to obtain information of the sub-canopy structures [18]. Most remote sensors can be operated from spaceborne, airborne, and terrestrial platforms. Spaceborne sensors have the advantage of large Field of View (FoV), however, the large distance limits the amount of detail that can be captured. Most spaceborne sensors belong to the optical and RADAR classes, while LiDAR based ones are operated from

spaceborne platforms as profilers due to technological (i.e., low pulse repetition and/or sampling rate) and distance (i.e., the speed of light is a constant) limitation. Several spaceborne sensors are in orbit to perform Earth remote sensing with different spatial, spectral and temporal resolutions. For example, the Moderate Resolution Imaging Spectroradiometer (MODIS) [19] and Advanced Land Observing Satellite Phased Array Type L-band Synthetic Aperture Radar (ALOS-PALSAR) [20] and Geoscience Laser Altimeter System (GLAS) provide low to moderate resolution data, the Multispectral Scanner (MSS) on-board Land Remote-Sensing Satellite (LANDSAT), and Synthetic Aperture Radar (SAR) sensors on board the COnstellation of Small Satellites for the Mediterranean Basin Observation (COSMO-SkyMed) provide higher resolution data (i.e., 1m - 30m) at the cost of a longer revisit times [21], and sensors such as Quickbird/IKONOS capture high resolution data with sub-metric accuracies [22]. A more detailed data acquisition of forests is done by mounting remote sensors on low flying airborne platforms (e.g., helicopters and drones), enabling them to capture finer resolution spatial and spectral details when compared to spaceborne platforms. Popular airborne sensors include Airborne Visible and Infrared Imaging Spectrometer (AVIRIS), Unmanned Aerial Vehicle Synthetic Aperture Radar (UAVSAR), and laser scanners such as the RIEGL VQ-780i. The highest resolution remote sensing data are often captured from terrestrial platforms, however, the limited FoV is a drawback. The huge amount of 2D and 3D information derived from multiple remote sensors in various platforms allow accurate estimation/measurement of forest parameters at a range of spatial, spectral, and temporal resolutions. Whatsoever, simultaneous acquisition of data from multiple remote sensors is often costly (due to inaccessibility and increased acquisition cost) and sometimes impossible (due to governmental policies). In addition, data from multiple sensors require preprocessing steps such as homogenization and registration, which are computationally expensive. In general, there is growing interest in more detailed measurements of the forests while minimizing the cost of data/acquisition [6; 23]. Thus the thesis contributes to the development of methods for individual tree level forest information extraction using single sensor data such as the high density LiDAR ones which contain accurate 2D and 3D details of forests.

LiDAR remote sensing has been used in forestry shortly after its invent in the 1960s. The technology uses the precisely measured round-trip time of a highly directed Light Amplification by Stimulated Emission of Radiation (LASER) beam, combined with the sensor position and the orientation information, to capture structural and spectral data of the scanned object. In case of forests, LiDAR acquires 3D profile data. The amount of detail captured depends on the laser-footprint size, the sampling frequency, the scanning frequency, and the height/distance of the sensor platform from the object. A large footprint, low sampling/scanning frequency, and large sensor height result in low-resolution

data, whereas, a small footprint, high sampling/scanning frequency, and small sensor height result in high-resolution data. LiDAR systems for forest analysis are popularly mounted on airborne and terrestrial platforms. The former set of systems is mounted on airborne platforms such as low flying aircrafts or helicopters, and the data collected are referred to as Airborne Laser Scanning (ALS) data. The latter set of systems is usually mounted on tripod stands, and the data collected are referred to as Terrestrial Laser Scanning (TLS) data. The ALS data can be used to precisely estimate the forest variables such as the tree height, the crown span, the stem diameter, and the biomass at the stand level (group of trees) [24] or the individual tree level [17]. Whatsoever, the amount of details in ALS data drastically decreases for subcanopy layers. On the other hand, the TLS data contain very fine details about the subcanopy layers including the texture of the stem bark, and the leaf structure [25], however, the scanning geometry of TLS results in data which contain limited information about the forest canopy layer. Thus, ALS systems are suitable for surveying and mapping large forest areas, whereas TLS data are usually employed for local forest inventories, and reference data generation for validating forest parameter estimation by ALS data. Advancements in scanner and sensor technologies in the last decade drastically increased the amount of data that can be collected from a unit forest area. For example, modern ALS systems such as the RIEGL VQ-1560i can record more than 50 points per meter square in a single scanning pass made at flying height of approximately 1 km at a speed of around 100km/hr [26], and TLS systems such as Leica HDS6100 can capture more than 25000 points per meter square at a distance of 10m [27]. This is a huge advancement compared to initial LiDAR systems such as the ones from the Optech which produced less than 2 points per unit meter square at a distance of approximately 500m, and less than 100 points from close ranges. A very high resolution point cloud data contain a huge amount of detail of the forest structure, that can be exploited to study forests at the individual tree level. The high density LiDAR scanning data contain comprehensive details of the spatial and spectral characteristics of the forests at the individual tree level including that of crown, stem, branch, and leaves. The availability of such data is triggering a paradigm shift in operational forest parameter estimation from the area, to the individual tree level [28; 29]. This calls for the need to develop automatic species classification and forest parameter estimation techniques that can maximally exploit the information in the data.

1.2 Motivation and Objectives

Recent high density small footprint LiDAR systems acquire data with a huge amount of tree level 3D structural information which can be used to accurately classify species

and estimate forest parameters. However, individual tree detection and delineation in LiDAR point cloud itself is a challenging problem especially in thick and complex forests, mainly due to reduced point density in subcanopy layers, over-toppling (i.e., dominant tree crowns often fully/partially topple over subdominant ones which make the latter undetectable in the canopy layer), and partial mixing of proximal tree crowns [18]. In this case, novel methods exploiting the 3D forest structural information in LiDAR data that are robust to partial crown mixing and point density variation, need to be developed in order to accurately detect and 3D delineate both dominant and subdominant trees. At present, most of the forest inventorying is performed at the area-level by using generalized field measurements (i.e., over an area). However, area-level inventorying methods lack a built-in species discrimination component which is critical to accurate forest parameter estimation and precision forestry [30]. The characterization of tree species and their spatial distribution is critical for sustainable forest management and understanding regional ecological processes. An important requirement of accurate individual tree level inventory is that individual trees are detected and delineated accurately [6]. State-of-the-art ALS data based automatic individual tree level inventorying methods have failed to challenge area-based ones, mostly due to lack of accurate single tree detection and delineation capabilities in multi-layered and complex forests [28]. Hence, there is a growing interest in developing methods that can accurately detect and delineate individual trees. [23; 31] Thus, the objectives of the thesis are to exploit the 3D structural information in high density LiDAR data to: a) accurately detect and 3D delineate individual tree crowns, b) classify individual tree species, and c) accurately estimate the stem location and the stem DBH.

1.3 Novel Contribution of the Thesis

The aim of the thesis is to develop fully automatic methods for extracting forest parameters at the individual tree level, by exploiting the 3D structural information in the high density LiDAR point cloud. The specific contributions of the thesis are the following:

1. An automatic tree detection and 3D crown delineation technique for multistoried forests using both 2D and 3D structural information in high density ALS data.

2. An efficient tree species classification techniques that exploit the internal and external crown structural information in high density ALS/TLS data.

3. An efficient approach to accurate stem localization, and direct estimation of Diameter at Breast Height (DBH) using 3D stem modeling in high density ALS data.

In the following subsection, a brief description of the method and novelty for each contribution is described.

Individual tree detection and 3D crown delineation in ALS data

High density small footprint multi-return/full-waveform ALS scanners capture a huge amount of structural data of individual trees in forests. The increasing availability of the high density data has provided the possibility of shifting operational forest parameter estimation from area/stand level to the individual tree level. However, accurate tree detection and 3D crown delineation are critical to accurate Individual Tree Crown (ITC) level analysis [6]. Several techniques that can detect and delineate 3D tree crowns exist in the literature. However, their performance in detecting subdominant trees is often low in multilayered forests due to crown proximity and reduced point density in the sub-canopy layers [23; 6; 18]. Thus, the first contribution of this thesis is a novel technique that detects and 3D delineates: a) the dominant crowns, and b) the subdominant trees which are invisible at the canopy layer due to overtopping-by/proximity-to larger or taller crowns. The method uses the 2D canopy level information to identify three dimensional (3D) candidate point cloud segments which are then separately projected into a novel space to detect and delineate both dominant and subdominant trees. The novelties of the proposed method include: a) dominant and subdominant tree crown detection with minimal omission and commission errors, and b) an accurate 3D crown delineation for both dominant and subdominant trees, in multistoried coniferous forest. The effectiveness of the proposed technique is demonstrated in the experiments on a high density (50 points/m^2) small footprint multi-return LiDAR dataset of a multistoried forests in the southern Alps located in Trentino, Italy.

Tree species classification using high density LiDAR data

Species knowledge is indispensable for accurate estimation of forest parameters. Every species has unique general crown structural characteristics that can be modeled and exploited to classify different species [32; 33]. Tree species differ in their leaf area, foliage distribution, and branching patterns, resulting in divergent crown structures [34; 35; 32; 33]. High density small footprint multi-return LiDAR data contain a lot of details on the internal and the external crown structure. Methods that model point distribution [36], return intensity [27] and crown shape [37] to achieve species classification exist in the literature. In particular, high density ALS data contains structural details of branches which are the building blocks of tree crown [35; 34]. However there has been no or minimal efforts towards the development of methods that can harness the potential of branch level structural differences to achieve species classification. Thus, in this thesis, we pro-

pose novel approaches to conifer species classification by modeling both the internal (i.e., branch level) and the external crown characteristics. The key contributions include: a) a robust model for internal crown structure modeling of conifers using the LiDAR data; 2) a robust set of efficient and scale invariant geometric features, representing the branch-level characteristics, derived using the proposed internal crown structure model; and 3) species independent feature extraction using a data-driven technique. All experiments were conducted on a set of conifers belonging to major European species including Norway Spruce, European Larch, Scot Pine and Scot Silver. The results confirm the effectiveness of the proposed methods over the SoA ones in classifying conifer species.

Stem localization and direct estimation of DBH in ALS data

The accurate estimation of stem location improves the accuracy of crown delineation and accuracy assessment of any parameter estimated at the tree level. Most stem localization methods based on the 2D canopy level information work on the unrealistic assumption that the stem is located directly below the highest point of the tree. Although many 3D stem detection algorithms exist in the state of the art, most of them require the stem section in the lower crown to have enough sample. However, in dense forests, the number of points in the lower section of the crown is often very small. Thus we propose a stem detection technique which models the stem based on the growth direction of the branches in the upper sections of the crown. In a branch point-cloud cluster, the point farthest from branch tip is very likely to be associated with the stem. The set of all such points is referred to as stem points, and they can approximately define the 3D stem. We model the 3D stem by regression fitting a cone on the stem points. Also, most SoA methods estimate the DBH using species-specific allometric models. However, the proposed method measures (i.e., directly estimates) the DBH from the parameters of the fitted cone without species knowledge. The main contributions are: a) a novel approach to estimate the stem position of conifer based branch direction, and b) an approach to directly estimate DBH by 3D shape based modeling of stem. All experiments were conducted on a set of manually delineated conifers belonging to three different conifer species (i.e., Norway Spruce, European Larch, the Swiss Pine) for which both the stem location and the DBH are known. The experimental results prove the method to perform better in stem localization, and DBH estimation with respect to the SoA methods.

1.4 Structure of the Thesis

The current chapter is a brief overview on forest information extraction from high density LiDAR remote sensing data. The chapter also gives a short description of the various

challenges in this context, the proposed solutions, and the key novelties. The rest of the thesis is organized into seven chapters.

Chapter 2 is on the fundamentals of airborne and terrestrial laser scanning, and key notions that benefit the understanding of the thesis. The remaining chapters illustrate details about the challenges addressed in the context of forest remote sensing using high density LiDAR data, and novel solutions.

Chapter 3 briefly recalls the SoA and related works in individual tree detection, tree species classification, and biophysical parameter estimation using high density LiDAR data.

Chapter 4 presents the need for single tree detection and delineation, and also the challenges involved. Further, the section describes in detail the proposed individual tree detection and 3D crown delineation method for multilayered conifer forests using high density ALS data.

Chapter 5 and chapter 6 focuses on tree species classification using high density ALS data. The method proposed in chapter 5 uses crown geometric information for conifer species classification, while, a novel data-driven approach to tree species classification is proposed in Chapter 6. Chapter 7 is on the proposed approach to tree species classification by crown geometric modeling in high density multi-scan TLS data.

Chapter 8 discusses the need for accurate stem localization in the context of biophysical parameter estimation at the individual tree level, and describes the proposed stem localization and direct DBH estimation method in detail.

Each chapter provides an introduction to the specific topics and a short review of the SoA that leads to the research gaps that are addressed in the thesis.

Chapter 2

LiDAR Fundamentals

The chapter recollects some fundamentals on LiDAR remote sensing. The concept of laser ranging, LiDAR profiling and LiDAR scanning are described in the first few sections. The thesis presents automatic techniques separately using ALS and TLS data, and thus later sections describe in details their data capturing process.

Remote Sensing (RS) encompasses a variety of technologies that remotely acquire spatial, spectral, and temporal information about an object/area of interest by analyzing the interaction of electromagnetic radiations with it. The main elements of remote sensing system are: a) an electromagnetic wave transmitter, b) interaction of wave with the object/area of interest, and c) the electromagnetic wave receiver which records the returned energy [38]. The properties of the received wave differ from the transmitted one based on the characteristics of object/area that it interacts, and the state of the wave propagation medium. Thus, the recorded data can be analysed for deriving information about the study area/object. Remote sensing technology is widely exploited for studying and monitoring terrestrial entities such as forest [19], ocean [39], and the atmosphere [40]. Remote sensing systems are broadly classified as active and passive, based on the electromagnetic energy source used for illuminating the object/area. The former set of systems uses artificial energy sources such as lasers or radio wave transmitters, while the latter set constitutes of scanner and radiometers which exploit the energy coming from natural sources such as the Sun. For Earth remote sensing applications, the sensors are mounted on space-borne [41], airborne [42] and terrestrial platforms [43]. In this thesis, we focus on the forest remote sensing using LiDAR data acquired from airborne and terrestrial platforms.

2.1 Basics of LiDAR Remote Sensing

Also referred to as laser altimetry, LiDAR is an active remote sensing technique that uses laser light to characterize an object/area of interest. The major elements of the LiDAR remote sensing include: a) a transmitter that fires a finite-length/intensity-modulated laser pulse at the object/area of interest, b) pulse interaction with the object/area of interest, and c) pulse energy getting reflected back to an optical sensor/receiver [44]. The return pulse energy P_{ret} is determined based on LiDAR transmission equation, and the time of return is dependent on the distance of the object from the sensor i.e., referred to as range. The transmission equation of LiDAR is given as [45],

$$P_{ret} = \frac{\rho M_L^2 D_r^2 D_{tar}^2}{4R_L^2 (R_L\gamma + D)^2} P_t \tag{2.1}$$

Where ρ being the reflectivity of the surface, $M_L \in [0,\ 1]$ is the loss factor, D_r is the receiver antenna/sensor-aperture diameter, D_{tar} as the target object/area diameter, R_L is the range, γ is the beam divergence, D is the diameter of laser-exit aperture, and P_t is the transmitted power. At large distances, the D is insignificant compared to $R_L\gamma$. Hence (2.1) reduces to (2.2).

$$P_{ret} = \frac{\rho M_L^2 D_r^2 D_{tar}^2}{4R_L^4 \gamma^2} P_t \tag{2.2}$$

A laser based transmitter-receiver system can be designed by using the aforementioned transmission equation, and can be used for range measurement of an object/area of interest. In the following sections, we discuss in detail the concept of laser ranging, LiDAR profiling, and LiDAR scanning, which are fundamental for understanding the thesis.

2.2 Laser Ranging

Ranging refers to calculating the shortest distance between the laser transmitter/receiver (Tx/Rx) and the object/area of interest. LiDAR based ranging is performed by measuring the time lag between the laser transmission and reception Δt (for pulsed lasers), and phase lag between the transmitted and received wave $\Delta\phi$ (for continuous waveform lasers) [44]. In pulsed laser systems, the range R_L is proportional to Δt and is calculated using (2.3), where c is the speed of light.

$$R_L = \frac{c}{2}\Delta t \tag{2.3}$$

While in the continuous waveform laser systems, the laser light is intensity modulated with a sinusoidal signal of wavelength λ_{IM}, and the range R_L is obtained by exploiting

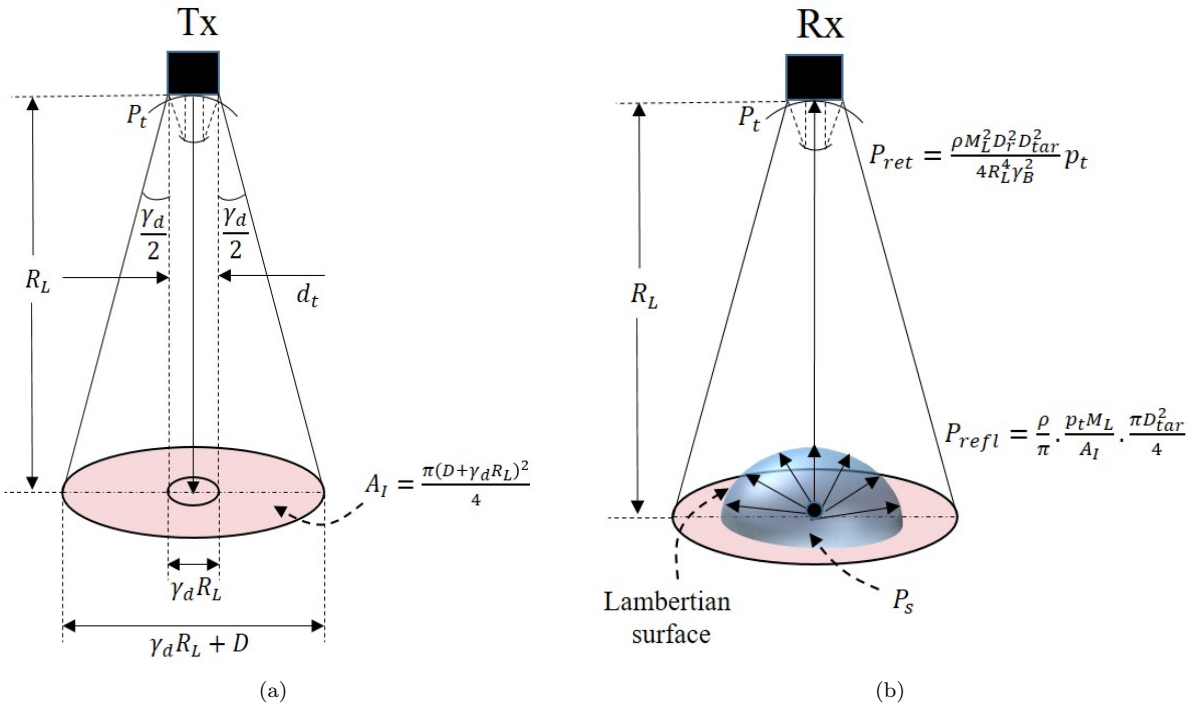

Figure 2.1: (a) The footprint created by the spreading of transmitted laser beam, (b) the Lambertian surface corresponding to a point reflector at the footprint center.

the phase difference between the transmitted and return wave phase $\Delta\phi$. The range is calculated in a continuous waveform systems using (2.4), where f_{IM} is the frequency corresponding λ_{IM}.

$$R_L = \frac{c}{2}.\frac{T}{2\pi}\Delta\phi = \frac{1}{4\pi}.\frac{c}{f_{IM}}\Delta\phi = \frac{\lambda_{IM}}{4\pi}\Delta\phi \tag{2.4}$$

The time (for pulsed laser systems) and phase (for continuous waveform laser systems) lag measurements are done using very precise electronic systems to minimize the error in the calculated range. It is worth noting that, range resolution in a continuous waveform laser system can also be improved by using shorter λ_{IM}, and hence is an advantage of continuous waveform systems over pulsed ones. Whatsoever, high power requirement and limited unambiguous range are issues associated with the continuous waveform systems, that limits its use to close range applications. For both pulsed and continuous waveform systems a higher ranging precision can be obtained using triangulation method by using the angle of intersection between two laser beams produced by either separate laser or formed by splitting of the single laser beam.

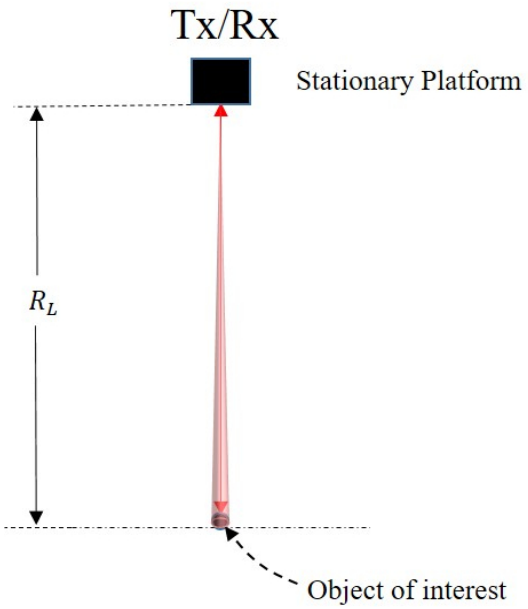

Figure 2.2: Laser ranging

2.3 LiDAR Profiling

By periodically performing laser ranging from a space borne or an airborne platform moving over the object/area of interest, the ranging instruments can be used to capture One Dimensional (1D) data at nadir points (which are uniformly separated) in the ground projection of the platform trajectory. The data so collected is referred to as the LiDAR/laser profiler data. LiDAR profiling done from a moving airborne or space based platform at height h from the sea level enables them in capturing the terrain profile of larger areas on the surface of Earth (Fig. 2.3). Alternatively, LiDAR profiling done from a terrestrial platform allows capturing the local terrain profile [46], and hence is popularly used in land surveying applications [44]. Here, the height difference between the laser ranger and the ground point is measured as the product of the slant range and the vertical angle of the ranger.

LiDAR Profiling of Forests

Periodic laser ranging performed from a low flying platform has been originally used for acquiring the surface topography, even in the presence of a thick canopy. Here, the laser pulse is fired vertically down towards the nadir point of the platform and the return(s) are used to define the characteristics of the object/area at the point, such as the land cover class and the surface elevation. The knowledge of the position and the altitude of the flying platform at each ranging instance allows determining the topography along the

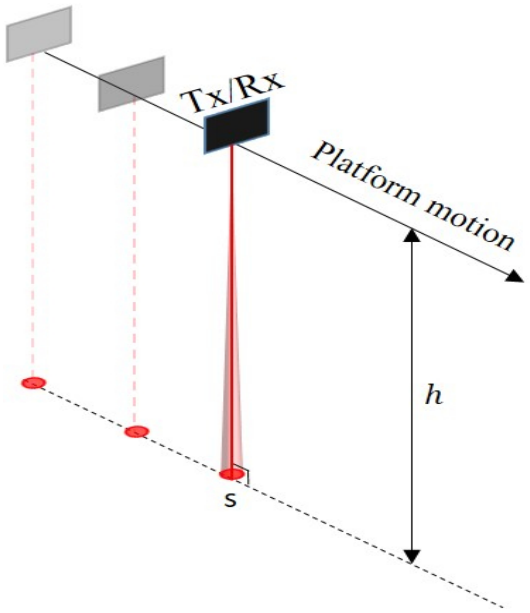

Figure 2.3: LiDAR profiling

ground projection of the platform trajectory. Profiler data acquired from multiple flights conducted with optimally selected trajectories over an area of interest can determine the 3D surface topography of the area. The laser pulse fired vertically from an airborne platform towards forest interacts with its vertical profile and hence get partially reflected back to the sensor. Each pulse provides at least one ranging and set of associated attribute measurements (e.g., the intensity and the scan angle) that characterizes the forest that falls within the laser footprint. LiDAR profiling of forest has been used to estimate tree height [47], canopy density [48], and biomass [49], along with forest area topography [50].

Despite huge distances and associated lower scan density, space based LiDAR profilers such as the large footprint space-borne full waveform profiling GLAS (onboard ICESat) and Advanced Geoscience Laser Altimeter System (AGLAS) (onboard ICESat-2) have also been successfully used to estimate the global canopy height [51]. The canopy matrices generated from GLAS and or AGLAS data are used to estimate aboveground biomass [52], and carbon [53]. Whatsoever, the performance of space based profiles is adversely affected by the atmospheric conditions, the low pulse width (which acts as a low pass filter which limits vertical resolution) and the low pulse energy (considering the large distance between the platform and the target). However, recent space-borne missions such as Global Ecosystem Dynamics Investigation LiDAR (GEDI) has onboard LiDAR systems capable of generating footprints as small as 25 m and high pulse firing rates as high as 242 times per second with a pulse power of 10 m, that can perform a more comprehensive sampling on even dense canopies.

2.4 LiDAR Scanning

The laser ranging instrument can be transformed into a laser scanner by using a scanning mechanism framework. The idea behind laser scanning is to collect data point(s) for a series of locations on the target object/area using the laser ranging technique. These data points when jointly considered can represent the surface topography and attributes of the object/area in 3D. Laser scanning is achieved by repeated/simultaneous laser ranging at a series of target locations from a linearly moving platform. Usually, a framework of custom optics and supporting mechanical structures is used to deflect laser pulse in the across-track direction to the direction of the platform motion. More specifically, a rotating mirror/prism placed at an inclination of 45° to the casted laser beam is used to cause the deflection [44]. The beam can be deflected along the whole length of the horizon in the across-track direction (i.e., the direction perpendicular to the movement of the platform, in the incident beam plane) by adjusting the orientation of the mirror. However, laser scanning in a terrestrial framework is usually performed at smaller deflection angles in order to reduce problems of low power at regions away from nadir, and large variations in footprint size. Thus the maximum deflection angle, and hence the FoV, is limited to smaller angular intervals by using a multi faced mirror. The rate of rotation of the mirror/prism determines the scanning frequency. Fig. 2.4 shows the basic laser scanning technique, with LiDAR transmitter (Tx)/receiver (Rx) system at a distance of h from the target surface producing a swath s. The scanning happens across the direction of the platform motion.

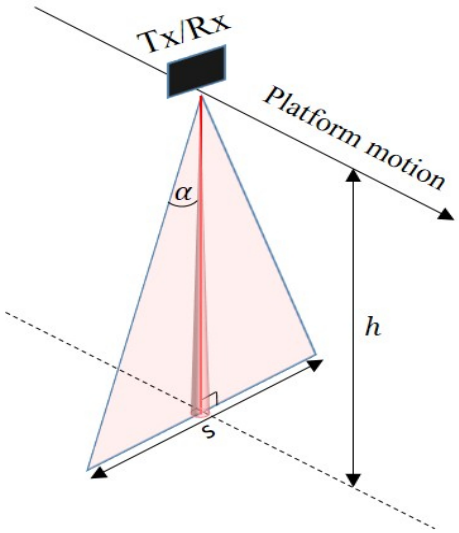

Figure 2.4: Laser scanning

The amplitude distribution (in time) of the pulse energy reflected back to the optical

sensor is based on the interaction of the pulse with object(s) in its path e.g. branches of a tree located at different heights. The peaks in the returned waveform correspond to the maximum energy reflections that happened along the path, and hence are the most informative sections of the distribution. Discrete return LiDAR systems detect only the peaks in the returns, and usually record one (first or last), two (first and last), few (e.g., four, eight) returns, depending on the application requirements. However, the alternate class referred to as the full waveform LiDAR systems record the amount of energy returned to the sensor for a series of very fine time intervals. Although it is memory intensive, the data collected have very high vertical resolution.

The number of pulses that is fired per second is referred to as the pulse rate, and determines the horizontal resolution of a LiDAR system. i.e., a higher pulse rate increases the horizontal resolution of the system by capturing more data points along the scan direction, and vice versa. Although it is safer (in terms of error) to have a single pulse in the air, the recent advancements in the precision pulse generation and return time measurement electronics allow multiple pulses to be in the air simultaneously. However, to do so, the measuring distance intervals should be greater than the range-ambiguity interval which is the speed of light divided by the pulse rate. The angular accuracy of the system also affects the horizontal accuracy. Although a high resolution angular encoder can provide a very precise angle measurement, the effective horizontal resolution of a LiDAR system is often limited by the laser beam diameter and beam divergence. The size of the footprint is also a factor affecting the accuracy of the measurements. However, the precision of the measured data depends mostly on the footprint size as the return signal is an average of the total reflections happening from within the footprint. For a particular footprint size, the averaging of overlapping point data improves the horizontal accuracy.

LiDAR scanning can be performed from airborne and terrestrial platforms, and are referred to as the ALS and the TLS, respectively. In this thesis, we focus our attention on information extraction from the airborne and the terrestrial laser scanner data.

2.4.1 Airborne Laser Scanning

Airborne Laser Scanning (ALS) performs LiDAR scanning from a stable low flying airborne platform such as helicopter, aeroplane and drone, to capture 3D details of an object/area on the Earth surface, from an aerial perspective. The basic modules of an ALS system are: a) a laser scanner that fires laser pulse towards the target object/area and detects the reflected pulse(s), b) the Global Positioning System (GPS) which provides accurate 3D positional information of the platform, c) an Inertial Measurement Unit (IMU) which continuously records the orientation details (i.e., the pitch , the roll, and

the yaw) of the platform, and d) an on-board computer interface that controls the laser scanning and data recording configurations.

The transmitted laser pulse travels the minimum distance at the nadir point, and the distance increases away from the nadir (for a flat terrain). Thus, ALS data are acquired strip-wise over the target area mainly to minimize the range errors. The pulse-energy-loss increases for larger scan angles, hence inducing data errors. In addition, the flying platforms are often not very stable in the air in terms of orientation and height. This instability also results in data errors. Accurate position and orientation data at the ranging instance allow correcting the positional errors in the data. In the case of ALS, accurate 3D positional information and the orientation information are derived from the using a GPS receiver, and the IMU, respectively. A Differential Global Positioning System (DGPS) which uses a reference signal from a base station is preferred to obtain maximum accuracy [44]. The on-board computer collects the scanner data, the GPS, and the IMU data continuously. Processing of the points can be done in an on-the-fly or post-acquisition fashion. The density of points collected in a single scanning pass is dependent on the pulse rate, the scanning frequency, the flying height, and the number of returns stored [54]. Increased accuracies can be obtained by using ground control points during strip adjustments aimed at stitching together different strips [45].

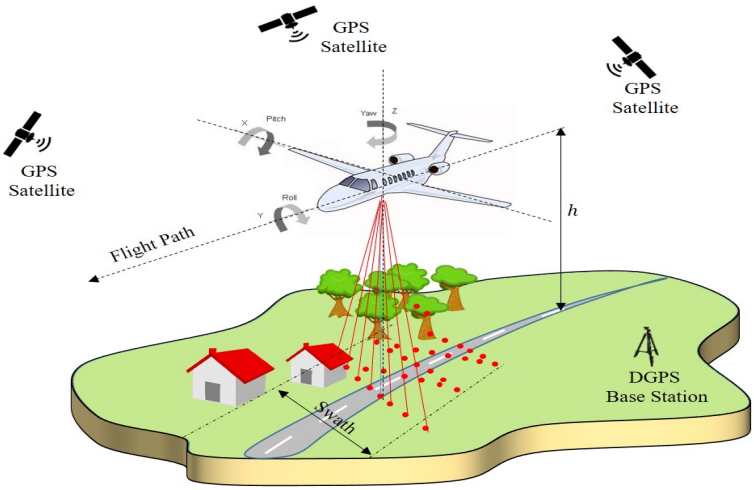

Figure 2.5: Airborne laser scanning

Airborne Laser Scanning of Forests

Airborne laser scanning conducted over forests reveals the 3D structure of forests by capturing data of the forest vertical profile. ALS laser beam footprint is usually very small and thus spans very fine sections of the tree crown, which makes the scanners useful

for acquiring data at the resolution of individual tree structures. Multi-return and full waveform systems capture huge amount of point sample along the vertical profile of tree crowns. In particular, the small footprint multi-return/full waveform systems capture very fine 3D tree crown structural characteristics (because of high range resolution). The first return usually corresponds to reflections from the canopy layer and the last return corresponds to the ground reflections (Fig. 2.6). The intermediate returns correspond to reflections from the middle layers of the forest (i.e., between the canopy layer and the ground). The intensity component corresponding to individual data point provides some spectral information depending on the laser wavelength. In forestry applications, the wavelength of the laser pulses is in the near-infrared part of the spectrum is typically 1040 nm or 1065 nm [44].

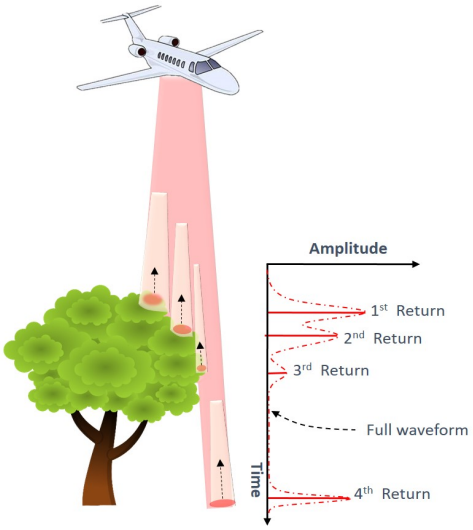

Figure 2.6: The laser beam scattering mechanism for an individual tree

.

The data collected by an ALS are a set of points in the 3D Euclidean space, with associated attributes such as scan angle, return number, scan direction and the point source ID. Compared to single-return systems which captures only one return against a fired pulse, multi-return/continuous waveform LiDAR systems can capture more than one return against a single pulse fired, resulting in a larger set of point data sample. Each data point also has a associate spectral attribute (i.e., intensity) that that is dependent on the frequency of the laser involved. Modern scanners have been able to scan in two or more channels (frequencies of the laser). Multispectral scanners have the capability to simultaneously capture the spectral responses using more than one laser frequencies, and hence are getting a lot of attention in tree species classification and forest inventorying [55].

2.4.2 Terrestrial Laser Scanning

Unlike ALS, the Terrestrial Laser Scanners (TLS) are instruments that capture 3D data of the area around a fixed position on the Earth surface. The principal components of a TLS scanner are: a) laser generator, b) a mirror that can be rotated along the vertical and the horizontal axis, c) the reflected beam receiving optics, and d) the range finder. Fig. 2.7a shows the principal components of the TLS instrument. TLS performs scanning in an automated manner by using a predetermined scanning pattern as mentioned in section 2.4. The beam width, and thus the horizontal resolution, in a TLS acquisition varies as a function of the initial beam diameter, the beam divergence, and the target distance. The horizontal resolution can be improved by employing smaller angular steps for the same scanning frequency.

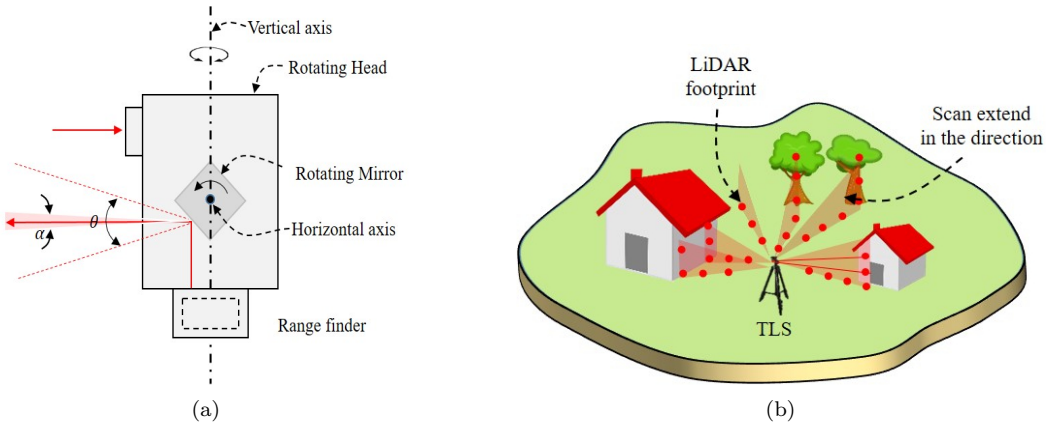

Figure 2.7: (a) TLS instrument and (b) Terrestrial laser scanning

Data collected from a TLS can be scanned to one of the three coordinate system: a) Scanner, b) Project, c) Global. The scanner and the project coordinate systems are established for individual and multiple scans, respectively. Thus they are beneficial for local studies. Co-registering the data in the scanner/project coordinate systems to a global coordinate system such as the WGS84 allow the data to be used for studies using information from other remote sensors, and also at a wider geographic scale [44].

The terrestrial acquisitions are affected by the topography of the area due to the varying ranges of the objects measured (from the scanning perspective) by the sensor. For example, the number of points captured linearly decreases with an increase in distance between the object and the scanner. In this case, a relatively homogeneous point density in different direction is ensured by partitioning the entire scan-area in smaller angular steps. The scanning is done accordingly to achieve a similar point density in each division. For complex landscapes, calculating optimal scan step along the horizontal and the vertical directions are critical to obtaining a homogeneous scan (Fig. 2.8).

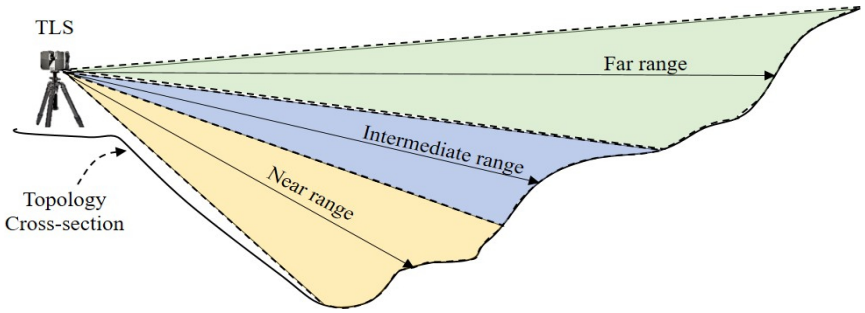

Figure 2.8: Scan partitioning

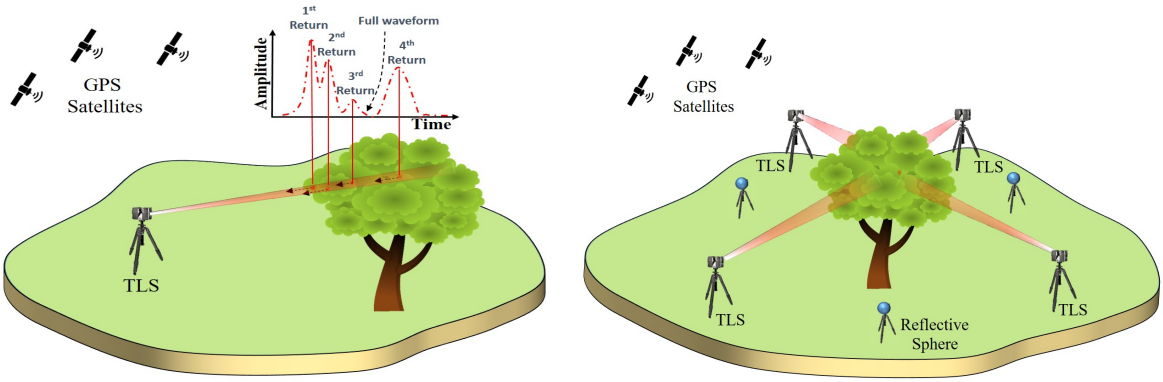

Figure 2.9: (a) Single-scan framework and (b) Multi-scan framework

Terrestrial Laser Scanning of Forests

The ability of the TLS to capture huge number of point sample of its surrounding objects is heavily exploited in forest studies at the individual tree level. For forest remote sensing, a TLS scanner is placed in a location which causes minimum occlusion of the surrounding trees in order to acquire maximum amount of detail. The data acquired using a TLS system differs from an ALS one in terms of acquisition geometry, and also the captured details are mostly complementary to each other [44]. For example, the TLS captures details of the lower crown section and the understory vegetation, however fails often in capturing canopy level details. Whereas most data captured by an ALS system are limited to the upper crown section.

TLS data are acquired using a single-scan or a multi-scan framework. The former framework restricts the data collection to the field of view of a single sensor. As a result, only a section of the surrounding trees are scanned (Fig. 2.9a). However, the latter framework merges data acquired from multiple scans performed from locations, allowing capturing of tree data from multiple perspectives. This allows a very comprehensive and uniform data acquisition on individual trees (Fig. 2.9b). The data collected by TLS are

a also a set of points in the 3D Euclidean space as is the case with ALS.

Chapter 3

State of the Art in Forest Remote Sensing using LiDAR data

The chapter provides the state of the art and related studies in LiDAR-based individual tree detection, species classification and forest parameter estimation.

Forest inventorying is performed using Area Based Methods (ABM) and ITC based methods [56]. The former relies on summary statistics calculated from the LiDAR data over an area to derive forest parameters, whereas the latter uses the delineated 3D point cloud of individual trees for species classification and forest parameter estimation. For example, Fig. 3.1 shows the schematic diagram illustrating key differences in height calculation between the ABM and the ITC methods. The major advantage of ITC level data over area based ones is the possibility to produce species-specific forest parameter estimates at fine resolutions. In addition, ITC methods have a better compatibility to reference field-inventoried data (which is always obtained from individual trees). Studies comparing ABM and ITC based approaches in the context of height estimates and forest carbon mapping [29] highlight the potential of the ITC based approaches to give improved performance over area based ones, as individual tree detection and delineation capabilities improve. The increasing availability of denser data from small footprint (i.e., 10-30 cm) systems [45] at declining acquisition cost [57] motivated development of methods to extract information at the ITC level. Hyyppa [58] and Persson [59] were among the first to confirm the possibility of deriving forest parameters and species information at the ITC level.

The thesis concentrates on exploring individual tree level based species classification and forest parameter estimation methods. Thus, section 3.1 discusses the state-of-the-art individual tree detection and delineation approaches which are fundamental to ITC based forest studies. Section 3.2 and section 3.3 recalls the state-of-the-art method in species classification, and forest parameter estimation techniques, respectively.

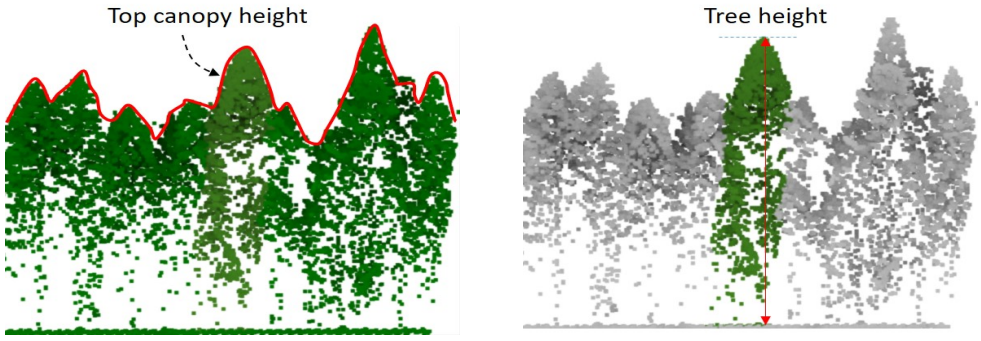

(a) (b)

Figure 3.1: Schematic diagram illustrating the key differences in height calculation between the ABM and the ITC method.

3.1 Individual Tree Detection and Crown Delineation

In the framework of forest analysis, the tree detection refers to identifying the ground location of the tree stem, while the crown delineation refers to identifying the tree crown boundary in 3D. Canopy Height Model (CHM) [60] based approaches have been conventionality and widely used for crown detection and delineation mainly due to their simplicity. In these approaches, crown delineation is performed by segmenting CHM, based on treetops detected using local maxima [60] or level set [61] method. The rasterization artefacts in the CHM combined with the irregularities in crown shape affect the crown detection and delineation accuracies, and hence are smoothened out using a Gaussian low-pass filter [62], [63]. Thus, optimal smoothing parameters are critical for accurate tree detection and delineation. They are often estimated by modeling topological relation of crown segments with one another [64], rule-based splitting and merging of crown segments [65], or methods based on local extrema calculated from combinations of normalised scale invariant CHM derivatives [62]. In case of mixed/multilayered forests with variable crown size (and thus no single optimal resolution), adaptively varying filter window size improved crown detection accuracy [60; 66]. Alternatively, multistage object-based approach to tree delineation using region growing approaches are also developed [67; 68]. However, the approach demands an overhead of fine-tuning of the search radius and merge conditions for optimal results. Although CHM based treetop detection techniques when used singlehandedly can detect and delineate most of the dominant crowns, they often fail to detect subdominant crowns. This is because of the partial (or complete) obstruction of their crown by the dominant ones, in addition to often being less prominent in the CHM.

The limited ability of CHM based methods in accurately representing tree crowns

motivated researcher to exploit the 3D information along the height profile. Exploiting the full potential of LiDAR data, several studies delineate tree crowns directly in the point cloud space. The simple k-means clustering applied to normalized point cloud, with seed points identified through CHM segmentation, highlighted the possibility of an accurate 3D crown delineation [69]. In an attempt to improve delineation of trees with irregular canopy size, Lee et al. applied region growing for generating initial 3D segments, and performed agglomerative clustering to accurately segment individual tree crowns [70]. A RANdom Sample Consensus (RANSAC) based geometric model fitting which iteratively determines the best set of points for a tree proved to perform well with sparse forests with variable tree heights [71]. In some studies, the horizontal spacing between tree crowns [72] and the variation in vertical density profiles of CHM segments [73] are exploited to delineate tree crowns. Methods performing 3D layerwise analysis on tree point cloud to mitigate the problem of reduced point density in the understory also exist in the literature [74]. For example, layer-wise segments derived through clustering of the point cloud segments in every layer are stacked together and inspected for overlap to detect potential tree crowns [75]. Voxel-based approaches also proposed in the literature. For example, Wang et al. delineated tree crowns using features derived from point cloud segments in every horizontal layer along the tree height. Each layer is divided into cells, and the points within each study cell are resampled into the local voxel space (within), to derive the projection images [76]. In a more recently proposed voxel-based approach, the complementary information derived from the treetop and the stem location are exploited for 3D tree crown delineation [77]. In a comparison study on different state-of-the-art crown delineation methods (performed on the same dataset), the accuracy varied from study to study from 25% to 90% [31]. The results prove that the accuracy is highly influenced by the crown delineation method. It is also proven that, in addition to forest type [78], spatial arrangement [79] and variation in tree size [80], forest structural diversity [81] also impacts the detection and delineation accuracies. It has been inferred that high stand density and large forest heterogeneity have adverse effects on delineation accuracy [31]. The point cloud density is also proved to have an impact on the accuracy of tree detection and delineation [82]. For example, decreased point density in the subcanopy layers results in less information about the subdominant and understory vegetation, and thus causes low detection and delineation performance .

Despite the availability of high density data, SoA methods are lacking in the ability to accurately detect and delineate both dominant and subdominant trees [75; 31; 78; 83]. Wang et al. proposed a hierarchical morphological approach to 2D crown data derived from voxel layers analysis along the forest vertical profile to delineate dominant and subdominant crowns in the 3D space [84]. Vega et al., proposed a multi-scale segmentation

at the point level, followed by a multi-criteria analysis of the segments for accurate crown localization and delineation. However, the accuracy associated with the subdominant tree detection is low mainly due to poor point density below the canopy layer [85]. In a bottom-up approach to detect and delineate tree crowns, Lu et al., first extracted tree trunks by exploiting the intensity difference between trunk and other parts of the tree, and assigning the remaining points to the trunk clusters based on a set of proximity rules (with respect to stem) [86]. Among studies using full waveform LiDAR data, [87], the ones based on ellipsoidal k-means clustering proved to provide good accuracies in multilayered forest. Here, the cluster centers of dominant trees are obtained from the CHM segments, while that of the subdominant trees are obtained in an iterative way using uniform seed placement which however often causes inaccuracies [88]. Paris et al. delineated dominant and subdominant tree crowns by a radial-sector-wise analysis of the vertical profile of the tree crown [18]. However, the method relies only on the crown boundary visible at the canopy layer to delineate crown, and hence it does not fully utilize the 3D information in the LiDAR data.

Whatsoever, efficient and robust (to various forest types/conditions) methods that can accurately detect and delineate 3D tree crowns in high density airborne LiDAR data are lacking, making ITC based methods less suitable for operational forest inventorying. Thus, statistical approaches to estimate tree count are also proposed for analyzing complex and multistoried forests. For example, Maltamo et al. [89] used a theoretical distribution to predict the stem number and the DBH of subdominant trees which are not visible in the canopy layer. The parameters of the distribution were calculated from a truncated diameter distribution of dominant trees [89]. With a similar objective, but under the assumption that the relative height of trees in a homogeneous Poisson stand determines the probability of observing them from the air, some authors estimated the subdominant stem count [90],[91], and predicted stem-diameter distribution without the knowledge of tree position [92]. Prior information of tree shape, when used in the MAP estimation of the position, the size, and the crown shape, also improves tree detection accuracy [93]. Nonetheless, statistical modeling of tree level parameters can be useful for: a) estimating the understory biophysical parameter in case of low point density, and b) correcting errors in the crown level parameters derived from the pure ITC technique.

TLS based Individual tree detection and delineation are mostly bottom-up approaches, due to the availability of huge amount of information about the lower sections of the tree (e.g., stem), due to hemispherical scanning performed from a ground platform. Tree detection in TLS data is based on the assumption that there is only one central truck for a tree, which is often modeled as elongated cylindrical structure [94]. Several tree trunk detection [94] and modeling [95] approaches are available in the literature. Many authors

delineated the stem, the branch skeleton, and the foliage of individual trees, by training the system to recognize individual components by using Gaussian mixture model fitting [96], 3D morphological analysis [97], and intensity of the LiDAR returns [98], and in the process delineated the individual tree crowns. Yang et al. first delineated individual tree trucks by clustering the segments detected using limited radius cylinders on every horizontal division of the tree point cloud. Crown delineation is achieved by allocating the remaining points to nearest tree trunks using a hierarchical minimum cut operator [99]. In any case, TLS data is primarily used in forestry for reference data collection, considering its ability to provide extremely accurate tree attributes such as the tree position and the DBH at sample plots [100; 101].

3.2 Tree Species Classification

Remote sensing based species classification has been traditionally performed by exploiting the spectral information in high resolution multispectral and hyperspectral data. However, the use of 3D spatial information in tree species classification problems has been gaining popularity with the increasing availability of high density LiDAR data [102; 103]. Törmä [102] was among the first to test the usability of low density small footprint single return airborne LiDAR data for deriving species proportions in forest stands. However, despite using a set of 28 descriptive statistical point cloud features for characterizing the species distribution, the maximum accuracy reported is only 59.3% due to limited information of the vertical forest profile. A similar low classification accuracy is also reported by Moffiet et al. [103] by deriving a different set of descriptive statistical point cloud features from single return LiDAR data. Several researchers also investigated the effectiveness of using small footprint high density multi-return LiDAR data for species classification. Pyysalo and Hyyppä [104] proved that the profile of distance of small footprint high density multi-return LiDAR data points from the stem along the vertical direction provides hints on the tree species. In [105], the height difference between the first and the last pulse from multi-return LiDAR systems is identified as a good feature for differentiating deciduous trees from conifers during leaf-off conditions. The underlying assumption here is that the last laser return is reflected from within the deciduous tree crown, while the same would get reflected back from crown-top in case of conifers. Holmgren et al. distinguished Norway Spruce from Scots Pine (both conifers) in small footprint high density LiDAR data using features derived from laser return proportions and point height distributions, and achieved an overall accuracy of 95.0% [106]. By generating moment and percentile features from the points, Orka et al. [107] classified spruce and birch trees in an unmanaged forest. Improved species classification performance is obtained by exploiting the high

vertical resolution of the 3D positional data in small footprint full waveform LiDAR data [108; 109]. By classifying spruce, larch and beech trees, Holmgren and Persson [110] and Hofle et al. [111] proved the potential of point data attributes such as the echo width and the backscatter cross section derived from the full waveform LiDAR point cloud (by modelling the waveform as a series of Gaussian components) in species classification. Studies have also demonstrated the potential of LiDAR data for classifying tree species in subtropical forest [109], boreal forests in the Nordic countries and Canada [107; 112], temperate forests in Europe [83; 36], and North America [113; 114].

Based on the fact that crown shape is species dependent, geometric model fitting techniques are also proposed as an effective species classification approach by some authors. For example, Kim et al. showed that height percentile value and features derived from fitting simple geometric shapes such as the cylinder, the cone and the sphere, on the tree crown are very useful for classifying deciduous and evergreen trees [115]. However, the use of leaf-off and leaf-on data increase computational complexity and operational cost. Vauhkonen et al. [116] successfully employed alpha shape based ITC matrices to achieve species classification of pine, spruce and birch. In [117], Ko et al. pointed out the importance of internal crown geometric features derived from LiDAR to perform tree species classification. They derived six geometric features, including two internal and four external crown structural features, from small footprint high point density multi-return airborne LiDAR data to achieve species classification. The classification of pine (coniferous), poplar (coniferous) and maple (broad-leaved) trees achieved an overall accuracy close to 90.0%. Whatsoever, it is worth noting that the study reports low classification accuracies within the conifer class. This is because the Merge and Split K-means based model used in the study is not able to accurately model the individual conifer branch clusters and hence produces inaccurate features which ultimately lead to poor classification performance. In [118], the authors have demonstrated that advantage of jointly employing point-space distribution and laser return-intensity features, along with internal and external crown geometric features for species classification in a boreal context.

In addition to structural information, the intensity of the backscattered laser beam gives spectral information that proved to be used for classifying tree species [119; 120]. Brandtberg et al. [62] tested the potential for intensity information for ITC level species classification using leaf-off data, and inferred that the return beam intensity has a dependency on the branch thickness and the reflectance properties of the bark. With leaf-on data, the mean return intensity is found to be influenced by crown structural parameters such as the crown density and gaps within the crown [121]. Whatsoever, the dependence of the return intensity on the scan angle, the flying height, and topography often induces variance in the data [27; 54; 122]. Thus strategies are proposed by several authors to

reduce the variance induced by the scan angle and the height factor [123; 122]. The use of leaf-on and leaf-off data provided additional information related to change in spectral reflectance of a tree, and is hence proved to be useful for species classification [37]. Many authors also considered the joint use of structural and spectral information in high density LiDAR data by deriving ITC matrices from both height and intensity attributes [27; 124; 125]. Recent approaches are oriented towards single sensor solution to species classification by using spatially and spectrally rich data from systems such as multispectal LiDAR [126].

By performing scanning from a ground-based platform, the so-called Terrestrial Laser Scanner (TLS) captures denser point clouds containing finer details of tree-structures including stem, crown, and leaves. In one of the initial attempts on species classification using TLS, Othmani et al. [127] derived surface texture properties of tree stem to differentiate between hornbeam, oak, spruce, beech, and the pine. However, the method demands an extremely high point density which are often infeasible to obtain in an operational survey. By deriving nine TLS features related to a tree stem and crown geometry, Lin et al. [25] attempted classifying between spruce, pine, aspen, and oak. Here, despite deriving unique features from the stem, the crown, the branch, and the leaf levels, the total accuracy obtained was just over 75%. This poor accuracy could be attributed to the inaccurate modeling of tree structure, and poor selection of features. In another endeavor to exploit TLS data for tree species classification, Lin et al. [25] derived 10 features at various levels starting from the overall crown shape to the leaf characteristics. However, despite branch being the building block of crown, only one feature (i.e., branch slope) is used to model the branch characteristics, resulting in a sub-optimal model, and thus an overall classification performance of 77.5% only.

Despite the fact that multi-sensor data assimilation is a costly and complex affair, some researchers studied the effect of combining complementary information for an accurate forest inventory [128; 129]. High resolution Near Infrared (NIR) images have been identified as a valuable source of complementary information for improving the performance of LiDAR based conifer-deciduous classification [130]. Some authors [131], [132] studied the use of high resolution multispectral images to derive species-specific details. However, the low spectral resolution of these data is a bottleneck for an efficient species classification. Instead, the fine spectral sampling achieved by hyperspectral sensors enables the discrimination of several species but at a lower spatial resolution. Hyperspectral data have been used in several studies alongside airborne LiDAR data [133], [134]. Sugumaran et al. used LiDAR and hyperspectral data jointly for tree species classification in urban scenarios [135]. In [136], the effectiveness of combining data from LiDAR, SAR, Landsat ETM+, and Quickbird data for forest parameter estimation was investigated. Their joint

use was found to be more effective than using LiDAR data only. However, the same study points out that LiDAR is the best single sensor for estimating the canopy height and the biomass of trees with good accuracy. This understanding has been a motivation for many studies on species classification using only LiDAR data [115], [117], [137].

3.3 Forest Parameter Estimation

Since the 1990s, a large number of scientific studies for extracting the biophysical information at the ITC level from LIDAR data has been proposed. The various parameters that are extracted include tree count [58; 83], tree height [58; 59], crown span [138; 139], crown volume [140], crown base height [141], stem volume [17; 36], DBH [142; 36], above ground biomass [143], and other parameters related to forest structure [144; 145].

Accurate stem location is a critical aspect to forest parameter estimation at the ITC level as it affects both 3D tree crown delineation and their linkage with the field data. The assumption in many stem detection studies is that the stem location is the ground projection of the treetop [31; 146; 147]. CHM is a 2D image of the canopy surface derived from the first return component of a multi-return LiDAR data. All CHM based treetop detection algorithms work under the assumption that the peaks in the CHM correspond to the treetops [59; 148; 149]. However, the resolution of the CHM, and the smoothening filter size have a large impact on the treetop detection accuracy and need to be optimized using area-based estimate of stem number [150] and/or crown radius [151]. Whatsoever, the single peak assumption is reasonable only for trees which generally have a tapered upper crown (e.g., conifers). Also, often a single tree crown may contain multiple peaks. These multiple treetops will be recorded against a single tree, resulting in reduced performance [31; 152]. The state of the art also includes object based methods to detect individual trees [67; 153]. However, methods which work directly on the point cloud were found to be more accurate in treetop detection as there is no error induced from CHM smoothening [154; 155; 156]. A general observation with point cloud is that the LiDAR point distribution (i.e., the histogram) along the height of the tree is minimum near the stem section [157]. This feature of the stem, modeled as a local dip in the histogram, combined with a region growing segmentation, is useful in delineating the stem [158]. Reitberger et al., identified potential stem points using a three step procedure: the first step discards the ground points, the second step identifies the crown base section in the point cloud and performs a 2D hierarchical clustering to identify points belonging the stem, and the final step eliminates clusters resulting from understory vegetation using a RANSAC based technique [83]. Histogram-based methods assume that there is at least a branch free section of the tree stem between the crown and the ground. The intensity of the laser

return is a measure of surface properties such as the texture and the roughness [86]. These properties are different for stem, leaf, and branch and are recorded as intensity variation in laser returns. In an intensity normalized data, high return intensity points usually correspond to tree stem and thus they are often leveraged to delineate stems [86]. Vertical slice-wise boundary detection technique, as in [159], that derives the horizontal span of the crown in each slice also allows detecting and delineating the 3D stem. The assumption here is that the ground projection of the data in horizontal slices containing only the stem will generate a 2D boundary spanning a relatively small area than the other section of the crown. Hybrid techniques for treetop detection were also proposed by some authors by combining the ALS data with a variety of a priori information [93; 160].

DBH is a biophysical parameter that is essential for accurately estimating forest biomass [161; 162] and modeling of carbon water relation [163]. Several methods based on low density ITC data indirectly estimate the DBH by deriving allometric relations with tree level variables such as tree height and/or crown span [17; 164]. However, the fact that such methods require apriori species knowledge, is a problem in operational DBH estimation. An alternative approach is to use supervised machine learning approaches (e.g., Support Vector Regression (SVR)) [165]. However, training data are sometimes difficult to retrieve. High density small foot-print multi-return LiDAR data contain accurate structural details which can be used to directly measure several tree level attributes. This is evident from the success of methods that delineate structural components of trees such as the crown [166], stem [83], and branches [167]. In this light, Rahman et al. [168] attempted measuring the DBH based on the variance of point distribution around a 3D line fitted on points corresponding to tree trunk. A direct estimation of the DBH on the point cloud is also proposed in [169] by analyzing the data point distances to a suitable tree skeleton. The methods assume that there is a section of stem in the lower crown section which is not occluded by branches/foliage. However, conifers such as Norway Spruce mostly have branches along its entire height profile.

Chapter 4

Individual Tree Detection and 3D Crown Delineation

Accurate crown detection and delineation of dominant and subdominant trees are crucial for accurate inventorying of forests at the individual tree level. State-of-the-art tree detection and crown delineation methods have good performance mostly with dominant trees, whereas exhibits a reduced performance when dealing with subdominant trees. In this chapter, we propose a novel approach to accurately detect and delineate both dominant and subdominant tree crowns in conifer-dominated multistoried forests using high density small footprint high density ALS data. Here, 3D candidate cloud segments delineated using a CHM segmentation technique are projected onto a novel 3D space where both dominant and subdominant tree crowns can be accurately detected and delineated. Tree crowns are detected using 2D features derived from the projected data. The delineation of crown is performed at the voxel level with the help of both 2D features and 3D texture information derived from the cloud segment. The texture information is modeled by using 3D Grey Level Co-occurrence Matrix (GLCM). The performance evaluation was done on a set of six circular plots for which reference data are available. The high detection and delineation accuracies obtained over the state of the art prove the performance of the proposed method.

Part of the chapter appears in:

1. Harikumar, A., Bovolo, F., and Bruzzone, L., ' A local projection based approach to individual tree detection and 3D Crown Delineation in multistoried coniferous forests using high density airborne LiDAR data.' , IEEE Transactions on Geoscience and Remote Sensing, Vol. 57, No. 2, pp. 1168 - 1182, Feb 2019.

4.1 Introduction

Accurate tree detection and crown delineation are fundamental to the ITC level forest biophysical parameter estimation [6]. However, the crown overlap and proximity make it a challenging task in the context of ALS data. Also, the amount of structural information in ALS data dwindles towards the subdominant forest layers. This dwindling further amplifies the challenges in crown detection and delineation in subdominant forest layers. Errors in detecting and delineating tree crowns affect the accuracy of any downstream operation including tree species classification and parameter estimation [88]. Tree detection and delineation in subdominant layers are important as trees in the layer as they: a) contribute to the forest biomass, and thus neglecting them results in errors in the biomass estimates, b) are part of forests and thus modeling them is necessary to understand the forest environment, and c) include young and or naturally dwarf trees.

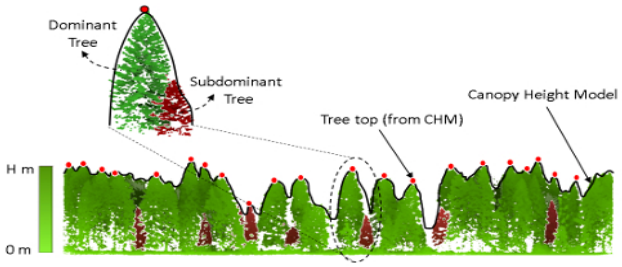

Figure 4.1: CHM based tree detection and crown delineation. The dominant and subdominant trees are shown in green and red, respectively.

Most state-of-the-art 2D and 3D crown detection and delineation algorithms (see section 3.1) work effectively in the case of trees in the dominant layers, however they show a reduced performance for trees in subdominant forest layers [85; 18]. In general, 2D CHM based approaches have a greater ability to delineate crowns in the dominant layers, while the 3D methods exploit the vertical profile information in ALS data and hence have a greater potential over 2D counterpart to delineate crowns even in subdominant layers. However, state-of-the-art 3D methods also often show suboptimal detection and delineation performance in the subdominant forest layers (see section 3.1).

Whatsoever, methods that can accurately detect both dominant and subdominant trees using high density ALS data are lacking in the literature. In particular One major challenge when using ITD is the under-detection of smaller trees [23]. Thus, here we present an automatic technique that can: a) detect and delineate both dominant and subdominant tree crowns in multistoried coniferous forest with minimal omission and commission errors, and b) accurately estimate the DBH. The proposed method uses both layer-wise 2D and volumetric 3D information in the ALS data to detect and delineate

trees.

4.2 Proposed Tree Detection and Delineation Method

In this chapter, we propose a novel method for detecting and delineating both dominant and subdominant trees in a multistoried coniferous forest by combining 2D and 3D information derived from ALS data. Here, the focus is on coniferous forests as: 1) they constitute close to 80% of the European forest and 2) they are important from both economic and ecological point of view. 3D candidiate tree crowns are extracted from the point cloud based on CHM segment boundaries extracted using a state-of-the-art technique. We reasonably assume that each 3D segment (which is henceforth referred as the 3D candidate segment) contains one dominant tree crown only, however, may contain a number of subdominant tree crowns. All LiDAR points in a 3D candidate segment are then projected onto a novel 3D Euclidean space, where detection and delineation of dominant and subdominant tree crowns are performed. The high level block scheme of the proposed method is shown in Fig. 4.2.

4.2.1 CHM Segmentation

Let $P = \{p_i \in R^3, i = 1, 2, ..., N\}$ be the set of N LiDAR points in the input point cloud. $T_{CHM} = \{t_j \in R^3, j = 1, 2, ..., T\}$ is the set of 3D tree top locations, where T is the total number of tree tops detected by the level set method [61] applied to the CHM. Segmentation is performed on the CHM by using the marker-controlled compact watershed algorithm [170] with T_{CHM} as seeds. The compactness of segments is controlled using $q \in [0, \text{inf}]$ [170]. Each CHM segment $C_i (i = 1, 2, 3..., T)$ corresponds to the 2D boundaries of a 3D candidate segment with one dominant tree and $S_i (i = 0, 1, 2, 3..., S)$ possible subdominant trees. The section of the 3D point cloud corresponding to individual CHM segments (i.e., 3D candidate segment) is extracted and analysed for: a) detecting the S_i subdominant tree crowns, and b) accurately delineating the dominant, and the S_i subdominant tree crowns.

4.2.2 Data Projection

Analyzing the 3D candidate segments to accurately detect and delineate tree crowns in the original 3D Euclidean space is challenging as: a) the subdominant trees have smaller crowns, and are often close to the dominant ones, thus making it difficult to identify and delineate them; b) there is no or minimal difference in the crown-structural/volumetric-textural properties of a dominant tree and any proximal subdominant one; This makes it

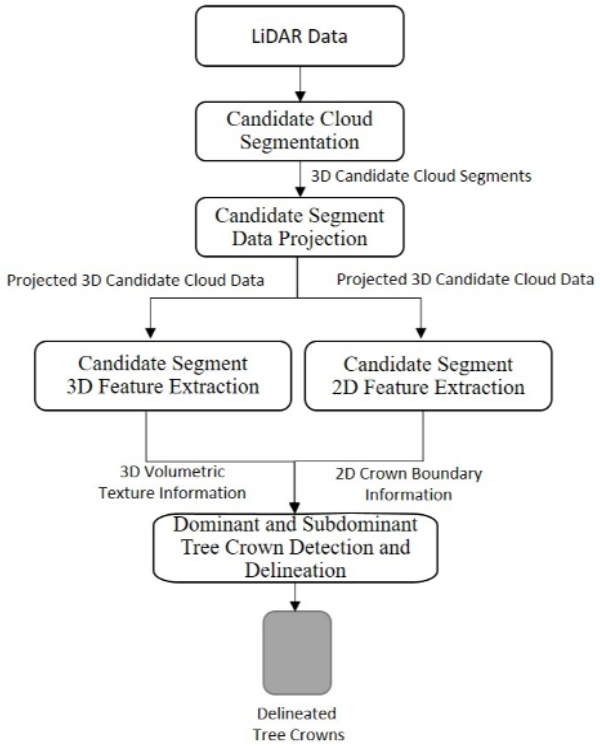

Figure 4.2: Block scheme of the proposed crown detection and delineation approach.

difficult to directly distinguish them using structural information in LiDAR data. Thus, we develop a technique that transforms the 3D candidate segment such that: a) smaller trees in it can be detected independently on their size and/or proximity to the dominant one; and b) a volumetric structure/textural modification is induced on the dominant tree crown without affecting its local branch structure, and any subdominant tree structure.

For each 3D candidate segment, we consider the neighborhood spanned by a cylinder with the axis along the dominant tree stem direction, and the radius r as the distance of the point farthest from the stem axis, and measured in a direction perpendicular to it. Here, the dominant tree stem is assumed to be vertically below the highest point $p_v = [x_v, y_v, z_v]$ in the 3D candidate segment. Any LiDAR point $p_i = [x_i, y_i, z_i]$ within the cylinder can then be uniquely projected into the novel space, spanned by the basis variables d, l, and z, using the projection equations (4.1), (4.2), and (4.3), which are designed to satisfy the transformation requirements.

$$d = \sqrt{(x_v - x_i)^2 + (y_v - y_i)^2} \tag{4.1}$$

$$l = 2\pi r\theta \tag{4.2}$$

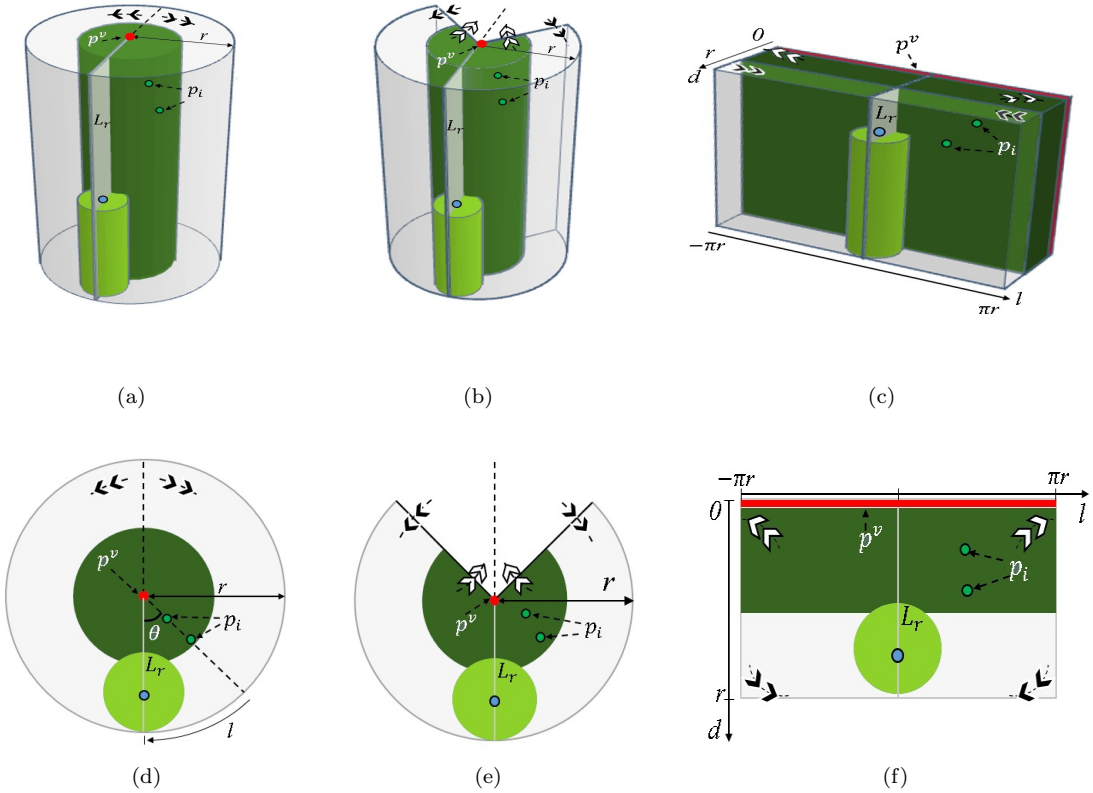

Figure 4.3: Perspective and top view of solid cylinder placement on the original point cloud space (a,d), cylinder roll-out (b,e), and projected space (c,f).

$$z = z \tag{4.3}$$

where, $\{x_v,y_v\}$ and $\{x_i,y_i\}$ are the set of horizontal spatial coordinates of p_v and p_i, respectively. Here, d is the shortest distance between a LiDAR point p_i and the stem, l is the length of the arc with radius r, θ is the smallest angle between the p_i and the reference plane L_r and z is the height of a point from the X-Y plane [171]. Interestingly, the transformation is equivalent to rolling out the space inside a solid cylinder into a cuboidal space (Fig. 4.3). It is worth noting that the transformation increases the distance between a pair of points (i.e., stretches the space) nearer to the axis of the cylinder, than to those located farther away from the axis. The amount of stretching is controlled by r; a larger r causes more stretching than a smaller r. In the case of conifers, branches grow outward from the central stem in directions nearly perpendicular to it. Thus, when the opening is performed along the stem of the dominant conifer, the section of every branch closer to the stem are pulled apart more than the section further away (see Fig. 4.3a-4.3c). It is worth mentioning that, in the projected space, the branches seem to emerge from a plane rather

than a line (i.e., stem). This adds up as an advantage of the projection, allowing the entire 3D candidate segment to be visualized and analyzed from a single-point perspective (Fig. 4.3c).

In the proposed transformation, the negative direction of L_r decides the vertical section where the cylinder is opened. L_r is selected such that it does not cross any subdominant tree crown. This is because any subdominant tree with part of the crown falling on either side of L_r (in the original space) is ripped apart to the either side of the rectangular cuboid (in the projected space). This undesirable situation leads to overestimation of subdominant tree count, hence reducing the crown delineation performance. Accordingly, we propose a Principal Component Analysis (PCA) based method which uses only the x and y components of the data for identifying the optimal reference plane direction. The assumption here is that conifers have a near-symmetrical crown, i.e., the spread of crown around the stem is near-symmetrical. However, the presence of subdominant trees disrupts this symmetry, and results in: a) data points further away from the main crown; and b) localized increase of point density (due to greater biomass per unit volume). In both the symmetry disrupting situations, the first principal component ($PC1$) is directed towards the subdominant trees, while the second principal component ($PC2$) points in an orthogonal direction. We choose L_r to be in the direction opposite to the resultant of PC1 and PC2, as it is very unlikely for that plane to pass through any of the subdominant tree point cloud even in complex situations where more than one subdominant tree exists in a 3D candidate segment. Fig. 4.4a shows an ideal 3D candidate segment containing one subdominant tree while Fig. 4.4e shows four subdominant trees near the dominant one. It can be observed that opening the point cloud along L_r derived as above, does not divide/rip apart the subdominant tree, in both the situations.

We also use the PCA analysis for detecting the presence of subdominant trees in a 3D candidate segment (as some 3D candidate segments may not have subdominant trees.) Let d_{min} and d_{max} be the distance of the points in the cloud that is maximally away from the stem in the direction of L_r and PC1, respectively. We identify these points by: a) fitting a maximally compact 2D convex hull on the x and y coordinate data of the point cloud, and b) finding the boundary points that are closest to, the line connecting the treetop point and its intersection in the convex hull boundary (in the respective direction). We consider the ratio of $\frac{d_{min}}{d_{max}}$ as an indicator of the presence of subdominant trees. A ratio close to 1 means that the distances in the two directions are similar, and hence the absence of a subdominant tree is assumed. Smaller ratios mean that the distances in the two directions are highly unequal, and hence refers to the presence of subdominant trees in the direction of PC1. Further analysis using data transformation is performed on 3D candidate segments for which the presence of subdominant trees

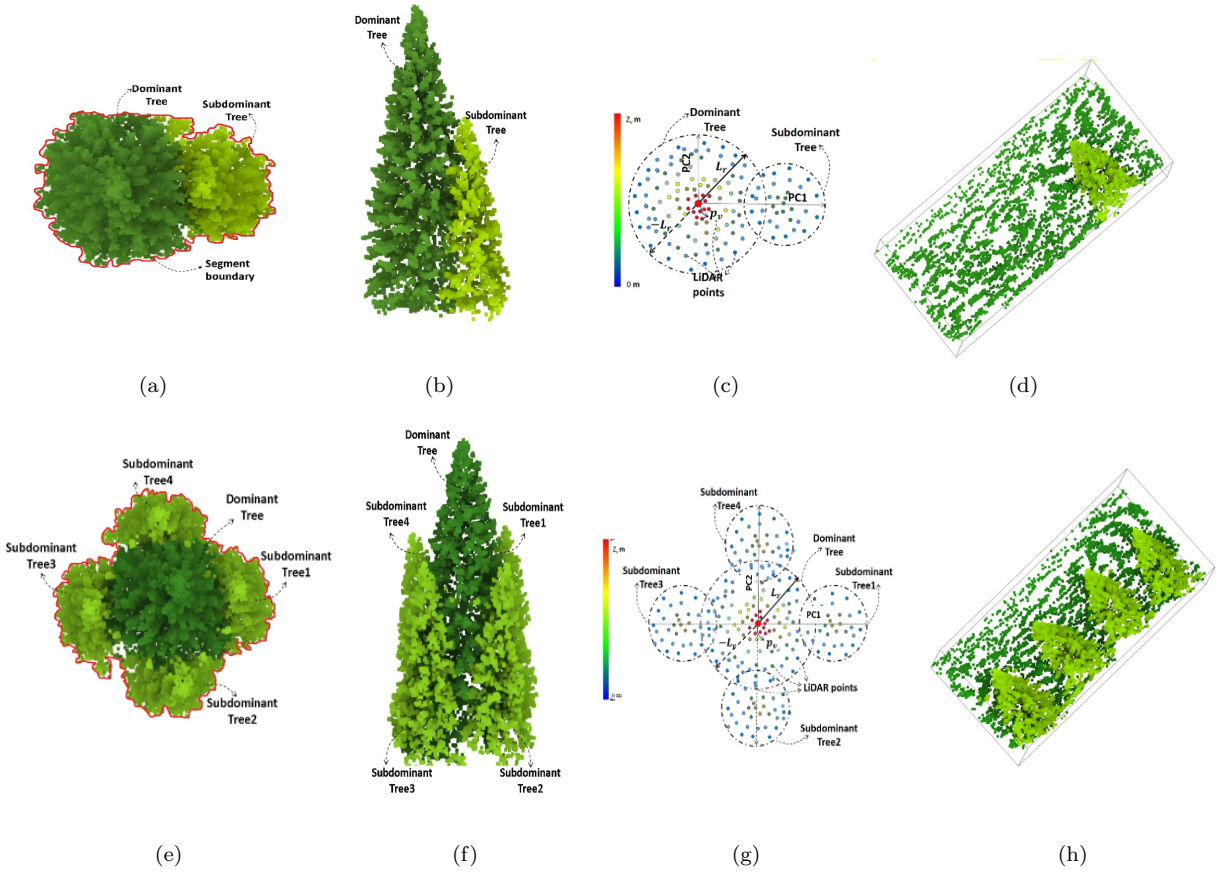

Figure 4.4: Subdominant tree growth scenarios: (a,e) the top view, (b,f) the side view, (c,g) the reference plane direction estimation, and (d,h) the projected point cloud. Cases with one (simple case), and four (complex case) subdominant trees are illustrated.

is detected. The data transformation is advantageous for differentiating the dominant from subdominant tree crowns as it: a) deforms mostly the shape of the dominant tree crown, while maintaining the local crown structure; b) does not (or minimally) deforms the subdominant tree crowns; and c) allows observing the points associated with all the dominant tree branches from a single-point perspective. Fig. 4.4 shows the original and projected 3D data corresponding to an example candidate tree CHM segment, for simple (i.e., with 1 subdominant tree) and complex (i.e., with 4 subdominant trees) situations. The red boundary line in Fig. 4.4a,4.4e represents the CHM segment boundaries.

4.2.3 Candidate Segment 3D Feature Extraction

We perform the texture analysis in the transformed space at the voxel level, where the optimal voxel size is obtained by using a semivariogram analysis. The sill location in

a semivariogram corresponds to the distance beyond which the correlation is minimum, and hence the distance at the sill is taken as the optimal voxel dimension. It is worth recalling here that the projection operation is equivalent to rolling out the space inside a solid cylinder (enclosing the 3D candidate segment data) placed along the stem of the dominant tree (Fig. 4.3). It should be noted that the intermediate stage (Fig. 5.1b,4.3e) is shown only to help visualize the spatial relationship between the initial and final states of the data. The rolling out affects mostly the dominant tree data, while the structure of subdominant trees is preserved. In the projected space, the branches of the dominant tree appear to grown straight up from the background plane, while the subdominant trees have their branches growing out from the respective stem locations. This induces a change in volumetric texture properties of the dominant tree crown, while maintaining the texture of the subdominant tree crowns. We exploit this variation in texture properties to delineate dominant and subdominant trees in the projected point cloud data.

In this chapter, we use the Grey Level Co-occurrence Matrix (GLCM) texture features calculated on the number of points in each voxel. By considering the number of voxel-pairs with similar point count in a particular direction and within a fixed neighborhood, 3D GLCM is derived and used to extract voxel-level texture information. Hence, for every voxel cell and a direction, a GLCM matrix is generated. Branches in the projected space often have slightly different vertical and horizontal tilts, resulting in directional variation in the local structure/texture. Thus, we derive GLCM matrices for 13 different directions, and averaged element-wise to get a single GLCM matrix [172]. In order to quantify texture variations from each averaged GLCM matrix, four Haralick texture features including energy, correlation, contrast, and homogeneity are calculated [173]. Although the feature extraction can also be performed on GLCM matrices generated with different neighborhood size and voxel distance, we restrict our analysis to the first order neighborhood and unit distance, respectively.

4.2.4 Candidate Segment 2D Feature Extraction and Boundary Detection

The l and z dimensions of each data point provide information about its position with respect to L_r, while d gives information about the distance of a point from the dominant tree stem. A 2D representation of the spatial variation in d on the $l-z$ plane helps to detect and delineate dominant and subdominant trees. The 3D data can be converted to a 2D representation by forming a square grid which spans the $l-z$ plane, and assigning values to each grid cell by selecting the largest d value falling within the respective cell. The grid size is chosen to be the same as that of the semivariogram. We refer to the 2D representation as the Candidate Segment Surface Model (CSSM), as it essentially models the spatial variation of the maximum d values in the projected data. It is worth

noting that the CSSM generation process is similar to that of the forest CHM in the original point cloud space, where the points with the maximum d values in each grid determine the exterior crown boundary instead. In general subdominant tree crowns, and thus the corresponding data points, exist farther from the stem of the dominant tree. As a result, the sections of CSSM representing the subdominant tree crowns have relatively larger d values compared to the dominant crown sections (Fig. 4.4d, and 4.4h). The presence of subdominant trees often results in an increase in biomass volume (due to leaves, branches, and stem) and in turn causes a local increase in LiDAR point density. It is worth recollecting here that the subdominant tree point cloud within the 3D candidate segment mostly remains unaffected by the projection, while the dominant tree point cloud (within the 3D candidate segment) is rolled out along its stem axis. As a result, the point density of the region spanned by dominant tree crown in the (l-z) plane is lowered by approximately half, while the density of the subdominant tree remains unaffected (Fig. 4.4b, and 4.4d). By using the number of LiDAR points (rather than the largest d within a grid) as the selected parameter, one can generate the Candidate Segment Density Model (CSDM).

We detect subdominant trees crown boundary by performing the simple k-means segmentation on the Gaussian smoothed candidate segment features. The number of clusters is set to 2 to extract the dominant, and the subdominant crown segments. We identify the foreground cluster (which represents the subdominant crowns) based on the mean values of pixels belonging to the cluster in the CSSM and CDSM. A larger mean value is found in the cluster containing the subdominant tree(s), and is selected as the foreground cluster. Each foreground segment boundary closely follows the subdominant tree crown boundary in the $l-z$ plane. For each segment boundary the local maximum in its upper half corresponds to the subdominant tree top, while the maximum extent of the segment along the l axis represents the maximum crown radius. Sometimes the segments of multiple subdominant trees merge due to crown proximity, creating a merged segment. However, in any case, the merge happens mostly below a certain crown height (due to the tapered-top characteristic shape of conifers), hence creating a local minimum between two local maxima. In these situations, the position of the local minima on either side of the local maximum determines the crown span. We implement this analysis by: a) identifying the upper half (along z) of the boundary segment, and assigning minimum values to remaining sections along l not spanned by the segment boundary; b) fitting a curve passing through all the upper envelope points; and c) detecting the local maximum/maxima and local minimum/minima of the fitted curve. This information about the position of the local maximum combined with the two local minima on its both sides, is used to create an approximate shape of the subdominant tree. In our case, we use an elliptical shape,

as it can model tree crowns effectively. The major axis length (a_e) and minor axis length (b_e) of the ellipse are assumed to be the local maximum height (i.e., the subdominant tree height), and the horizontal distance between the local minima on either sides of the local maximum (i.e., the subdominant tree crown width). The center of the ellipse is placed at half the height of a local maximum. The ellipse is used as an input to accurate detection and delineation of the 3D tree crown.

4.2.5 Dominant and Subdominant Tree Crown Detection and Delineation

We achieve crown delineation in the projected 3D space by performing segmentation of the voxels based on the texture properties. The segmentation is performed on the so-called multispectral scalar image which is obtained by pixel by pixel averaging of the gradient image obtained against the individual texture features [174]. Whatsoever, the point density within the tree crown in the original space decreases from the exterior of the crown towards the stem, and also from the top of the crown towards the bottom. Consequently, in the projected space, the point density decreases in the direction of the positive d axis and decreases in the direction of decreasing z axis. In other words, the point density varies within a tree crown. This can affect the performance of most volumetric segmentation (i.e., 3D segmentation) techniques. However, the point density variation within a horizontal layer along d is small. Thus, we perform segmentation on the interpolated image of the layer-wise texture data. The number of layers along d is defined by the voxel size.

All voxels whose centers are located below a threshold $d_t = \frac{d_{min}r}{d_{max}}$ belong to the dominant crown, While the remaining voxels contain the subdominant crown(s). Individual subdominant crown(s) is extracted at the voxel level by stacking the group of all structurally similar voxel cells from different d layers. For each tree, segments from all d layers that has the major portion of its area falling within the respective elliptical boundary (derived from 2D analysis of candidate segment in Sec. 4.2.4) are stacked. We perform multivariate marker-controlled watershed algorithm [174] on interpolated texture feature maps to identify such segments in individual d layers. A spatial Gaussian filtering is applied to each texture layer in order to smoothen out any local irregularity and to avoid oversegmentation. The stacked voxel segments define the 3D crown of the subdominant tree(s) in the projected space. Every data point inside the projected segment is then assigned to one of the voxel cells, based on the proximity of a point to the center of a voxel cell. The index of points belonging to the individual stacked-voxel segments define the point cloud of a tree in the original space. Any unassigned point is assigned to one of the tree cloud segments based on proximity.

However, CHM based segmentation may result in a subdominant tree crown being split

between 3D candidate segments (Fig. 4.5a) (i.e., section of the subdominant tree crown is allocated to different proximal 3D candidate segments) and hence will be detected and delineated as separate trees in the respective 3D candidate segments (Fig. 4.5b). This results in an overestimation of subdominant tree count, and an underestimation of the crown size. To address this issue, we merge subdominant tree clusters if they have: a) similar crown boundary parameters on data points in the G most external d slices of the 3D candidate segment. These are the ones corresponding to the largest d values. Here we consider $G = 2$ to include enough points for crown segment boundary estimation (i.e., $\cup(d_D, d_{D-1})$ (Fig. 4.5c). Elliptical crown boundary parameters a_e and b_e are calculated as in section 4.2.4 and used for similarity estimation; and b) the Euclidean distance p_S^t between the highest point in the respective slices is small. For each subdominant tree cluster, we represent these parameter values as a 3D vector $t_d = [a_e\ b_e\ p_s^t]$. Clusters pairs with the Euclidean difference between corresponding t_d vectors less than a threshold are merged. It is worth noting that the proposed split-crown merging technique works also for complex situations where a crown is split into more than two parts.

We consider the horizontal position of the highest point in the delineated point cloud as the location of the tree. The maximum radius of a delineated crown is calculated as the perpendicular distance of the point that is maximally away from the line connecting the highest point in the subdominant tree segment and its projection on the ground.

4.3 Experiments and Results

4.3.1 Study Area and Dataset

The study area is a multistoried coniferous forest in the southern Italian Alps, in the municipality of Pellizzano located in the Trentino region in Italy. The altitude of this mountainous terrain ranges from 900 m to 2000m above sea level. The area has an extent of 3200 ha with the geographic center point of $46^0 17' 31.00''$ N and $10^0 45' 56.49''$ E. High density ALS data were acquired between 7th and 9th of September 2012 using a Riegl MS-Q680 sensor. The acquisition was performed from an airborne platform flying at an average height of 660m above ground level with a speed of around 180km/hr. The pulse repetition frequency was 400 KHz and recorded a maximum of four returns for each laser pulse fired. The major tree species include the Norway Spruce (Picea abies), the European Larch (Larix decidua), and the Silver Fir (Abies alba).

The experiments were conducted on a set of 6 plots (Fig. 4.6) containing both dominant and subdominant trees. The radius of each plot is 25m. The plot centers were measured using a survey grade differential GPS, which provided a root mean square error of 0.25m in a separate validation. The position of trees within a plot was measured with respect

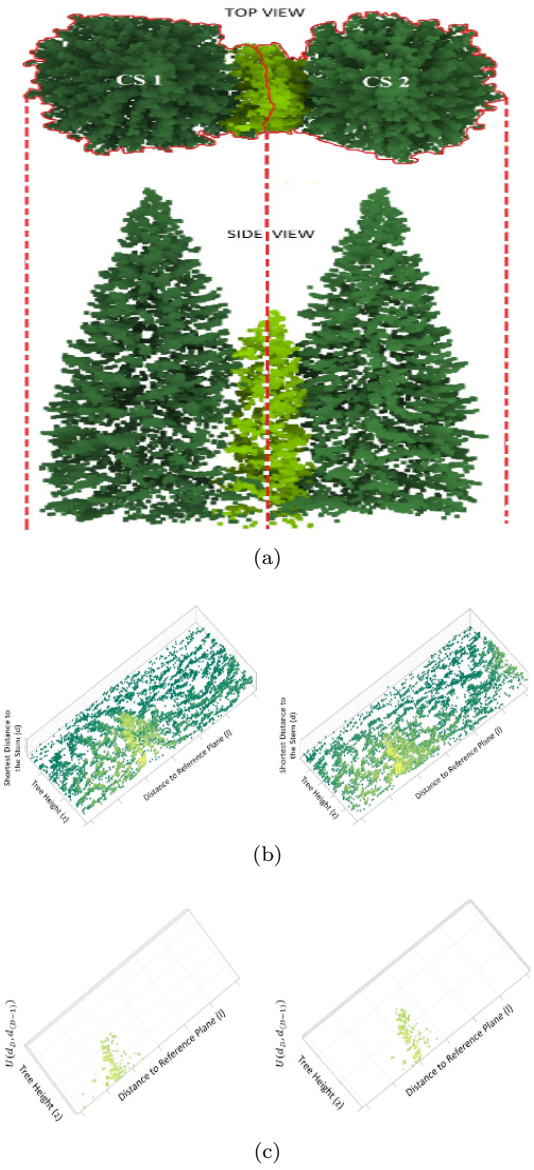

(a)

(b)

(c)

Figure 4.5: (a) Top and side view of two proximal 3D candidate segments (CS1 and CS2) with a split subdominant tree crown, and (b) shows the corresponding projected 3D candidate segment, and (c) $\cup(d_D, d_{D-1})$.

to the center of the plot using an ultrasound instrument with high measurement accuracy of 0.25m. The height, the DBH (at 1.3m above the ground), and the species are also available from an in situ survey. Basic statistics of the DBH and the crown radius, for individual plots are given in Table 4.1. The height of individual trees was estimated using regression models (4.4) based on a set of reference trees for which height is also known.

$$h_i = \alpha_0 + \alpha_1 ln(DBH_i) + \epsilon \tag{4.4}$$

where h_i is the height of i^{th} tree, DBH_i is the DBH of the i^{th} tree, and ϵ is the error term in the regression function. The α_0 and α_1 are regression parameters [88]. Regression models were derived for each species in the dataset separately. The estimated height is used for correcting/rectifying the positional errors of trees [175]. Each delineated tree i derived using the proposed and the state-of-the-art method is linked to a tree j in the reference data based on the distance d_{ij} obtained using (4.5). For the case with multiple trees satisfying the distance criteria, the most proximal tree is linked to the reference data. Only clusters which fall completely within the boundary of the plot are included for the validation. However, a few trees near the plot boundary which satisfy the inclusion condition are not used in the validation due to lack of field data, i.e., such cases counted to a total of seven trees.

$$d_{ij} = \sqrt{(r_{xy}^2 + (r_z/3)^2)} \tag{4.5}$$

where the r_z is the vertical distance, and r_{xy} is the horizontal distance between the highest point in the delineated tree i and the nearest reference tree j. A delineated tree is linked to a reference tree only if d_{ij} is less than 1.5m + $2DBH$, in order to allow for positioning and height errors or else is considered as a Commission Error (CE) [88]. The DBH estimation for every tree is performed using the model (4.6) that employs the tree height and the crown diameter as the independent variables.

$$DBH_i = f(b_0 + b_1\sqrt{h_i} + b_2\sqrt{d_i})^2 + var(\epsilon) \tag{4.6}$$

where DBH_i is the estimated DBH (in millimeter) of the i^{th} tree, and h_i and d_i are the tree height (in decimeter) and the crown diameter (in decimeter), respectively. The b_0, b_1 and b_2 are model parameters. The coefficients of the model used for Norway Spruce are $b_0 = -3.524$, $b_1 = 0.729$ and $b_2 = 1.345$, whereas for other species the model coefficients are $b_0 = -3.733$, $b_1 = 0.807$, and $b_2 = 1.144$ [176]. As non-linear transformations were used for the dependent variables, the DBH estimates will be biased, and the effect is mitigated by bias correction [177]. The attenuation bias (due to crown diameter measurement errors) associated with the Norway Spruce model and other species models are negligible, and are observed to be -0.065 and -0.072, respectively.

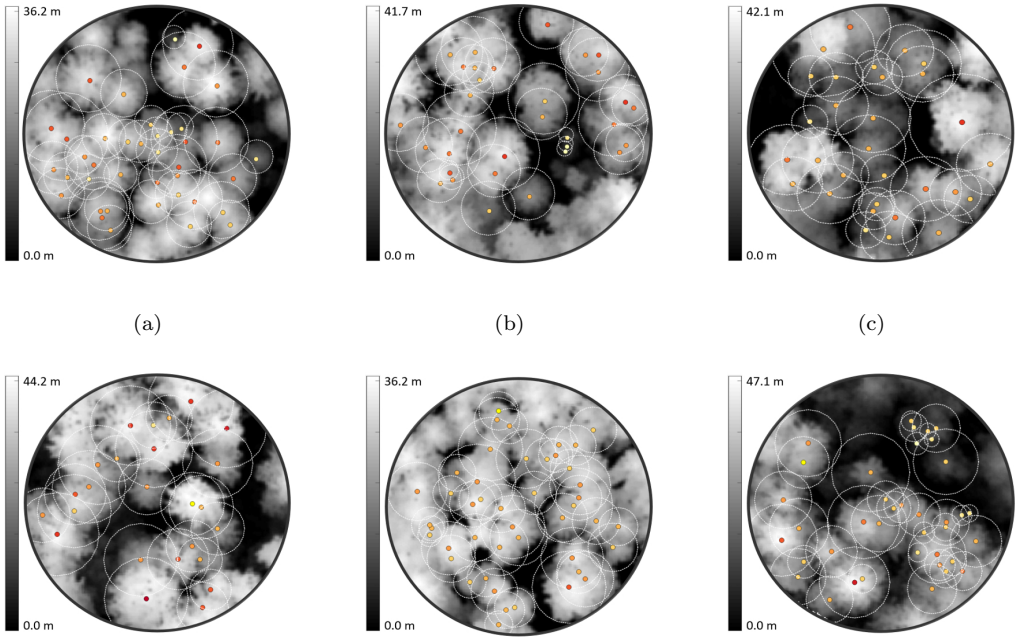

Figure 4.6: (a)-(f) High density LiDAR data CHM representations of the plots with individual tree tops (in red) and respective maximum crown extents (white dotted circles). The points represent the crown center, and is colored based on the DBH value. Small to large DBHs are represented in shades from yellow to red.

Table 4.1: Statistics of the structural characteristics of the trees in the dataset considered for automatic segmentation.

Plot	**#Trees**	**DBH (cm)**		**Crown Radius (m)**	
		Range	**Mean**	**Range**	**Mean**
H1	40	9.0 - 76.0	39.6	1.3 - 7.0	3.7
H2	32	9.0 - 78.0	44.0	2.0 - 7.5	5.2
H3	30	16.0 - 77.0	35.5	2.6 - 7.8	4.4
H4	25	20.0 - 92.0	53.4	3.7 - 7.7	5.8
H5	45	25.0 - 67.0	35.1	2.1 - 6.9	4.2
H6	38	9.1 - 81.0	33.6	1.3 - 6.8	3.6

4.3.2 Experimental Results and Discussion

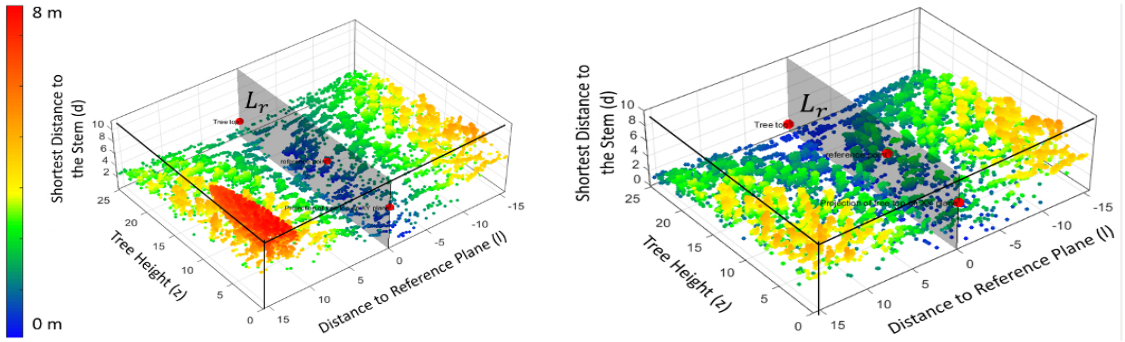

(a) (b)

Figure 4.7: Projected point cloud of a 3D candidate tree segment: a) with a subdominant tree, and b) without any subdominant tree.

The performance quantification was conducted on the six plots to investigate the operational effectiveness of the proposed method. The dominant tree tops detected using the level set algorithm are used as the markers for the marker-controlled compact watershed segmentation on CHM, which in turn is used to delineate 3D candidate segments. The compactness parameter q is set to 1 as it was found to be optimal for minimizing the over-segmentation errors [170]. The spatial resolution of the CHM was chosen on the basis of the average number of LiDAR points/m^2, while the 2D Gaussian filter parameters were tuned to minimize false peaks in the CHM. In our case, the CHM resolution and the Gaussian filter size are selected to be 0.25 and 5 x 5, respectively. Fig. 4.8 shows the watershed segments for plot H1. The watershed segment boundaries are used to generate the 3D candidate segments, i.e., all points within a CHM boundary are assigned to the respective segment. However, CHM smoothening results in points to remain unassigned near/outside the CHM boundaries. Thus, unassigned points are assigned to the nearest candidate segment. Fig. 4.10 shows the candidate tree segments for four scenarios with one, and four subdominant trees, respectively. Each candidate data segment is then projected into the proposed space to detect subdominant trees. Fig. 4.7a and Fig. 4.7b show the 3D visualization of the projected data with and without a subdominant tree, respectively. Here, large d values associated with the subdominant trees are shown in shades of red, while the low values correspond to the background/dominant tree crown points, and appears in shades of yellow and green.

The projected space is divided into voxels. The optimal voxel size is obtained against the range of an exponentially fitted semivariogram. However, the range is set to 0.5m for

the case in which semivariance does not saturate. Fig. 4.11(a-d) show the projected point cloud of dominant segments with one, two, three and four subdominant trees, respectively. For each projected segment, the CSM is computed on the d values (Fig. 4.12). The crown of subdominant trees maximally stretches along the z direction (i.e., along the height of the tree). We exploit these characteristics to minimize the local variation of d in the $l - z$ plane, and reduce false peak detection, by using a rectangular spatial filter with the longer side along the z axis. For our dataset, the 6 x 3 rectangular Gaussian filter with $\sigma = 1$ was found to optimal in removing false peaks caused due to locally protruding branch points. The location of a subdominant tree top (red dots in Fig. 4.13) combined with the nearest valley points on its either (blue dots in Fig. 4.13) side are used to define the boundary of the subdominant tree. Fig. 4.14 shows the elliptical boundaries of the subdominant crowns detected in the projected space for cases with one, two, three, and four trees.

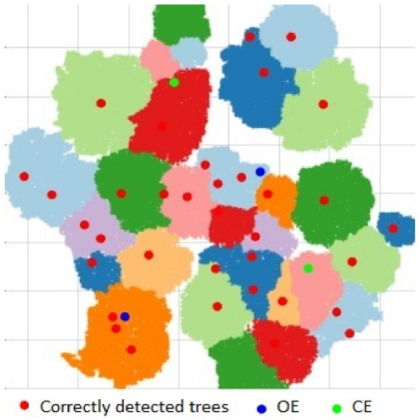

Figure 4.8: The candidate tree segments for the plot H1 are shown as color-filled polygons.

The delineation of subdominant tree crowns is performed by exploiting the tree top location, and the 2D crown boundary information modeled from the CSM using the ellipse. The projected space is divided into d_{max}/v voxel layers, where d_{max} is the maximum d value of points in P, and v is the voxel size derived using the semivariogram. Texture segmentation of each voxel slice/layer is done using a marker-controlled watershed algorithm as: a) it allows detecting spatially confined and homogeneous local segments even in the presence of large variance in the data, b) the situation is similar to the case of crown segmentation in a CHM (for which it is largely used), and c) it is simple. Here, the gradient magnitude is used as the segmentation function, the foreground markers are obtained by using the opening-by-reconstruction and the closing-by-reconstruction morphological operations, and the background markers are obtained by considering the watershed ridge lines obtained from the binarization (using Otsu's method [178]) of the

original image with the foreground markers superimposed. All segments falling to the subdominant voxel layers and within the respective ellipse are separately stacked to identify the 3D subdominant crown segment(s). Fig. 4.15 shows the voxel layer segments stacked together to obtain the 3D crown segment of subdominant trees for different subdominant growth situations. All voxel layer interpolated texture feature maps are separately smoothened using the rectangular Gaussian filter with $\sigma = 1$. Point cloud segment of the subdominant tree(s) are obtained by identifying the projected points contained by the 3D voxel set. The mapping to the original space is done using a unique index that is assigned to every data point. Subdominant tree clusters with $t_d < 1.8$ are merged into a single cluster. The value of t_d was obtained using the trial and error method. The objective here was to minimize CE for a set of manually selected 3D candidate segments in the 6 plots for which subdominant crown split occurred.

We compared the proposed method with a point cloud based tree detection and delineation technique, henceforth referred to as the SoA method [18]. The method uses level set analysis on CHM to detect dominant tree apexes, and perform an angular analysis around them to delineate individual crown boundaries. The crown boundary for a tree is derived based on the first local minimum detected on the angular sectors considered around the apex. Further, a sector-wise analysis is performed on the delineated 3D dominant tree segments to detect and delineate any subdominant crown [18]. The dominant and subdominant trees were detected and delineated by employing angular sector-splits of 4 and 8, respectively. The quantization steps for vertical profile analysis is set to 29, and was estimated using the method in [18].

Table 4.2 shows the detection accuracies obtained by the proposed method, and the SoA method, for the six sample plots. The proposed method improves the overall detection accuracies by around 5% when compared to the SoA method. The overall accuracy of the proposed tree detection method varies from 88.0% to 96.8% for the six automatically segmented plots. The better performance of the proposed method can be mainly attributed to the projection technique which selectively induces a structural change in dominant tree cloud, thus improving the separability between the dominant and the subdominant cloud segments. This possibility is lacking in the SoA method which is based on a more complex sector-wise analysis that tends to result in tree crown being shared between 3D candidate segments. Thus, the algorithm will identify part of the subdominant crowns in each candidate segment, (and detect it as separate trees) resulting in larger CE (see table 4.2). Whereas, the proposed method minimizes the crown splits by suitably selecting the direction of the reference plane in the projection. The proposed method performs the crown detection analysis in the 3D space, rather than on a projected 2D space as it is the case with the SoA method. Thus it allows the maximum exploration

of the structural information in the ALS data. For this reason the method can better detect small subdominant trees which are lost when using other methods. Hence reducing the Omission Errors (OE). Fig. 4.9 shows the histogram of the detected trees by the range of DBH class. The proposed and the SoA method show similar performance for subdominant trees with DBH greater than 40. However, the proposed method was able to detect a larger number of smaller trees (i.e., with DBH less than or equal to 40), when compared to the SoA method. Whatsoever, the performance on detecting trees with DBH less than 20cm is minimum for both the proposed and the SoA methods. This low performance can is attributed to the low point cloud density in lower forest layers. In any case, the proposed method correctly detected a larger number of trees, which proves its effectiveness.

Table 4.2: DET, CE and OE obtained with the proposed and SoA methods.

Plot ID	**Trees**	**Proposed Method**			**State-of-the-art Method**		
		DET	**CE**	**OE**	**DET**	**CE**	**OE**
H1	40	38 (95.0%)	2 (5.0%)	2 (5.0%)	35 (87.5%)	4 (10.0%)	5 (12.5%)
H2	32	31 (96.8%)	1 (3.0%)	1 (3.0%)	29 (90.0%)	3 (9.3%)	3 (9.3%)
H3	30	27 (90.0%)	2 (6.6%)	3 (10.0%)	28 (93.3%)	4 (13.3%)	2 (6.6%)
H4	25	22 (88.0%)	2 (8.0%)	3 (12.0%)	21 (84.0%)	2 (8.0%)	3 (12.0%)
H5	45	40 (88.8%)	3 (6.6%)	5 (11.1%)	38 (84.4%)	3 (6.6%)	7 (15.5%)
H6	38	36 (94.7%)	3 (7.8%)	2 (5.2%)	33 (86.8%)	4 (10.5%)	5 (13.1%)
Total	210	194 (92.3%)	13 (6.1%)	16 (7.6%)	184 (87.6%)	20 (9.5%)	25 (11.9%)

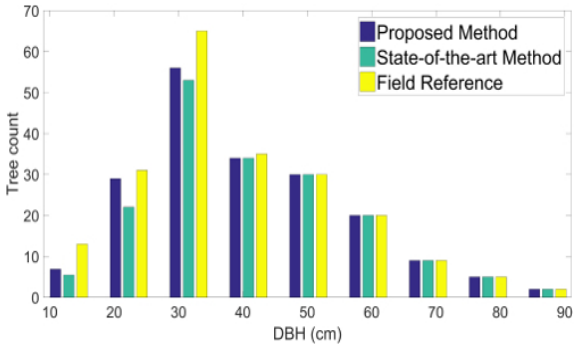

Figure 4.9: Overall detection accuracy obtained on the 6 plots, across different DBH classes.

Fig 4.10 - 4.16 shows the step-wise mechanism for crown delineation performed on 3D candidate segments of various complexities. It can be seen that the algorithm is able to detect both dominant and subdominant trees for simple (1 tree in the 3D candidate

segment) and complex (more than 1 tree in the 3D candidate segment) growth scenarios. The crown delineation performance evaluation was performed on the correctly detected trees. Table. 4.3 shows the Mean Error (ME), the Mean Absolute Error (MAE), and the Mean Squared Error (MSE) of the DBH estimates obtained using the proposed, and the SoA method, on the 6 plots. As expected, the proposed method is able to better estimate the DBH of the trees. However, both the proposed and the SoA method underestimate DBH in average. This can be attributed to the low point density in the subdominant layer, and Gaussian smoothing done on the 2D and 3D features. The relatively lower ME, MAE and RMSE provided to the proposed method confirm the average ability of the proposed technique to mitigate the omission errors. The same analysis have been conducted by dividing the dominant-subdominant pairs in 3 groups of delineation complexity defined in terms of proximity among the trees: Group 1 includes the pairs with dominant-subdominant tree distance in the range 0m - 2.5m; Group 2 includes the ones with distance in 2.5m - 5.0m, and Group 3 is the set with pairs of trees being more than 5.0m far from each other. For both the proposed and the SoA method the DBH estimation error is found to be larger for trees with smaller distance (i.e., the ones in $PL1$). As we move to less complex situations (Groups 1 and 2) the estimation mean error in DBH decreases. Table 4.4 shows the ME, MAE, and RMSE associated with the three groups, for the proposed and the state-of-the-art method. This is in accordance with the fact that the crown delineation accuracy improves as the trees are further away from one another, due to smaller overlap. However, the proposed method performs better in these cases as well by resulting in a ME that is less than half the one provided by the SoA method.

Table 4.3: The ME, the MAE, and the RMSE accuracy of estimated DBH for the proposed and the state-of-the-art method.

Method	**ME**	**MAE**	**RMSE**
Proposed	-0.4 cm	5.5 cm	7.3 cm
SoA	-0.2 cm	5.8 cm	7.9 cm

In general, the proposed approach accepts the reality of underdetection of subdominant trees, and shifts the conceptual analysis from tree object to tree-approximate object referred to as candidate segment. Two major problems with the state-of-the-art methods include the crown overlap and occlusion effect and point density variance. The proposed method mitigates the former problem (i.e., crown overlap) using a novel data projection that facilitates the feature extraction from point cloud segments representing individual trees. The method exploits the slice-wise 2D feature extraction together with the locally extracted 3D voxel level features to address the latter issue in airborne LiDAR data.

Table 4.4: The ME, the MAE, and the RMSE accuracy of estimated DBH for the proposed and the state-of-the-art method by delineation complexity.

Dominant to Subdominant Distance	**Method**	**ME**	**MAE**	**RMSE**
Group 1 (0.0-2.5 m)	Proposed	-0.6 cm	5.8 cm	7.7 cm
	SoA	-0.3 cm	5.9 cm	8.2 cm
Group 2 (2.5-5.0 m)	Proposed	-1.0 cm	5.8 cm	7.5 cm
	SoA	-0.7 cm	6.7 cm	7.9 cm
Group 3 ($>$ 5.0m)	Proposed	-0.2 cm	5.5 cm	5.9 cm
	SoA	-0.2 cm	5.9 cm	6.1 cm

Whatsoever, the candidate segments are extracted using CHM segmentation, and hence error in segmentation at the candidate segment level is propagated in the down-the-lane analysis. For this reason, the method is most optimal for conifer forests which generally gives minimal crown segmentation errors due to the tapered crown shape of conifers, than for temperate or boreal forest with generally more broadleaved trees.

4.4 Conclusion

In this chapter, a novel local projection based tree detection and 3D crown delineation is proposed for high density ALS data. The proposed method detects both dominant and subdominant trees in multistoried conifer forests. 3D candidate segments are first extracted and then separately analyzed in the projected space to detect and delineate both dominant and subdominant trees. The tree crowns are delineated in 3D by exploiting the projection-induced texture variation extracted using GLCM features. The average crown detection accuracies obtained is 92.3% and the RMSE errors associated with the DBH estimates is 7.3cm. Possible future works include leveraging on the intensity information in ALS data, and using datasets with larger point density which include more texture information (e.g., the Terrestrial Laser Scanning data), to improve tree detection and crown delineation. The performance of the method need to be evaluated for boreal and temperate forest in order to study the possibility to generalize the method to the use in forests with various characteristics.

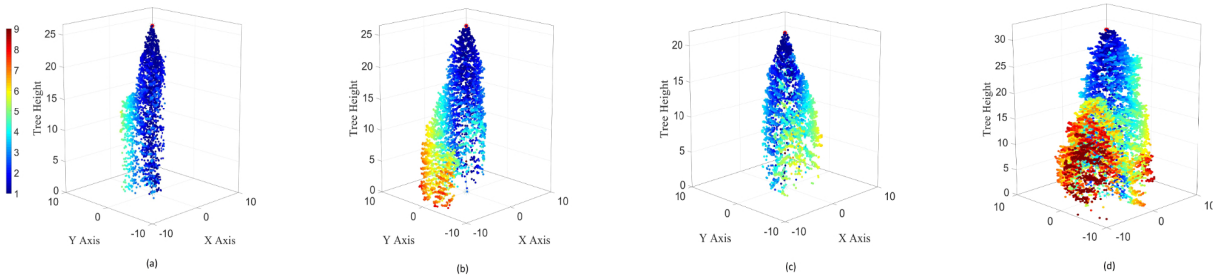

Figure 4.10: Point cloud of 3D candidate segments in the original space with: (a) one, (b) two, (c) three, and (d) four subdominant trees. The colorbar shows the distance of a point to the projection axis.

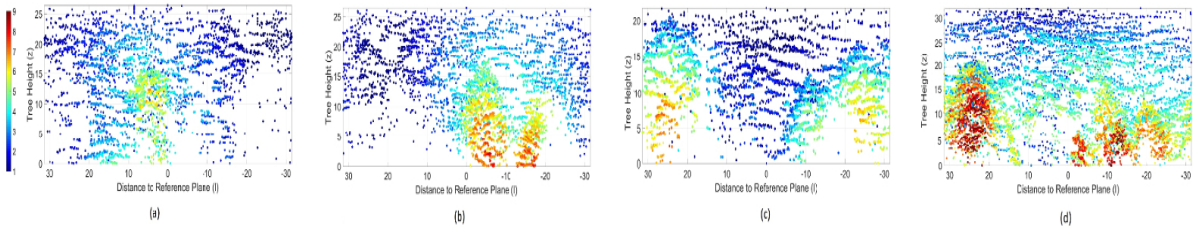

Figure 4.11: Projected point cloud of the 3D candidate segment with: (a) one, (b) two, (c) three, and (d) four subdominant trees.

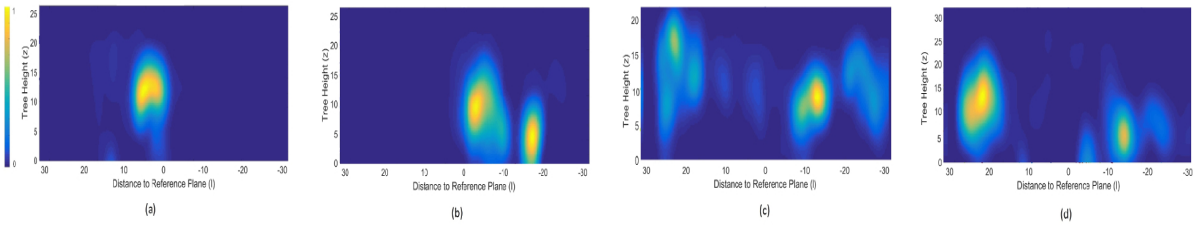

Figure 4.12: The CSSM map derived from the projected 3D candidate segment data with: (a) one, (b) two, (c) three, and (d) four subdominant trees.

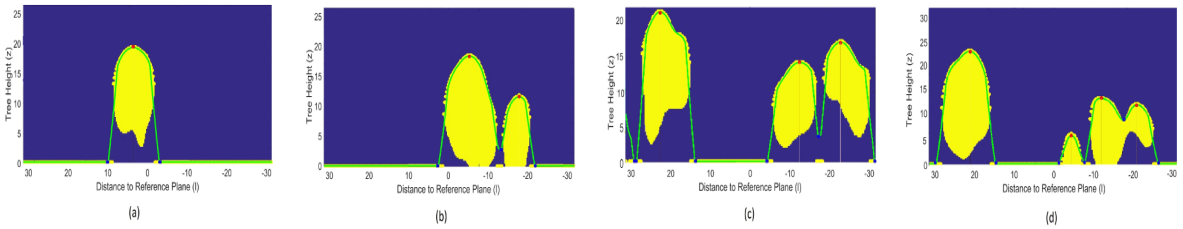

Figure 4.13: The segmented projected 3D candidate segment map with: (a) one, (b) two, (c) three, and (d) four subdominant trees. The local maxima (red dots) and local minima (blue dots) derived from the foreground segment (yellow) are used to define the elliptical boundary.

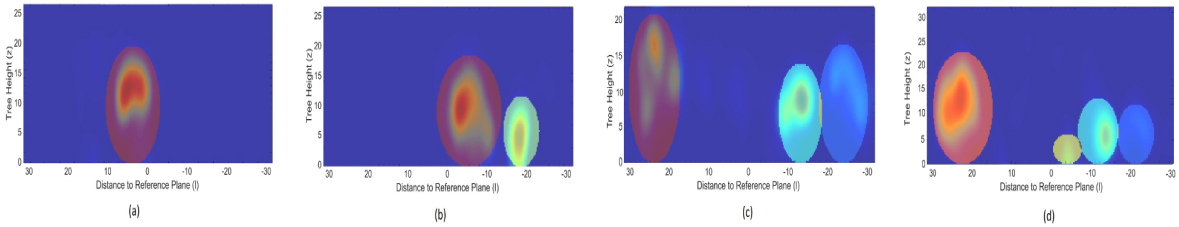

Figure 4.14: Elliptical tree crown boundary obtained on the projected 3D candidate segment map binary images with: (a) one, (b) two, (c) three, and (d) four subdominant trees. The elliptical crown boundaries derived from CSM for subdominant trees are shown in unique colors.

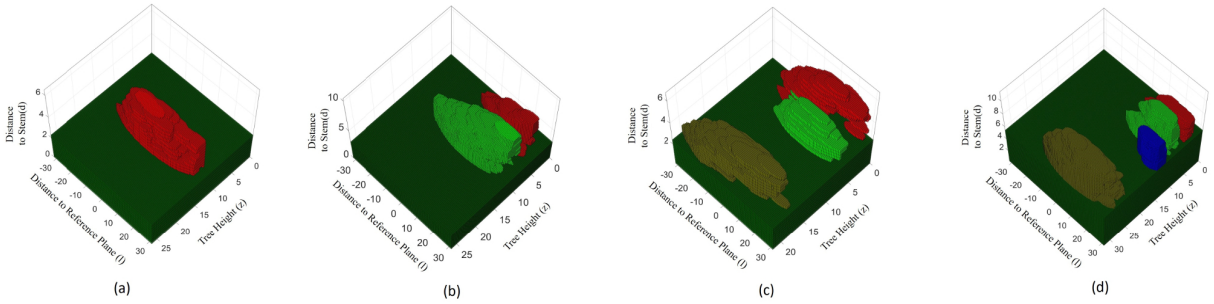

Figure 4.15: Stacked segments from different voxel layers for: (a) one, (b) two, (c) three, and (d) four subdominant trees.

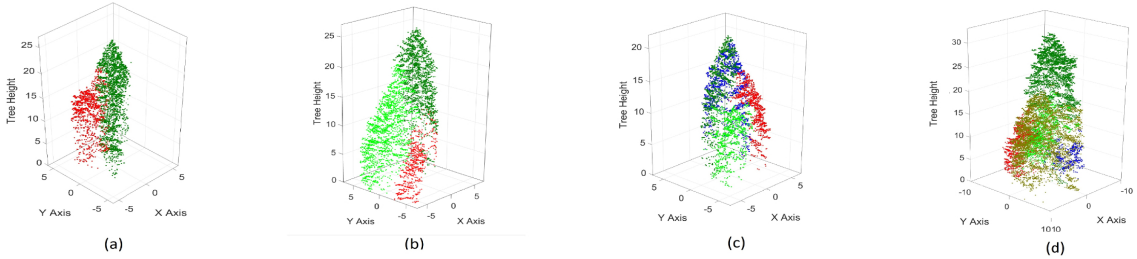

Figure 4.16: The tree point cloud segments for: (a) one, (b) two, (c) three, and (d) four subdominant trees.

Chapter 5

Tree Species Classification using Crown Geometric Information in ALS Data

Tree species information is crucial to precision forest management and related studies. The structural details of the forest vertical profile can reveal key information on tree species. In this chapter, we propose a novel method for conifer species classification based on the use of geometric features describing both the internal and external structure of the crown. The Internal Crown Geometric Features (IGFs) are defined based on a novel internal branch structure model which uses 3D region growing and Principal Component Analysis (PCA) to delineate conifer branches accurately. IGFs are used together with External Crown Geometric Features (EGFs) that capture the overall crown characteristics to perform conifer species classification. Three different Support Vector Machines (SVM) have been considered for classification performance evaluation. The experimental analysis conducted on high density ALS data acquired over a portion of the Trentino region in Italy proves the effectiveness of the proposed method.

5.1 Introduction

Tree species knowledge is fundamental for activities such as ecological [1], biodiversity [179],and climate change studies [180]. Small footprint multi-return airborne LiDAR

Part of the chapter appears in:

1. Harikumar, A., Bovolo, F., and Bruzzone, L., ' An internal crown geometric model for conifer species classification with high density LiDAR data.' , IEEE Transactions on Geoscience and Remote Sensing, Vol. 55, No. 5, pp. 2924 2940, Feb 2017.

scanners (see section 2.4.1) such as the Leica ALS80 and the RIEGL LMS-Q680i, can produce dense point clouds of forest structures. For example, in multi-return mode, the Leica ALS80 can record more than 50 sample/m^2 in a single scanning pass conducted from a height of about 1km and at a ground speed of 100 km/h. Hence data acquired by these systems contain a large amount of information on the tree crown including that of the branches. The large amount of spatial information acquired over forests allows to perform an accurate classification of tree species [181] and to better estimate parameters such as tree height, crown area, and biomass [182]. A review of the literate (section 3.2) confirms that most ALS data based methods are developed for classifying trees belonging to different taxonomical classes [183], [118]. However, methods for identifying the species of a tree belonging to the same taxonomic class (e.g., conifers) are lacking. Accordingly, here we focus on developing an effective technique for extracting crown structural information using small footprint high point density multi-return ALS data. In particular, we focus on conifers as they are very important from an ecological point of view and also dominate the European forests.

In this chapter, we introduce a novel method that utilizes the structural/geometric information present in small footprint high point density multi-return ALS data for identifying the species of a tree belonging to the conifer class (i.e., Pinopsida). Conifer species classification using ALS data is challenging due to the high similarity in their external crown shape (i.e., the external crown characteristics). Concerning the internal crown characteristics (i.e., the branch structure inside crown), conifers have a linear main stem with branches growing outward from the stem, in an approximately linear fashion, almost perpendicular to the stem. The separation between conifer branches increases as we move from the stem toward the external part of the crown. This makes the branches more distinguishable near the exterior of the tree crown (Fig. 5.1). However, each conifer species shows specific stem/branch attributes that makes it different from the others. Accordingly, we developed a robust method that: 1) models the internal structure of a coniferous tree from the ALS data; 2) defines robust, efficient and scale invariant geometric features representing the branch level characteristics of conifers based on the proposed internal crown structure model; 3) demonstrates the relevance of internal crown geometric features; and 4) performs effective conifer species classification. Experimental analysis was conducted on a dataset acquired by an airborne high density ALS system by conducting multiple passes over a study area located in the north west part of the Trentino region in Italy. Validation was concentrated on four major European conifer species, i.e., the Norway Spruce (NS), the European Larch (EL), the Swiss Pine (SP) and the Silver Fir (SF). However, the method can be extended to the classification of other conifer species. In our experiments, linear Sparse C-SVM, non-linear C-SVM, and non-linear multi-kernel

(a) (b) (c) (d)

Figure 5.1: Examples of the four different coniferous species considered in the study; (a) Norway Spruce (Picea Abies), (b) European Larch (Larix Decidua), (c) Swiss Pine (Pinus Cembra), and (d) Silver Fir (Abies Alba).

C-SVM (MK C-SVM) classifiers were used. Linear Sparse C-SVM is used for feature relevance analysis. This is because linear Sparse C-SVM has the capability to assign larger weights (i.e., hyperplane parameters) for relevant features, while smaller weights are assigned to the remaining features. Accuracy assessment was conducted by comparing classification results achieved by the three above mentioned classifiers.

The rest of the chapter is organized as follows. Section 5.2 describes the proposed method to model the internal branch structure and briefly illustrates the theory of SVM classifiers involved in the experiments. Section 5.3 introduces the dataset and the study area, and provides experimental results. Section 5.4 draws the conclusion of this work.

5.2 Conifer Species Crown Structure Characterization and Classification

Here, we propose an effective method for conifer species classification based on the structural properties of conifers derived from small footprint high point density multi-return ALS data. The approach assumes that the LiDAR point clouds corresponding to individual conifer trees have been isolated (see example in Fig. 5.3a). Any method available in the literature (e.g., [184], [185], [186]) can be employed to this purpose. Starting from the individual tree LiDAR point cloud, two sets of crown geometric features are derived that describe the tree crown from two complementary perspectives: i) the external one; and ii) the internal one. The former set includes six External Crown Geometric Features (EGFs) that capture the external behaviours of crown structural characteristic of conifers. The

latter set includes six novel Internal Crown Geometric Features (IGFs) that model the internal behaviour of conifers crown. This is achieved by exploiting the branch structure. The twelve features are used for conifer species classification. In our experiments SVM has been employed to this end with different kernels and architectures [187], [188]. The block scheme of the proposed approach is given in Fig. 5.2.

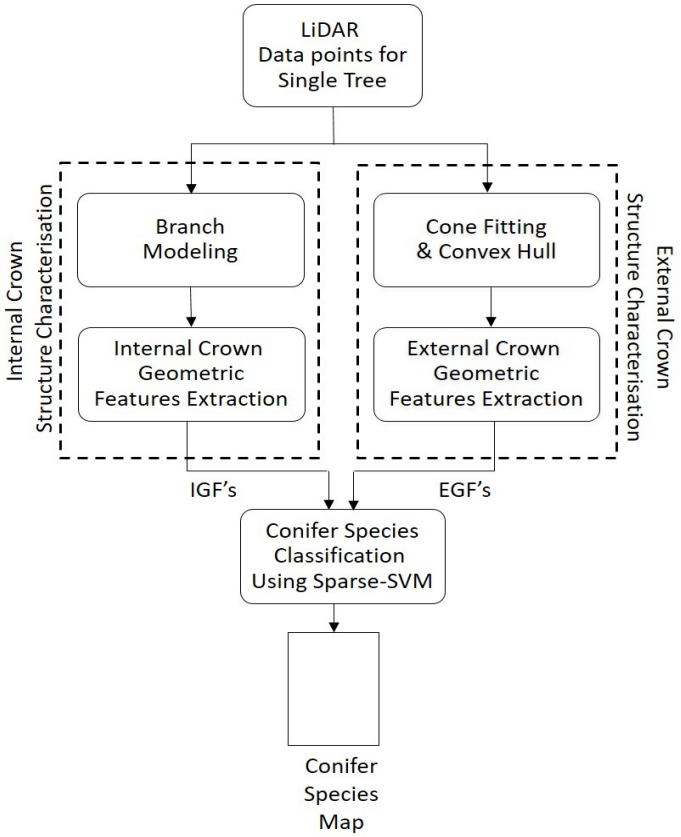

Figure 5.2: Block scheme of the proposed approach to conifer species classification.

5.2.1 Internal Crown Structure Characterization

In order to properly model the internal crown structure of conifers crown, let us observe that: i) conifers have a linear/vertical central stem; ii) branches grow from the stem outward; and iii) branches are linear and compact and have a direction which is almost perpendicular to the stem and reach the maximum distance from each other at branch tips [35]. The internal crown structural characteristics of conifers can be defined by studying the basic branch parameters. [34; 35]. Thus, we propose to identify individual branches of conifers. Conifers have a monopodial growth form (a single, straight trunk with side branches) with strong apical dominance [189], and as a result branches have an

approximately ellipsoidal shape. For this shape, length, width, compactness, density, and symmetry attributes are the basic parameters that can be used to define the structural characteristics of branches, and thus are used in this study.

We have assumed the following notations to describe LiDAR data at the tree level. Let $P = \{p_1, p_2 \ldots, p_N\}$ be the LiDAR point cloud representing a single tree, where $p_n \in P$ is the spatial position of each point belonging to the tree in the small footprint high density multi-return LiDAR cloud. p_n is fully described in a 3D Euclidean feature space by its x_n, y_n and z_n Cartesian coordinates. Let M_T be the central stem and B the total number of branches that constitutes the conifer skeleton. In the LiDAR point cloud of a single tree, each branch can be modeled as a cluster of points (referred to as branch cluster) $c_b = \{p_n; n \in I_b\}$, where I_b is the index set of all the LiDAR points belonging to c_b. The set $C_B = \{c_b, b \in [1, B]\}$ of B branch clusters obtained by grouping LiDAR points in P represents the entire conifer tree crown. It is worth noting that the laser sampling can be non uniform from the spatial point of view (thus different trees may show a large difference in the numbers of LiDAR sample) and that the number of reflections is relatively large near the external part of the tree crown and relatively smaller towards its interior (i.e., near the stem).

Considering these properties, we developed a conifer branch modelling technique that applies 3D region growing [190] to the data and identifies LiDAR points associated with each branch. However, the accuracy of region growing (and in-turn the accuracy of the internal crown structural model), highly depends on the seed point initialization. Here, we consider the LiDAR points most proximal to the actual conifer branch tips as the optimal seed points for three reasons: 1) the structural properties of conifer branches (i.e., compact and having tapering tips) allow an accurate identification of branch tips in high density LiDAR data; 2) conifers branch tips are prominent in high density LiDAR point cloud; 3) maximum separation between branches occurs at the branch tip (i.e., near the exterior of the crown), and this ensures that the seed points are uniformly separated or at least not confusingly close to each other. We refer to the region growing seed points as the branch tip points.

In case of conifers, it is highly likely that the boundary points of LiDAR point cloud are also the branch tip points. In this chapter, branch tip detection is achieved by the boundary detection algorithms in [191]. The algorithm finds the indices of those LiDAR points which define the smallest surface enveloping the entire point cloud. The compactness of the surface is controlled by a variance parameter that can take values between 0 and 1. When the parameter is set to 0, the surface becomes the least compact, and the surface becomes the most compact when the parameter is set to 1. Due to high density of LiDAR points, often multiple points near the same branch tips are selected as bound-

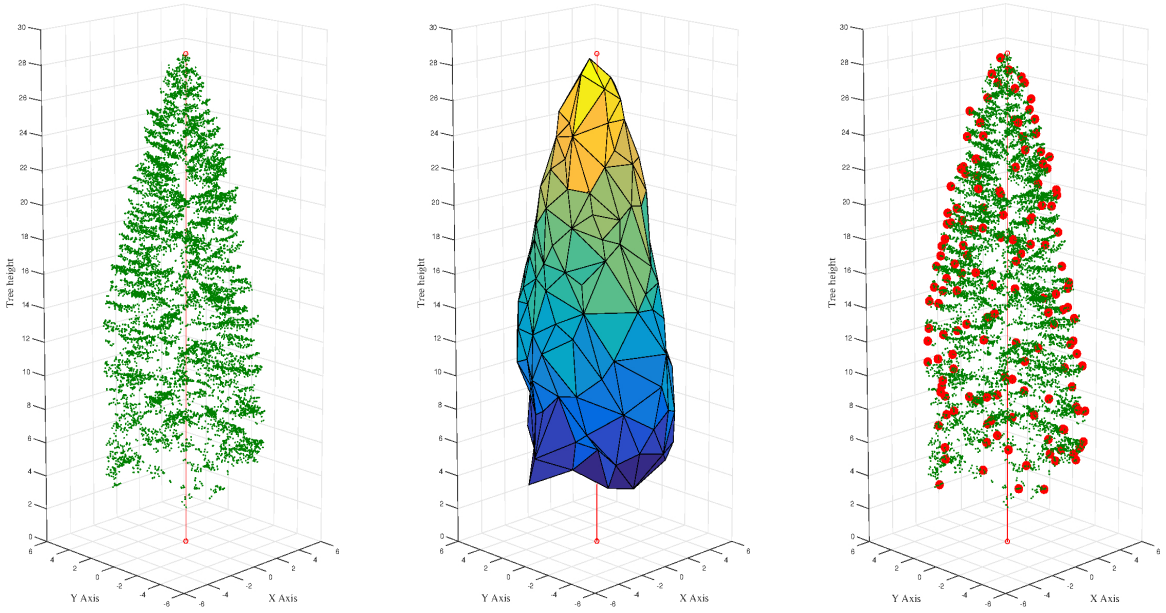

(a) (b) (c)

Figure 5.3: Internal crown structure modelling of conifers. (a) Input LiDAR point cloud for a tree (green dots). (b) The convex hull formed on the cloud. (c) Detected branch tips points (red dots).

ary points. However, only the most distant point (among the multiple boundary points) from the stem is considered as the optimal branch tip point. The space spanned by the candidate boundary points is dependent on the species. Moreover, the branch width/size varies along the height of the tree, i.e., the lower branches are larger and wider than the branches near the tree top. Hence we use an adaptive thresholding calculated using an inverse linear function of the branch tip point value z_i. The adaptive threshold takes into account also the variation in branch width/size along the height of the tree, i.e., the lower branches are larger and wider than the branches near the tree top. A convex hull formed from the boundary points is shown in Fig. 5.3b, and the boundary points after thresholding are shown in Fig. 5.3c.

The branch tips obtained using the boundary detection technique in [191] are the most external LiDAR points in every branch cluster. To define branches, a region growing is performed by progressively grouping LiDAR points, seeding from the identified branch tip points, according to a proximity criterion in the Euclidean space. The proximity calculation is performed on a four dimensional vector including the spatial coordinates of the LiDAR points, and the neighbourhood point density S_n. The neighbourhood point density S_n of the n^{th} LiDAR point sample p_n and can be calculated for each LiDAR point as:

$$S_n = \frac{Y_B}{\sum_{i=0}^{K} D_{ni}} \tag{5.1}$$

where Y_B is the number of nearest neighbours (a constant) of the n^{th} LiDAR point $p_n \in P$, and D_{ni} is the Euclidean distance between the n^{th} and the i^{th} LiDAR point. Thus, S_n will be large for those points which have close neighbours and viceversa. However, the LiDAR point density becomes considerably low towards the interior of the tree [192], [193], and as a result the inter-point distance (i.e., D_{ni}) becomes large, resulting in low S_n value. In effect, the closer to the stem, the more unreliable is the 3D region growing procedure. Hence, the growth process is stopped when the inter-point density difference becomes larger than a certain threshold. This threshold has been derived empirically by experimental analysis accomplished on a large set of conifers. Thus, sample close to the stem are not assigned to any branch cluster yet. Branch clusters with small number of points (i.e., < 10 points) were found to provide unrealistic branches and hence are not modeled. Such branch clusters mainly occur near the tree tops (due to small branch length) and also near the bottom (due to low point density).

Each incomplete branch cluster is usually highly correlated and linear in the 3D Euclidean space. This is evident since its overall shape can be approximated with a highly oblige ellipsoid (Fig. 5.5). Accordingly, the geometrical properties of individual branches can be approximated to the ones of the ellipsoid. To estimate the parameters of the b^{th} ellipsoid, Principal Component Analysis (PCA) is applied to the LiDAR points of branch clusters $c_b, b = [1, \ldots, B]$ (e.g., yellow points in Fig. 5.5) thus obtaining three principal components (PCs). PC1 is the axis along which data show the maximum variance and thus it is usually directed towards the stem of the tree. The angle between PC1 and the stem corresponds to the slope of the branch. PC2 and PC3 (i.e., the second and third largest variance components) provide information about the branch's horizontal and vertical width. Eigenvalues λ_1^b, λ_2^b and λ_3^b associated with the three PCA axis represent the ellipsoidal dimensions and thus the branch cluster dimensions. For each branch cluster, a regression line can be fitted in the 3D Euclidean space, which closely represents the wooden part of the branch. We refer to this as the branch line and it gives an approximate direction of the branch. For the purpose of cluster completion, all the points near the stem that were not allocated previously, are now assigned to one of the B branch clusters based on the proximity of the point to the branch line. Such points are very small in number and do not have much influence on the branch parameters.

The branch lines together with the stem provide a representation of the internal crown structure of a conifer (i.e., the conifer skeleton) (Fig. 5.4). Accordingly, the skeleton can be used to extract Internal Crown Geometrical Features (IGFs) that model the tree branch structure and are useful in distinguishing species.

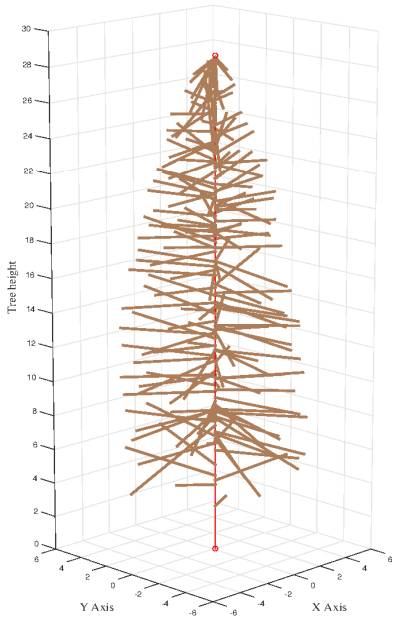

Figure 5.4: Conifer branch skeleton

Here, we define a set of six IGFs at tree level that depends on six corresponding branch-level features that derive from the proposed internal crown model. The set of branch-level features is as follows:

(a) *Branch length* L_b: distance between the b^{th} branch tip and the tree stem computed along the direction of its respective PC1.

(b) *Branch slope* α_b: angle between the direction of the PC1 of the b^{th} branch cluster and the stem.

(c) *Branch compactness* K_b: average of the perpendicular distance of LiDAR points in the branch to the corresponding branch line.

(d) *Branch width* W_b: calculated as the Eigenvalue along PC2 i.e., λ_2^b.

(e) *Branch symmetry* S_b: ratio between eigenvalues λ_2^b and λ_3^b. If the value is 1, the symmetry of the branch is considered to be maximum, whereas when the value tends to ∞ (i.e., $\lambda_2^b >> \lambda_3^b$) the branch is considered to be completely asymmetric or flat.

(f) *Branch density* D_b: number of LiDAR points associated with the b^{th} branch cluster c_b. Although, the feature does not capture the actual branch density, the feature value is directly correlated to the actual branch density.

The six IGFs are calculated for each branch and a feature-wise averaging is performed, thus obtaining values of the six features at the tree level. These features form half the number of feature that are given as input to the classifier in the final step of the proposed approach. Table 5.1 gives the analytical definition of the six tree level IGFs derived from the internal branch structure model. Trees at various stages of their growth will have different branch lengths and hence we normalize the features such as B_l, B_k and B_w by the Tree Height H_T. The average branch density B_n is divided by N in order to filter out variations caused by point cloud density.

Table 5.1: Proposed internal crown geometric features

Feature Id	Description	Equation
B_α	Average branch slope	$\frac{\sum_{b=1}^{B} \alpha_b}{B}$
B_l	Average branch length	$\frac{\sum_{b=1}^{B} L_b}{B \cdot H_T}$
B_k	Average branch compactness	$\frac{\sum_{b=1}^{B} K_b}{B \cdot H_T}$
B_w	Average branch width	$\frac{\sum_{b=1}^{B} W_b}{B \cdot H_T} = \frac{\sum_{b=1}^{B} \lambda_2^b}{B \cdot H_T}$
B_s	Average branch symmetry	$\frac{\sum_{b=1}^{B} S_b}{B} = \frac{\sum_{b=1}^{B} \frac{\lambda_2^b}{\lambda_3^b}}{B}$
B_n	Average branch density	$\frac{\sum_{b=1}^{B} D_b}{B \cdot N}$

5.2.2 External Crown Structure Characterization

High density LiDAR data also provide detailed level knowledge about the external shape of tree crown (Fig. 5.3a). Among the state-of-the-art algorithms for extracting information about the external crown geometry, shape fitting and convex hull based are the most popular. EGFs, which are derived using parameters of a regression-fitted geometric shape [194] and convex hull [195], obtained against the point cloud of a tree, are effective for tree species classification [117]. Fitting geometric shapes allows to have an idea of the

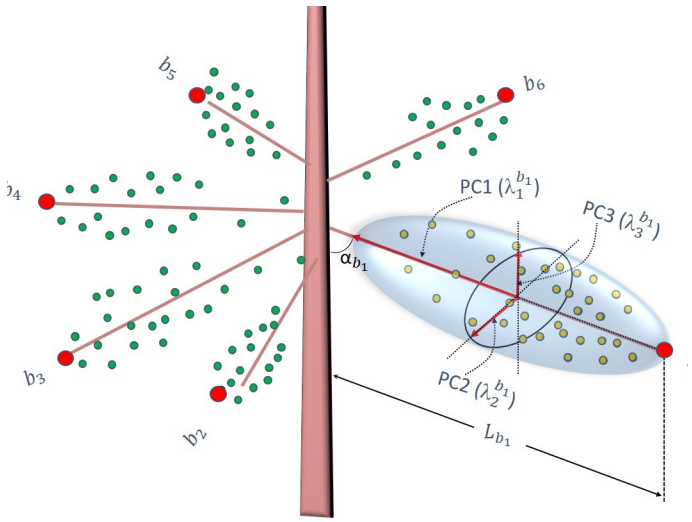

Figure 5.5: Illustration of the proposed branch model and of the related parameters.

general crown shape, whereas convex hull (based on the hull parameter α_{hull}) provides the smallest 3D surface that contains all the data points of a tree and thus provides information such as the crown volume, the surface area and the density. Conifer species have a similar typical conical crown shape that in some studies has been described with a generalized cone or paraboloid [196] [197]. For this study, we assume a simple cone shape and focus on features that are derived after shape-fitting. Whatsoever, considering the similar conical crown shape of conifers, it is expected that external crown geometrical features (EGFs) are less informative than IGFs, for species classification.

In order to fit a cone to the LiDAR point cloud of a tree, four cone parameters need to be estimated. These include the three coordinates of the cone vertex $V_c = [x_c, y_c, z_c]$, and the cone angle $a = tan(\alpha) = \frac{r_c}{h_c}$, where the angle α is the opening angle (semi-vertical angle),and r_c and h_c are the base radius and height of the cone (i.e. conifer in this case) respectively [198]. The general equation of a cone can be written as

$$(x_i - x_c)^2 + (y_i - y_c)^2 = (z_i - z_c)^2 a^2, \forall i \in [1, N] \tag{5.2}$$

where, x_i, y_i, z_i are Euclidean coordinates of the i^{th} LiDAR point sample in the tree. The parameters of the best fitting cone (Fig. 5.6a) can be obtained by fulfilling the least square condition:

$$\hat{a} = \underset{a}{\operatorname{argmin}} \sum_{i=1}^{N} \epsilon_i^2 = \underset{a}{\operatorname{argmin}} \sum_{i=1}^{N} (a_i - a)^2$$

where, (5.3)

$$a_i = \sqrt{\frac{(x_i - x_c)^2 + (y_i - y_c)^2}{(z_i - z_c)^2}}$$

$\hat{a}$ is the optimal parameter value, obtained by fulfilling the least square condition, defining the best-fit cone that represents the external crown shape for the tree approximately. The initial vertex coordinates can be chosen to be the spatial coordinates of the highest LiDAR data point in the cloud. The optimal vertex can be different from the initial coordinate and is updated accordingly with a_i (see equation 5.3) . Among the several EGFs available in the literature, we selected the six least correlated EGFs mentioned in [117]. The features are derived from the parameters of best fitting cone and convex hull. For each tree LiDAR point cloud. They include the following parameters:

(a) Volume of convex hull V_{hull}, divided by the number of points within the tree crown N.

(b) Difference between the convex hull volume and the fitted cone volume V_{cone}, to the convex hull volume.

(c) Regression error $RMSE_{cone}$ associated with the cone fitting. It can be computed by solving the $\left(A^T A\right)^{-1} A^T Q$, where A is the matrix derived from the derivatives of the Taylor expansion (which is applied to linearize the non-linear equation of the cone) of a_i around the cone vertex, V_c. The equation of a can be derived from (5.2), and Q is $(a_1, a_2, a_3, ..., a_N)$. The regression error associated with the least square cone fitting is a species dependent feature, as it does not consider only the general shape of the tree, but also the point density and distribution inside the canopy of the tree.

(d) Average of the distance of each point d_n, to the closest facet of the convex hull.

(e) Standard deviation of distances from each point to the closest facet of the convex hull.

(f) Ratio between the crown height H_C and tree height H_T.

Table 5.2 summarizes the considered external crown geometric features and provide their equations.

Table 5.2: External crown geometric features

Feature Id	Description	Equation
T_v	Volume of the convex hull by the number of points within the crown [199].	$\frac{V_{hull}}{N}$
T_d	Difference between the convex hull and fitted cone volumes compared to the convex hull volume [199].	$\frac{V_{hull}-V_{cone}}{V_{hull}}$
T_ϵ	Root mean squared error from regression fitting of cone [199].	$\frac{RMSE_{Cone}}{N}$
T_l	Average of distance d_n of each LiDAR point to the closest facet of convex hull [199]	$\frac{\sum_{n=1}^{N} d_n}{N}$
T_σ	Standard deviation of orthogonal distances from each point to the convex hull [199].	$\sqrt{\frac{\sum_{n=1}^{N}(p_n-T_l)^2}{H_T}}$
T_h	Crown height divide by Tree height [199]	$\frac{H_C}{H_T}$

5.2.3 Conifer Species Classification

In the last step, IGFs (Table 5.1) and EGFs (Table 5.2) are given as input to an automatic classifier that associates each tree with its species. Although any classifier could be employed, we use the Support Vector Machine (SVM) as it is very efficient and versatile [200] and has been successfully used in remote sensing applications. Three different SVM configurations has been used. Sparse C-SVM with linear kernel enhances the magnitude of feature weights (i.e., the weights of the relevant features are accentuated while the weights of the non relevant ones are attenuated) and thus is good to understand feature relative relevance. Both single and multi-kernel SVM architectures using both linear and non-linear kernels have been considered with the objective of achieving the highest classification accuracy and hence used for feature quality assessment in this chapter.The rest of the section briefly summarizes the theory of the above mentioned classifiers. Let $F = \{\vec{\mathrm{v}_\mathrm{i}}\}_{i=1}^{N_G}$ be the set of training feature vectors. N_G is the total number of training sample and $\vec{\mathrm{v}_\mathrm{i}} \in R^f$, f is the number of features. Let $U = \{u_i\}_{i=1}^{N_G}$ be the set of corresponding class labels in the training set, where $u_i \in$ {-1 1}. In our case, the input vector $\vec{v_i}$ is defined as the normalized set of IGFs and EGFs, i.e., $\vec{v_i} = [B_\alpha, B_l, B_k, B_w, B_s, B_n, T_v, T_d, T_\epsilon, T_l, T_\sigma, T_h]$.

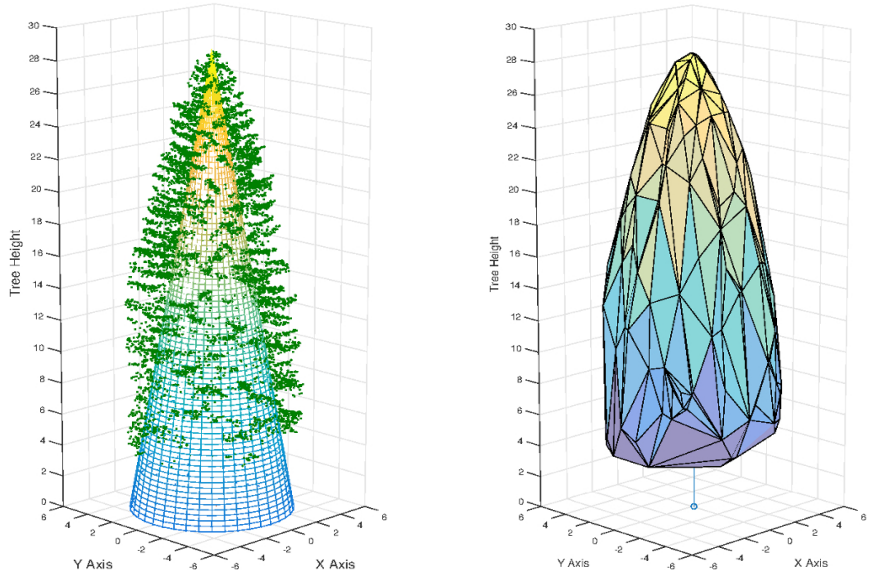

(a) (b)

Figure 5.6: Representation of (a) the regression cone fitting on the LiDAR point cloud of a Norway Spruce tree, and (b) shows the convex hull obtained for the same tree

.

The SVM aims at estimating an optimal separating hyperplane defined by the parameters $\vec{\mathrm{w}}$ and e, which are the weight vector and the bias, respectively [188]. The estimates of $\vec{\mathrm{w}}$ and e, for the C-SVM and MK C-SVM are obtained by solving the optimization problem in (5.4).

$$\begin{aligned} \min_{\vec{w},\xi,e} \quad & \frac{1}{2}t + C\sum_{i=1}^{N_G}\xi_i, \\ \text{subject to} \quad & u_i(\vec{\mathrm{w}}^T f(v_i) + e) \geq 1 - \xi_i, \forall i = 1, \ldots, N_G, \\ & \xi_i \geq 0, \end{aligned} \tag{5.4}$$

The function $f(v)$ for the C-SVM is a single kernel $K(v, v')$, whereas for the MK C-SVM it is a multiple kernel $\sum_{m=1}^{M_k} d_m K(v, v')$, where M_k is the number of kernels, and $\sum_{m=1}^{M_k} d_m = 1$. $K(.,.)$ is a given positive definite kernel associated with a reproducing kernel Hilbert space. In our case we use Radial Basis Function (RBF) kernel for both C-SVM and MK C-SVM. The terms ξ and C in (5.4) are the slack variables and the tuning parameter, respectively. Linear Sparse C-SVM performs classification by exploiting the sparsity in the input feature space, and emphasises the relevance of features (i.e., their weights), while reducing the relevance of noisy and/or correlated features. In the case of

Sparse C-SVM, the optimal feature selection and the SVM learning processes are achieved simultaneously. Although popular in other fields, Sparse C-SVM has not been widely used in remote sensing and hence we provide some details on it. The estimates of $\vec{\mathrm{w}}$ and e are obtained by solving the optimization problem in (5.5).

$$\begin{aligned} \min_{\vec{w},\xi,e,t} \quad & \frac{1}{2}t + C\sum_{i=1}^{N_G}\xi_i, \\ \text{subject to} \quad & u_i(\vec{\mathrm{w}}^T f(v_i) + e) \geq 1 - \xi_i, \forall i = 1,\ldots,N_G, \\ & \xi_i \geq 0, \\ & ||\vec{\mathrm{w}}||_2^2 \leq t \\ & ||\vec{\mathrm{w}}||_1^2 \leq gt \end{aligned} \tag{5.5}$$

The Sparse C-SVM formulation shown in (5.5) is the same as that of the C-SVM or MK C-SVM (5.4) except for the two additional constraints on $\vec{\mathrm{w}}$. The (5.5) is rather a simplified version of the original optimization problem in [187]. The simplification of the problem is achieved by replacing the cardinality constraint in the original problem with a weaker non-convex constraint, i.e., $||\vec{\mathrm{w}}||_1^2 \leq \sqrt{g}||\vec{\mathrm{w}}||_2^2$ [187]. This weaker non-convex constraint can be further relaxed to a convex form by bounding the norm $L2$ constraint on $\vec{\mathrm{w}}$ by a variable t, and the $L1$ norm constraint on $\vec{\mathrm{w}}$ by gt, where t is a constant. Hence, the aforementioned non-convex constraint can be split into the following constraints $||\vec{\mathrm{w}}||_2^2 \leq t$ and $||\vec{\mathrm{w}}||_1^2 \leq gt$ [187]. The $L1$ constraint on weight vector $\vec{\mathrm{w}}$ allows it to be Sparse (i.e., some values of $\vec{\mathrm{w}}$ could be 0), while the $L2$ constraint minimizes the number of elements of $\vec{\mathrm{w}}$ to be shrunk to zeros. Hence, only few relevant features are considered while generating the hyperplane. The individual elements of $\vec{\mathrm{w}}$ quantify the relative importance of a feature with respect to the others.

Fig. 5.7 shows an illustration of the hyperplanes obtained with a standard linear SVM and a linear Sparse C-SVM for a 2-class 2D problem. C-SVM considers both the features 1 and 2 to define the hyperplane, whereas linear Sparse C-SVM creates the hyperplane based on the feature 1 only. Similar considerations hold for a higher dimensional feature space. Using a subset of the original features makes the process computationally more efficient, at the cost of a small decrease in the classification accuracy w.r.t. C-SVM or MK C-SVM. If a multi-class problem needs to be solved, one-against-one or one-against-all approaches can be employed as for standard linear SVM [201].

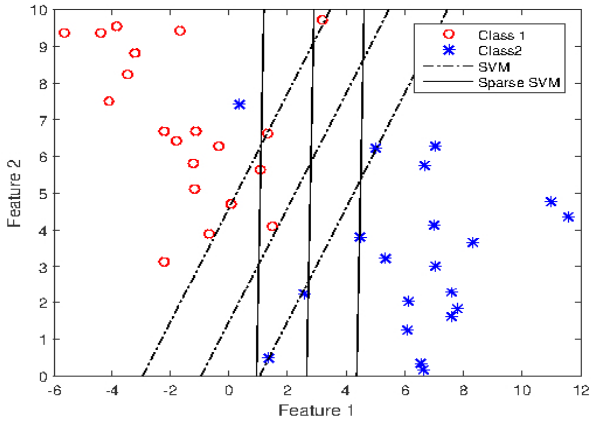

Figure 5.7: Illustration of the hyperplanes formed by the C-SVM and the Sparse C-SVM in an R^2 space. The Sparse C-SVM ignores one dimension (i.e. Feature 2).

5.3 Experiments and Results

5.3.1 Study Area and Data Set

The study area is located in the Italian Alps, in the municipality of Pellizzano at about 40 km northwest of Trento (a city in the North of Italy). The area contains valleys and mountainous terrains. The approximate extent of the area is about 3200 ha, and the altitude varies from 900 to 2000 m above the sea level. The forest in this region is heterogeneous with both coniferous and broad-leaf species. The dominant coniferous species include the Norway Spruce (Picea Abies), the European Larch (Larix Decidua), the Swiss Pine (Pinus cembra) and the Silver Fir (Abies Alba). Minority coniferous species are European Black Pine (Pinus Nigra) and Scots Pine (Pinus Sylvestris). Among the broadleaf species European Beech (Fagus sylvatica L.) dominates over Sycamore Maple (Acer Pseudoplatanus L.), Hop Hornbeam (Ostrya Carpinifolia Scop.), Field Elm (Ulmus Campestris), and Sessile Oak (Quercus Petraea Liebl). Here attention is devoted only to the four major coniferous species. The ALS data were acquired between 7^{th} and 9^{th} September 2012 from an airborne platform flying at an altitude of 660 m with a speed of 100 Km/Hr. The acquisition sensor is a Riegl LMSQ680i. The frequency of the laser scanner is 400 KHz and up to four returns were recorded. The point density varies from 10-50 points per meter squared due to the mountainous terrain of the study area. The flight was repeated several times to generate a dense point cloud with density varying from 50 to 200 points/m^2. As expected, a high density point cloud is observed below the flight path (i.e., near nadir) whereas the density of the point cloud decreases off-nadir. The density of LiDAR points is maximum in the crown region and reduces toward the interior

section of the trees. Further, point density is maximum near the tree top and minimum at the bottom. The ground sample collection was conducted in the same month as that of the data acquisition. Among them, a set of 200 reference trees, manually delineated from the point cloud, was created, that includes 50 trees each of the Norway Spruce (NS), the European Larch (EL), the Swiss Pine (SP) and the Silver Fir (SF) species. On the one hand, the NS, EL, and SF are relatively tall trees and are geometrically more similar to the assumed conifer characteristics. On the other hand, the SP is shorter with slightly different characteristics. SP class is included in the study as: a) it is one of the major species in Europe, and 2) it allows to evaluate the robustness of the proposed modelling technique. Table 5.3 shows the tree and crown height statistics of the tree sample. In order to validate the effectiveness of the proposed internal crown model and of the features derived from it, the crown of trees in the reference set was manually detected. In this way, the validation procedure does not suffer from: 1) propagation of error due to automatic tree delineation techniques and, 2) the presence of structurally damaged trees (as this is not investigated in this research). However, for operational use, automatic segmentation methods [182], [104], [186] can be employed, followed by a noise filtering to avoid isolated points around the crown. LiDAR points corresponding to understory vegetation were manually removed (but automatic methods from the literature can be employed as well [202], [186]) since they do not follow the conifer crown model. Selected trees show in average 12000 points from multiple scanning passes.

Table 5.3: Basic statistics of the structural characteristics of the sample conifer on the considered dataset

Tree	**Number**	**Tree height (m)**			**Crown height (m)**		
Species	**of Trees**	**Max**	**Min**	**Mean**	**Max**	**Min**	**Mean**
NS	50	44.97	22.36	31.51	35.0	19.0	26.31
EL	50	37.64	16.92	28.32	30.0	15.0	21.84
SP	50	39.57	13.49	30.35	34.0	10.0	24.52
SF	50	23.66	10.51	17.56	20.0	9.56	15.53

5.3.2 Experimental Results and Discussion

A direct evaluation of the performance of the proposed internal crown modelling technique would require reference information at the branch level. This is not feasible for the ALS dataset used in the study as: a) the data were acquired almost 9 years ago and any field data collected now would be incompatible with the ALS data, and b) it is very expensive in terms of time and money to perform an accurate branch level field-data collection. Thus, we adopted a validation set that includes qualitative analysis and an

indirect quantitative assessment. The results obtained using the proposed internal crown model are compared with the ones obtained by relying on a state-of-the-art (SoA) one. Merge and Split K-means clustering approach to internal crown structure modelling is used as the SoA method [117]. It applies k-means clustering to LiDAR data with random seed initialization, and performs a merging and splitting operations on the cluster to identify final valid branch clusters. In our experiments, the k has been set to be equal to the number of branch-tips identified using the proposed technique. For each tree, the branch tips were identified using the convex hull based technique with the variance parameter α_{hull} set to 0.5. The threshold (at crown bottom height) for multiple branch tip removal was set to 2.0, 3.8, 2.8 and 1.9 for NS, EL, SP and SF, respectively. In this way, we give clear advantage to the reference technique that has not the intrinsic capability to estimate the number of expected branches. The reader is referred to [117] for further details on the merge and split k-means based branch detection approach. In our method, the branch clusters were identified using the region growing performed on the point cloud, starting from the identified seed points. The growing is stopped when the neighbourhood threshold density becomes lower than the 0.3% of the density near the branch tip (where the density is likely to be the maximum). K was set to 5 for all the cases.

From the qualitative point of view, a visual comparison of the internal crown model obtained with the proposed model and with the SoA one was conducted for several trees in the reference set. Figures 5.8, 5.9, 5.10, 5.11 show examples of: a) the tree LiDAR point cloud, b) the branch model obtained with the SoA approach, and c) the branch model obtained with the proposed approach, for each of the four considered species. It can be observed that the proposed model is able to better capture the branch structure for all the considered species. This becomes more clear in the upper right part of Fig. 5.8. It can be observed that all the branch clusters have been correctly captured by the proposed method, whereas the SoA method fails to do so. The poor modelling capability of the SoA model is mainly caused due to isotropic groping preferences and random initialization of the k-means clustering. This choice, combined with the complexity of the LiDAR point cloud, often make it difficult to identify valid branch clusters. The proposed model overcomes the drawbacks by employing the convex hull based technique. Recalling that IGFs are attributes associated to the branches, their reliability depends on the branch model accuracy. Accordingly, it is expected that IGFs extracted from the SoA branch model are less reliable than the ones extracted from the proposed one while classifying species.

In order to quantitatively assess the above statement, IGFs were extracted by employing both the proposed and the SoA internal crown model. The EGFs were computed as well. An indirect quantitative validation of both the internal crown structural model and

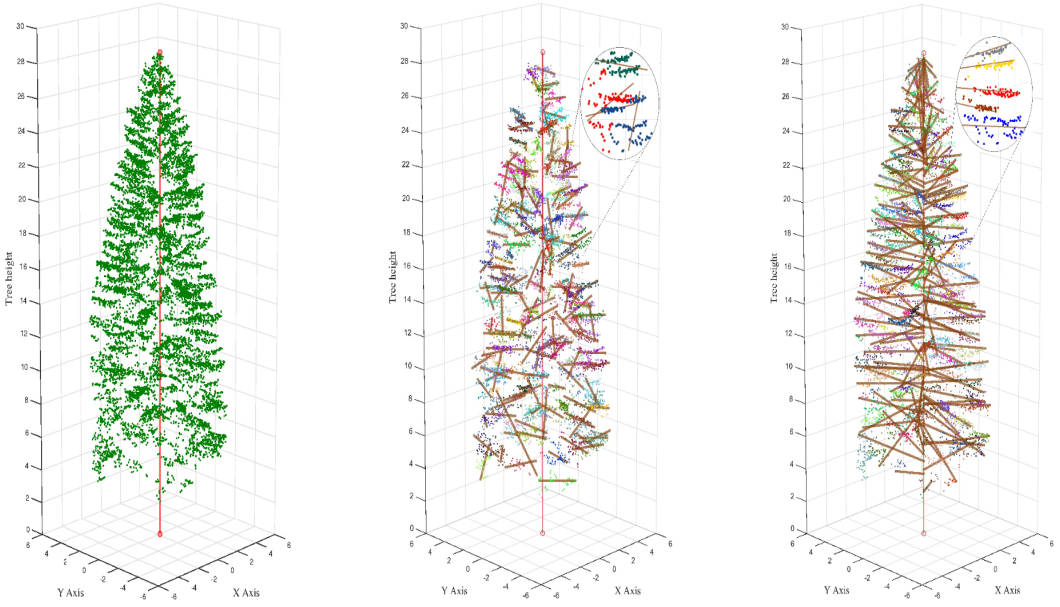

(a) (b) (c)

Figure 5.8: Example of results on a Norway Spruce tree, (a) show the raw LiDAR data, (b) the results obtained by the SoA model, (c) the results obtained by the proposed model.

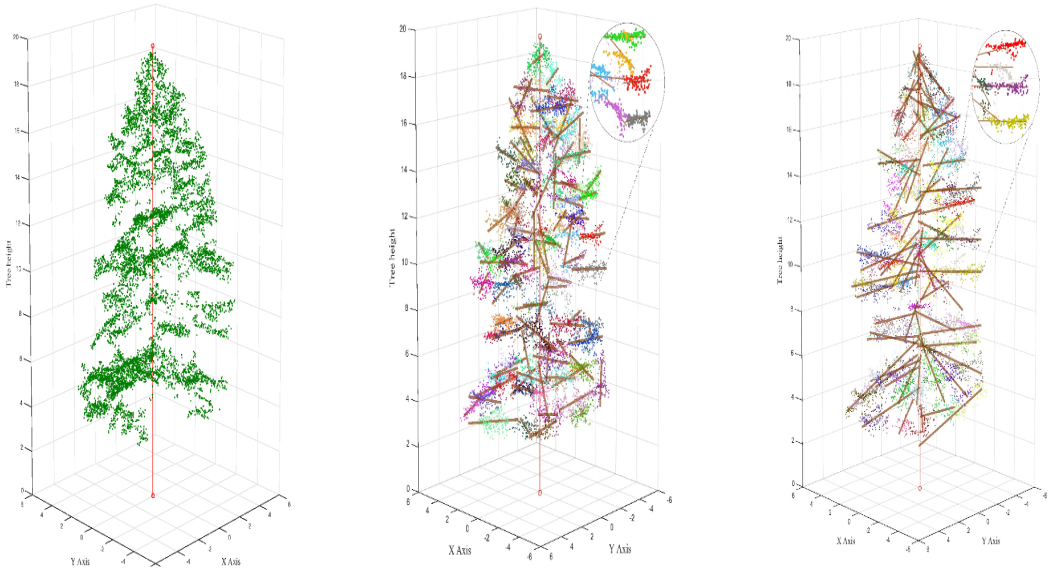

(a) (b) (c)

Figure 5.9: Example of results on a European Larch tree, (a) show the raw LiDAR data, (b) the results obtained by the SoA model, (c) the results obtained by the proposed model.

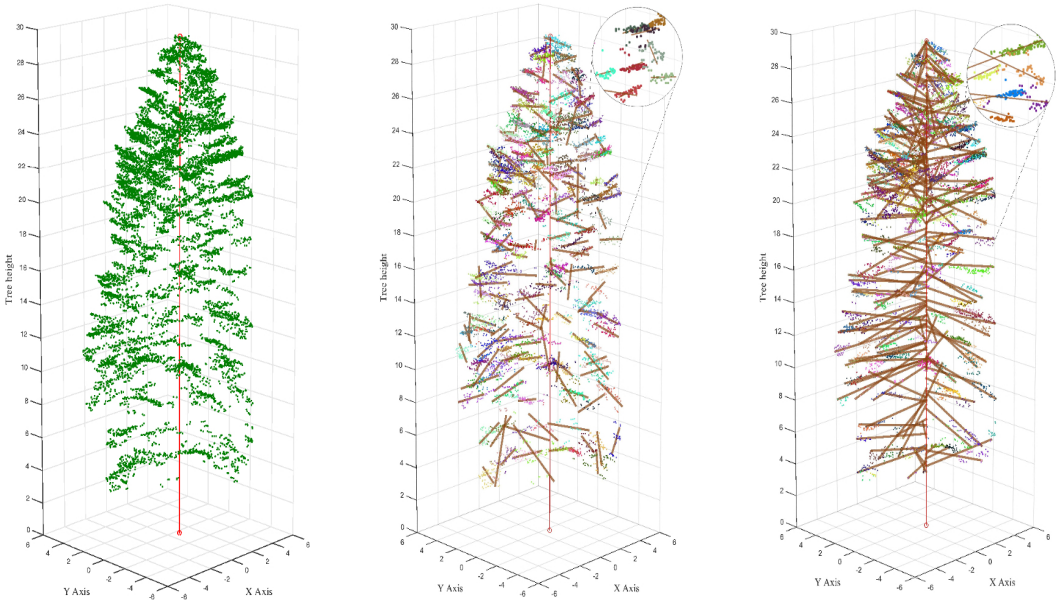

(a) (b) (c)

Figure 5.10: Example of results on a Swiss Pine tree, (a) show the raw LiDAR data, (b) the results obtained by the SoA model, (c) the results obtained by the proposed model.

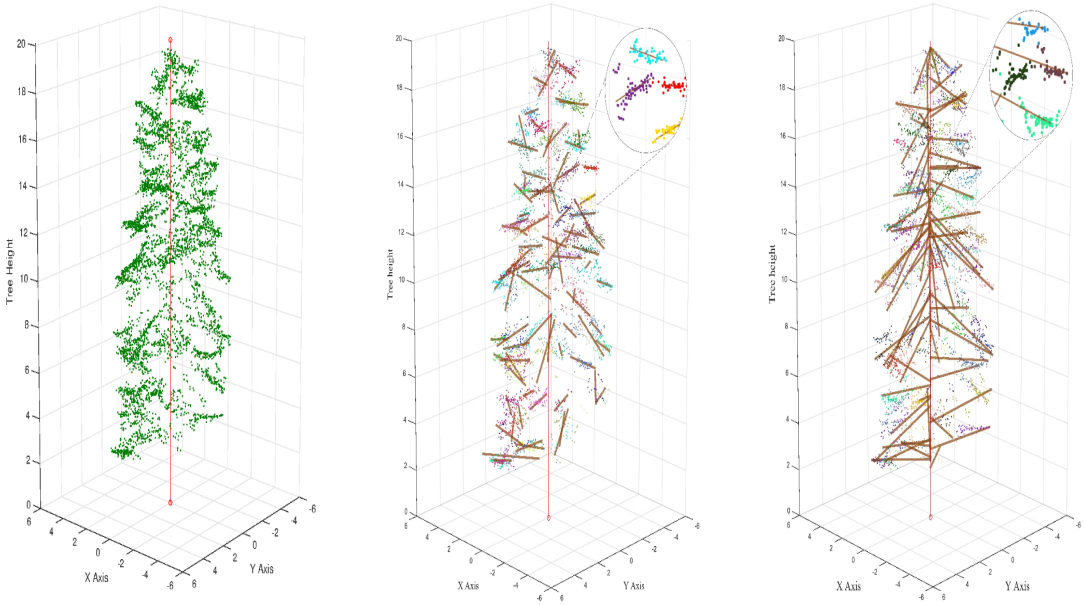

(a) (b) (c)

Figure 5.11: Example of results on a Silver Fir tree, (a) show the raw LiDAR data, (b) the results obtained by the SoA model, (c) the results obtained by the proposed model.

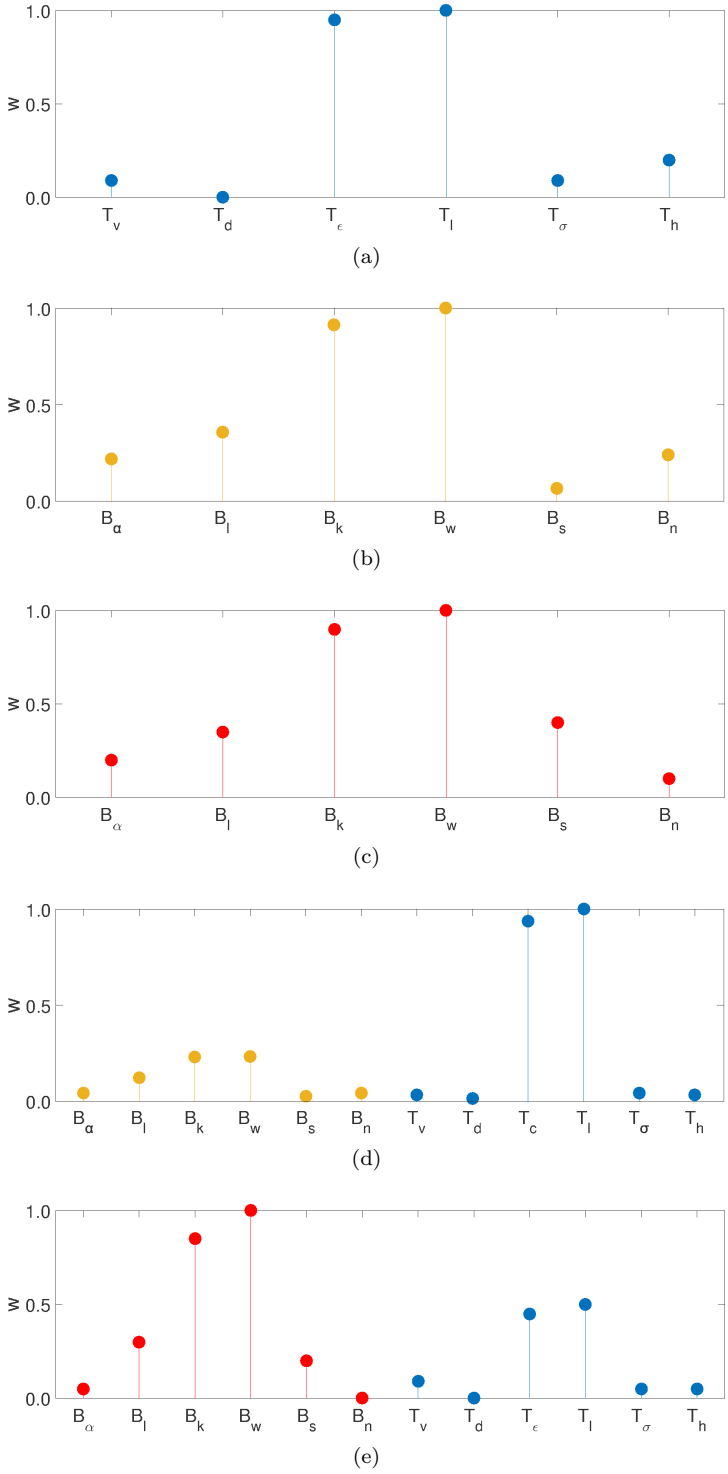

Figure 5.12: The Sparse C-SVM weights obtained when employing: (a) only EGFs, (b) only IGFs computed on the SoA model (c) only IGFs computed on the proposed model, (d) the IGFs from the SoA model together with the EGFs, and (e) the IGFs from the proposed model together with the EGFs.

the proposed IGFs was achieved by analyzing: i) the feature weights estimated during the Sparse C-SVM training phase; and ii) the Sparse C-SVM, C-SVM and MK C-SVM classification accuracy. The experiments were conducted on the following feature combinations: i) External Crown Geometric Features (EGFs); ii) IGFs extracted from the state-of-the-art model (IGFs-SoA); iii) IGFs extracted from the proposed internal crown model (IGFs-proposed); iv) IGFs extracted from the state-of-the-art model and the EGFs (IGFs-SoA and EGFs); and v) IGFs extracted by the proposed internal crown model and the EGFs (IGFs-proposed and EGFs). For all the cases the better the performance, the better is the considered set of features and thus the corresponding internal crown model. The feature extraction step requires about 15 seconds for each tree on a 64-bit Windows 10 machine with 8.00 GB of RAM and IntelXeonCPU E3-1240 V2. Thus, for operational use, the performance can be improved using parallel computing.

For all the classifiers, the training was conducted by means of a 4-fold cross-validation. The 60% of the total sample (i.e., 120 trees) were employed in the cross-validation procedure, and the remaining 40% (i.e., 80 trees) was used for validation. The validation set was selected such that 20 trees for each of the four species were included. Considering that the sample dataset size is small, the process was repeated 20 times and the results are analysed as the average over the 20 runs. The training procedure aimed at estimating: i) the optimal C parameter for each classifier, and ii) the optimal kernel parameters for C-SVM and MK C-SVM. Here an RBF kernel was used, thus the spread γ of the kernel(s) was estimated. For Sparse C-SVM, C values were considered in the range $[10^{-6}, 10^{6}]$ with an exponential step of 10^{1}. For all combination of features, the best average accuracy on the validation set was found for $C = 10^{5}$. For C-SVM, C was considered in the range $[2^{-15}, 2^{15}]$ with an exponential step of 2^{1}, whereas γ varied in the range [0.001, 10] with an exponential step of 10^{1}. The best average accuracy was achieved with $C = 2^{8}$ and $\gamma = 0.01$ for the EGFs, the IGF-SOA and the IGF-Proposed feature sets, and with $C = 2^{9}$ and $\gamma = 0.01$ for the remaining sets. For MK C-SVM, C was considered in the range $[2^{-15}, 2^{15}]$ with an exponential step of 2^{1} (like for the C-SVM), and a total of 9 RBF kernels were selected. The 9 corresponding γ values were selected by using the C-SVM optimal γ value as a guideline. Accordingly, γ values for MK C-SVM were selected close to 0.01 (i.e., 0.002, 0.004, 0.006 ,0.008, 0.010, 0.012, 0.014, 0.016 and 0.018). It is worth noting that the input data are from a single source and hence large variations in γ are not expected. The optimal C for MK C-SVM was found to be 2^{10}. Feature values were normalized before giving them as input to the classifiers [203].

Let us first analyse the feature relevance obtained as the weights of the trained Sparse C-SVM (linear soft margin, implemented using CVX [204]). The feature weights are a result of the class separability analysis performed by the Sparse C-SVM, i.e., a higher

feature weight shows that the feature is relatively more relevant when compared to the others [205]. The weight values for most EGFs are small and thus they are less relevant for conifer species classification (Fig. 5.12a). This behavior was expected as conifers have very similar external crown characteristics. Nonetheless, the cone fit error (T_ϵ) and the average distance of LiDAR points to the closest facade of the convex hull (T_l) showed to be promising features and this agrees with our observation that the crown shape and the point density variation around the stem are slightly different for different species. Fig. 5.12c shows the normalized features weights obtained in the proposed set up. The Sparse C-SVM assigned maximum weights to the branch width B_w and average branch compactness B_k. This is in alignment with our visual examination (a close look at Fig. 5.8, 5.9, 5.10, 5.11 shows that each tree species shows a unique branch width and branch compactness). Both B_w and B_k are independent of variations in both the point cloud density and the maturity of the tree, and hence are good features for species classification. While the average branch slope B_α, the average branch length B_l, the average branch symmetry B_s, and the average branch density B_n, were assigned lower weights. This implies that the B_l and B_α are less useful features at least for discriminating the species considered in this study. In case of B_α, the low weight value is a result of variation in branch slopes along its height. The low weight values for B_l is connected to the fact that trees of the same species and similar height can vary in their crown diameter, and thus show different branch lengths. Although, the average branch symmetry was expected to be a good feature to classify tree species, the results proved that they are less relevant for the four species considered in this study. This is attributed to the fact that branches of different species have similar ratio values. For example, the Norway Spruce and the Silver Fir seem to have different branch sizes. However the ratio between the branch width and the branch height is very similar. The average branch density is a good feature for species classification if the ALS sampling density is uniform throughout the acquisition, However in our case, the large variation in the point cloud density, due to combined effect of target material, range variation, and footprint size on the return power (see (2.2)), makes it less relevant with the current set of species. I.e., the relevance of features will differ for different set of species.

It is worth noting at this point that the weight values show only the relative importance of the features, and hence a direct comparison of the values across experiments involving different set of features is meaningless. For example, while classifying between Norway Spruce and European Larch, the branch width attribute has the maximum weight (this is in accordance with the fact that, birch has wider branches than spruce), while between Norway Spruce and Scot Pine, the branch density attribute is more relevant. However by jointly providing as input the IGFs-proposed and the EGFs to the Sparse C-SVM, it is

possible to compare the importance of the IGFs-proposed and the EGFs. The Fig. 5.12e shows the weight obtained for this feature combination. It is evident that the EGFs have been identified as relatively less important than the IGFs-proposed.

The normalized weight values obtained for the IGFs-SoA are shown in Fig. 5.12b. The features B_k and B_w have higher values and hence are more relevant. This is in line with our expectation for the same reasons mentioned previously. B_l, B_α, B_s and B_n have relatively smaller weights. We also tested the case in which the IGFs-SoA along with the EGFs were provided as input to the Sparse C-SVM. The Fig. 5.12d shows the normalized feature weights. As one can see, the EGFs were assigned higher weight values than any of the features in the IGFs-SoA set. The box-plots in Fig. 5.13 confirm the quantitative separability analysis. It can be seen that the highest weights are assigned to those features with non-overlapping means and minimum variance.

Since EGFs are extracted independently of branch geometric model, they can act as a benchmark for feature quality comparison between the IGFs-SoA and the IGFs-proposed features. By comparing weight assignments for the IGFs-SoA and the EGFs, and IGF-proposed and the EGFs, one can see that the IGFs-SoA have been identified as poor features in comparison to the EGFs whereas the IGFs-proposed proved to be better features than the same EGFs.

Let us now compare the average classification accuracy computed over the 20 runs and obtained on the five feature sets by using the Sparse C-SVM, the C-SVM (LIBSVM [206]) and the MK C-SVM (SimpleMKL Matlab tool [207]). Table 5.4 summarizes quantitative results. It is clear from Table 5.4 that the classification performance is higher when using the IGFs-proposed set rather than the IGFs-SoA feature set, both with and without the EGFs. This means that the proposed model is more accurate than the SoA one. Therefore the features derived from the proposed internal crown model are more effective.

Table 5.4: Average classification accuracy on the validation set for different sets of features.

Feature Set	**Classification Accuracy (%)**		
	Sparse C-SVM	**C-SVM**	**MK C-SVM**
EGFs	68.5	72.2	71.5
IGFs-SoA	75.8	79.2	79.7
IGF-proposed	81.2	86.0	86.6
IGFs-SoA and EGFs	80.9	86.9	87.7
IGF-proposed and EGFs	85.3	89.1	89.5

Furthermore, Table 5.4 points out that the MK C-SVM performs better w.r.t the Sparse C-SVM and C-SVM. Thus, we evaluate the species classification performance based on the accuracy provided by the MK C-SVM. As expected, the use of the EGFs only led to lower performance, i.e., an overall accuracy of 71.5%. An increment of performance of about 8.0% and 15.0% was achieved when using the IGFs-SoA and the IGFs-proposed feature sets, respectively. It is worth noting that the use of the proposed internal structural model significantly increased the overall classification accuracy, with respect to the use of features derived from the state-of-the-art one. This improvement confirms the effectiveness of both of the proposed internal structural model and the proposed IGFs. When both the IGFs and the EGFs are given as input to the Sparse C-SVM, the classification accuracy increases further reaching 87.7% with the IGFs-SoA features, and 89.5% with the IGFs-proposed features. The accuracy improvement achieved by the joint use of EGFs and IGFs is of about 8.0% and 3.0% when the state-of-the-art and the proposed model are used, respectively. Tables 5.5 and 5.6 show the confusion matrix (including user's accuracy (U.A.) and producer's accuracy (P.A.)) for the IGFs-SoA and the EGFs, and the IGFs-proposed and the EGFs experiments, respectively. The best result over the 20 runs was selected. As one can see, the number of errors is smaller for all the species when using the IGFs-proposed feature set.

Table 5.5: MK C-SVM confusion matrix of the best case over 20 runs on using the IGFs-SoA and the EGFs feature set.

Classification	Field Data				U.A.%
	NS	EL	SP	SF	
NS	17	0	2	1	85.0
EL	0	19	1	0	95.0
SP	1	0	19	0	95.0
SF	2	0	1	17	85.0
P.A.%	85.0	100.0	100.0	82.6	O.A. 90.0 %

In general, state-of-the-art methods (see section (3.2)) derive internal geometric information from the ALS data with no or minimal use of aprori information on tree crown structure which can greatly benefit in accurate crown modeling / feature extraction. Thus, the proposed method prove the importance of including aprori information on the general structural characteristics of trees in accurately modeling internal geometric features and, hence in accurately identifying tree species at the ITC level. However, it is worth noting that the relevance of geometric features might differ for different set of species, as key structural differences might be different for different set of species and or forest

Table 5.6: MK C-SVM confusion matrix of the best case over 20 runs on using the IGFs-proposed and the EGFs feature set.

Classification	Field Data				U.A.%
	NS	EL	SP	SF	
NS	18	1	0	1	90.0
EL	0	19	0	1	95.0
SP	0	0	20	0	100.0
SF	2	0	0	18	90.0
P.A.%	90.0	95.0	100.0	90.0	O.A. 93.7 %

types. The study also proves that the internal structural features are more relevant than external ones for classification of tree species belonging to the same taxonomical class, and hence stressing on the need for future research to better model the internal crown structure.

5.4 Conclusion

In this chapter, we proposed a method for modelling the internal crown structure of the conifers from small footprint high point density multi-return airborne LiDAR point clouds. The internal crown structure modelling is performed using a set of six novel features capable of characterizing the individual branch. The six proposed features are jointly used with six external crown geometric features taken from the literature for improving the classification accuracy by modelling also the external crown geometry of the trees. Accuracy assessment was performed by using three different SVM classifier including the Sparse C-SVM, the C-SVM, and the MK C-SVM. A set of five experiments were conducted to study the individual and the joint performance achieved by using the proposed and standard features taken from the literature. All experiments were conducted on a set of 200 tree sample belonging to the four major European conifer species (i.e., the Norway Spruce, the European Larch, the Swiss Pine, and the Silver Fir). Experimental results point out that the proposed internal crown model leads to the generation of more effective features with respect to the state-of-the-art one. Furthermore, the joint use of the proposed internal crown geometric features together with standard external crown geometric features provides sharply higher classification accuracies in conifer species classification than the use of external crown geometric features only. This proves the effectiveness of the proposed method that makes it possible to obtain satisfactory results in species classification without the use of any multispectral or hyperspectral image. As future works,

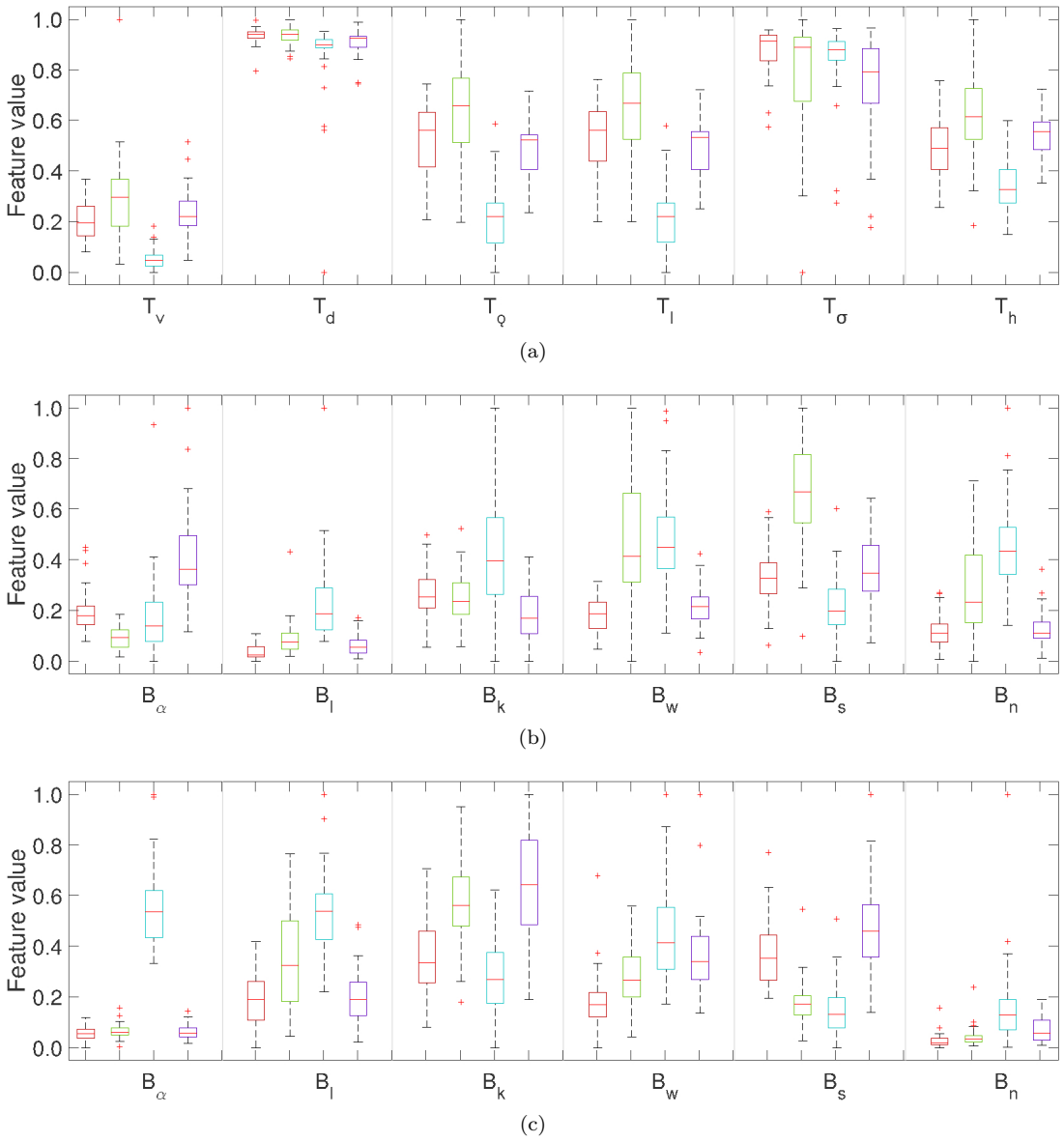

Figure 5.13: Box plot analysis of (a) EGFs, (b) IGFs-SoA and (c) IGFs-proposed, for Norway Spruce (red color), European Larch (green color), Swiss Pine (light blue color) and Silver Fir (purple color), respectively.

we plan to design additional internal crown geometric features to improve conifer species classification accuracy and to consider the effects of crown-overlap and under-story vegetation on the modelling process and hence on the final classification accuracy. Moreover, we plan to extend the method to characterize partially damaged trees (e.g., trees with missing branches and/or having unsymmetrical crown shapes). Also the performance of the method on other forest types such as boreal and temperate needs to be evaluated.

Chapter 6

A Data Driven Approach to Tree Species Classification in ALS Data

In this chapter, a data-driven tree species classification approach that maximally exploits the structural information in small footprint high density multi-return ALS data is proposed. The idea here is to perform a volumetric analysis of single-tree-point-cloud in order to extract robust features that characterize both the key internal and the external crown structure. The method captures the spatial distribution of the LiDAR points within the crown by generating a feature vector representing the three-dimensional (3D) crown information. Each element in the feature vector uniquely corresponds to an Elementary Quantization Volume (EQV) *of the crown. Three strategies have been defined to generate unique EQVs that model different representations of the crown components. The classification is performed by using a Support Vector Machines (C-SVM) classifier using the histogram intersection kernel that has the enhanced ability to give maximum preference to the key features in high dimensional feature space. All the experiments were performed on a set of 200 trees belonging to Norway Spruce, European Larch, Swiss Pine, and Silver Fir (i.e., 50 trees per species). The classifier is trained using 120 trees and tested on an independent set of 80 trees. The proposed method outperforms the classification performance of the state-of-the-art method used for comparison.*

Part of the chapter appears in:

1. Harikumar, A., Paris, C., Bovolo, F., and Bruzzone, L., ' A novel data-driven approach to tree species classification using high density multireturn airborne lidar data.' , In SPIE Remote Sensing, International Society for Optics and Photonics, 2018 Sep, Berlin, Germany.

6.1 Introduction

Species knowledge at individual tree level can augment the accuracy of forest inventory, facilitate ecological [1], biodiversity [179], and climate change studies [180]. Every tree species has unique structural characteristics that can be used to classify them [32; 33]. A wide variety of species dependent structural features can be derived manually from ALS data both at stand level and the individual tree level. For instance, Holmgren et. al. [121] derived 20 statistical features from the spatial attributes of point cloud to classify the three major Nordic species. Increased number of manual features are derived from individual tree point cloud by Lin et. al. (42 features from 4 characteristic groups) [125], and Li et. al. (extracted 79 Features from 2 characteristic groups). In general, features proposed in the literature (see section 3.2) lack generality as most of them are designed for a specific forest type, species and sensor, i.e., the relevance of such features depends on the forest type and the species/sensor type. Thus, we propose an automatic data-driven feature extraction approach that fully takes advantage of the structural information provided by airborne LiDAR data, in order to derive features that are independent of the forest type, species and sensor for individual tree species classification.

In the proposed approach we approximate the entire crown using a cylinder, and divide it into smaller Elementary Quantization Volumes (EQVs) that allow a detailed/fine analysis of its structure. Every EQV contains a section of the crown/data points. Thus for each EQV, features that are representative of the crown section (e.g., the point count) can be derived from the attributes of the enclosed points. Three different elementary volume quantization strategies are proposed and compared in the experiments. However, quantization created a large number of features which, lead to large dimensional feature space, and is often problematic in parametric classification problems due to Huges effect [208]. Here, we perform species classification on the normalized set of features derived from the EQVs using a non-linear Support Vector Machines (C-SVM) classifier based on the histogram intersection kernel which has the ability to accurately manage the relevances of the input features to obtain maximum classification performance. A sensitivity analysis on the crown division parameters allows selecting the best elementary volume and its dimension for the considered tree species.

The structure of the rest of the chapter is as follows. The proposed method to tree species classification is elaborated in section 6.2. The details about the dataset, the experiments, and the results are mentioned in section 6.3. Finally, section 6.4 concludes the chapter.

6.2 Proposed Method

The proposed method assumes that a set of segmented individual tree crowns delineated using any existing state-of-the-art techniques [59; 166] is available. For each segmented crown, the proposed method first captures the spatial distribution of the LiDAR points within the crown by quantizing the crown-volume into EQVs. The attribute(s) of an EQV is used to accurately characterize the local crown structure. A feature vector that represents the 3D crown structure(s) is derived by progressively stacking the EQV attributes and used as input to a C-SVM classifier to generate the conifer species map. Fig. 6.1 shows the architecture of the proposed approach.

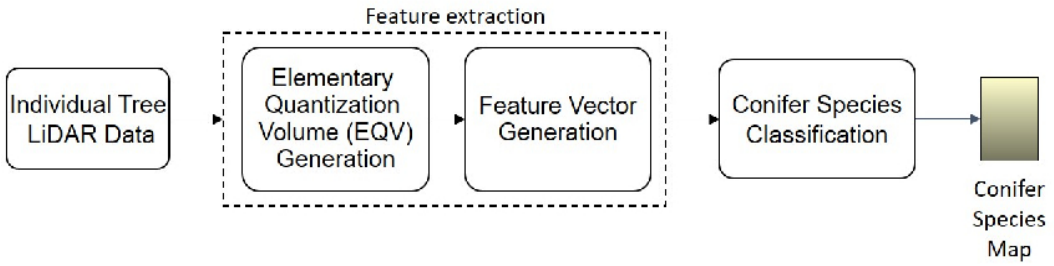

Figure 6.1: Flowchart of the proposed conifer species classification method.

6.2.1 Problem Formulation

Let $P = \{p_i\}, i = [1, N]$ be the set of LiDAR points corresponding to the segmented point cloud representing an individual tree, where p_i is fully described in a 3D Euclidean feature space by its x_i, y_i and z_i Cartesian coordinates. Let p_v be the highest point in the cloud, and g_v be its projection of the XY plane. Let L_t be the line connecting p_v and g_v, which represents the vertical axis of the tree point cloud. The maximum radius r_t of the tree crown is considered as the shortest distance between the point p_e and L_t, where p_e is the farthest point from L_t. In this chapter, a cylinder is considered for crown span modeling, considering its ability to approximately represent the bounding volume of the crown structure. The cylinder with the axis L_t and the base radius r_t can include the entire point cloud of a tree with height h_t. Fig. 6.2 shows the cylindrical parametric model used to define the bounding volume of the delineated LiDAR point cloud associated with a conifer.

6.2.2 Feature Extraction

The distribution of points in the space provides information about several crown structural characteristics. Thus, we derive a feature vector that includes maximum information

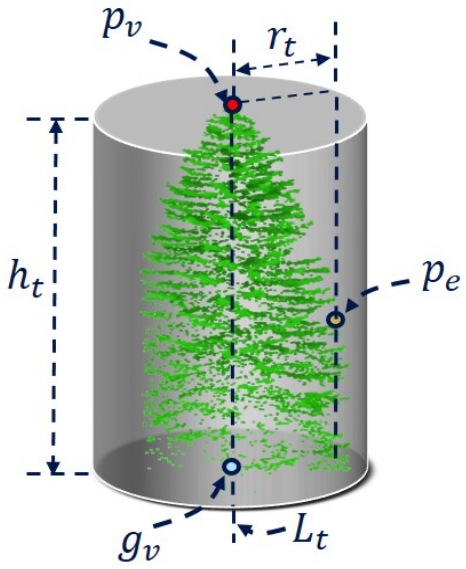

Figure 6.2: Cylindrical parametric model used to define the bounding volume of the segmented tree point clouds.

about the spatial variation of attribute(s) (e.g., the point density) within the point cloud. We define the space spanned by the cylinder using the angular $A \in [0, 2\pi]$, radial $R \in [0, \infty]$ and height $H \in [0, \infty]$ dimensions. Any point in the space can be defined by the vector $\vec{S}_i = [\alpha_i\ r_i\ h_i]$, where $\alpha_i \in A$, $r_i \in R$, and $h_i \in H$.

We extract detailed crown structural information in the point cloud by quantizing the space spanned by the cylinder along the A, the R and the H dimensions to derive smaller 3D volumes called as the EQVs (Fig. 6.3). Each quantization strategy captures a unique perspective of the crown. The first strategy performs quantization along the A and H dimensions and is referred to as EQ_1. Here the cylindrical volume (around L_t) is simultaneously quantized into A_N angular sections and H_N height divisions (Fig. 6.3a). This is useful for studying crown characteristics such as branch proximity/density (with one another) at different angular height EQVs around the tree stem. The second strategy EQ_2 performs quantizations of the cylindrical space around L_t into R_N radial sectors and the H_N height divisions simultaneously (Fig. 6.3b). This kind of quantization allows capturing the density variations along the radial direction of the crown, at different height-divisions. The third strategy EQ_3 simultaneously quantizes the cylinder into R_N radial, A_N angular, and H_N height divisions. Thus, it can be considered as the combination of EQ_1 and EQ_2. Quantization along each dimension can be done in a Tree Independent (TSI) or Tree Dependent (TSD) way. In the former, the EQV size along each dimension is made absolute (i.e.,tree independent). The absolute EQV size can be calculated using (6.1) where r_{max} and h_{max} are the maximum radius and height in the considered set of

trees. While the latter method determines the EQV size based on the maximum crown span of each tree, i.e., in a relative (i.e.,tree dependent) fashion. The relative EQV size can be calculated using (6.2).

$$\delta\alpha^{TSI} = A_N,\ \delta r^{TSI} = \frac{r_{max}}{R_N},\ \text{and}\ \delta h^{TSI} = \frac{h_{max}}{H_N} \tag{6.1}$$

$$\delta\alpha^{TSD} = \frac{2\pi}{A_N},\ \delta r^{TSD} = \frac{r_t}{R_N},\ \text{and}\ \delta h^{TSD} = \frac{h_t}{H_N} \tag{6.2}$$

Irrespective of the method, the number of height sections V generated after quantization is equal to A_N, R_N, and $A_N R_N$ for the EQ_1, the EQ_2, and the EQ_3 quantization strategies, respectively. Each EQV EQV_i, $i \in [1, VH_N]$, includes a unique set of points which is representative of the section of the crown that it encloses. One or more attribute(s) a_{EQV} can be derived from EQV_i to represent the properties of the considered crown section. We refer to the set of EQVs spanning the same space in the A and R dimensions as the Height Section. The attribute vector $\vec{a}_{EQV_v}$ of the v^{th} height section U_v, $v \in [1, V]$ (similar colored cells in Fig. 6.4a) is obtained by progressively stacking the $a^i_{EQV_v}$, $i \in I_v$ of the the individual EQVs in the height section into a vector $\vec{a}_{EQV_v} = [a^1_{EQV_v}, a^2_{EQV_v}, \cdots a^{H_N}_{EQV_v}]$. Here, I_v is the set of indices of EQVs in the height section U_v. The feature vector V_T is obtained by stacking individual $a_{E\vec{Q}V_v}, v \in [0, V]$ (Fig. 6.4b).

In our case, the point count is selected as a_{EQV} as it accurately represents the internal crown structure. However, the density of LiDAR data is different for each tree due to the geometric side effects of ALS scanning. Thus, the feature attribute V_T needs to be normalized. The first normalization strategy is the is a height section normalization, and is referred to as the Height norm. Here the normalization is performed independently for each attribute vector $\vec{a}_{U_v}$ belonging to individual height sections U_v, $v \in [1, V]$ in V_T. The attribute vector associated to the v^{th} height section $\vec{a}_{U_v}$ can be defined as $\vec{a}_{EQV_V}, v \in [1, V]$.

$$V_T = [\vec{a}_{U_1}, \vec{a}_{U_2}, \cdots \vec{a}_{U_V}], \text{where}\ \vec{a}_{U_v} = \left[\frac{\vec{a}_{EQV_v}}{max(\vec{a}_{EQV_v})}\right] \tag{6.3}$$

The second normalization, hereafter referred as Max norm, normalizes the V_T based on the maximum attribute value in the single tree feature vector as follows,

$$V_T = \left[\frac{[\vec{a}_{U_1}, \vec{a}_{U_2}, \vec{a}_{U_3}, ... \vec{a}_{U_V}]}{max([\vec{a}_{U_1}, \vec{a}_{U_2}, \vec{a}_{U_3}, ... \vec{a}_{U_V}])}\right], \text{where}\ \vec{a}_{U_v} = \vec{a}_{EQV_v} \tag{6.4}$$

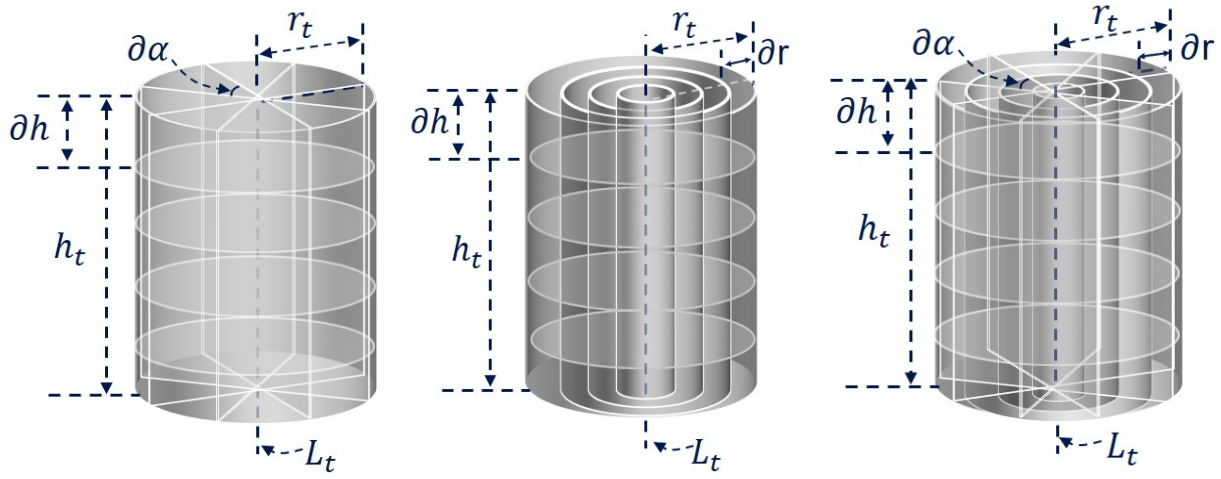

Figure 6.3: The proposed division strategies proposed includes, (a) EQ_1 , (b) EQ_2, and (c) EQ_3 quantization

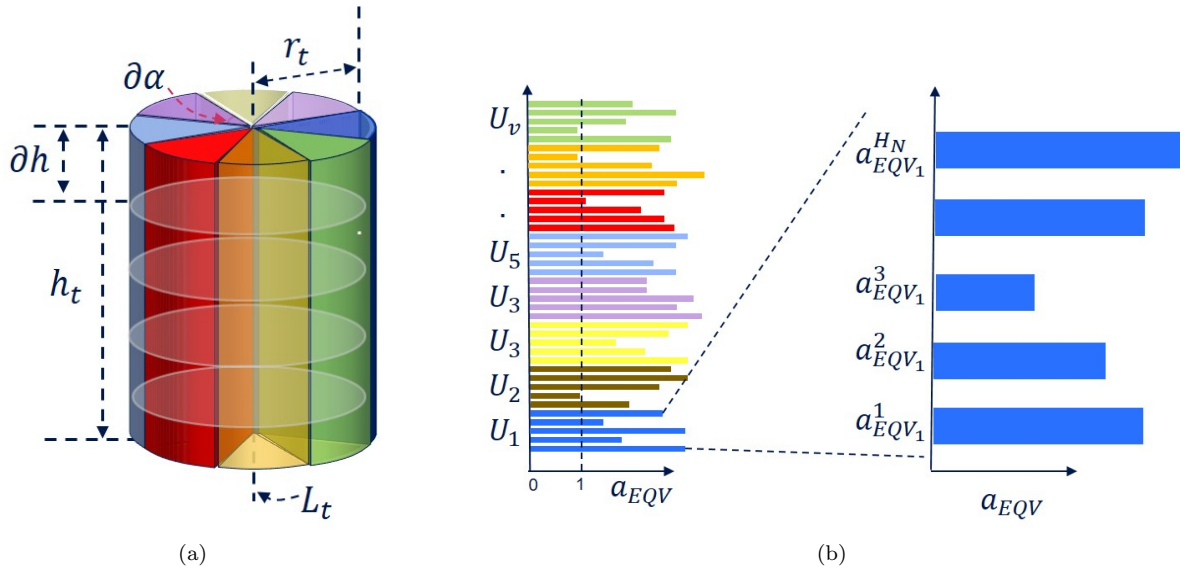

Figure 6.4: (a) Height sections generated from the EQ_1 quantization are shown in unique colors, and (b) The final feature vector obtained by stacking individual height sections.

6.2.3 Conifer Species Classification

The feature vector, where each element represents the point density of individual EQVs, encompasses the entire crown structural information. The features are automatically weighted using a generalized linear classifiers such as the C-SVM that focuses on finding the optimal separating hyperplane between the feature vectors of any two classes of in-

terest, while providing a measure of feature relevance [209]. The objective function of the SVM has the following dual form,

$$\begin{aligned} \underset{\zeta}{\text{maximize}} \quad & \sum_{i=1}^{l} \zeta_i - \sum_{i=1}^{l} \sum_{i=1}^{l} \zeta_i \zeta_j y_i y_j K_{hist}(v_i, v'_j) \\ \text{subject to} \quad & \sum_{i=1}^{l} \zeta_i y_i = 0, C \geq \zeta_i \geq 0. \end{aligned} \tag{6.5}$$

Here $x^i, i = [1 : l]$ and $y^i, i = [1 : l]$ are the training sample, and the corresponding labels, respectively. l is the number of training sample and ζ is the Lagrangian multiplier. In this case, a histogram intersection kernel [210] $K_{int}(.,.)$ is used considering its improved ability over other kernels (such as the RBF) to: a) assign maximum weights to key features, and b) reduce computational load in the feature projection step. The optimal hyperplane parameters α can be estimated by solving the maximization problem framed in (6.5).

6.3 Experiments and Results

6.3.1 Study Area and Dataset

The study area is a mountainous forest terrain in the municipality of Pellizzano located at about 40 km northwest of the city of Trento in Italy. The forest is mainly dominated by conifers and includes species such as Norway Spruce (Picea Abies), European Larch (Larix Decidua), Swiss Pine (Pinus Cembra), and Silver Fir (Abies Alba). The ALS data were acquired between 7^{th} and 9^{th} September 2012 using a Riegl LMSQ680i sensor operated at a scanning frequency of 400 KHz from an airborne platform flown at an altitude of 660 m with a speed of 100 Km/hr allowing acquisition of 10 - 50 points/m^2. The variation in point density is a result of altitude variation from 900 to 2000 m and the effect of scan direction. The flight was repeated several times to obtain very high density cloud of 50 to 200 points/m^2. All experiments were conducted on a set of 200 conifers, with 50 trees each belonging to Norway Spruce, European Larch, Swiss Pine, and Silver Fir. The classifier is trained using 120 trees and tested on an independent set of 80 trees (20 per species).

6.3.2 Experimental Results and Discussion

The shape and dimension of the EQVs are unique for each of the proposed quantization strategy. For all experiments, the angular $\delta\alpha$, the radial δr, and the height δh steps are obtained based on the quantization parameters (i.e., A_N, R_N and H_N). Here, $A_N \in [5, 45]$

(incremented by 5) and $R_N \in [2, 16]$ (incremented by 1) and $H_N \in [50, 160]$ (incremented by 10) define the range for searching the optimal quantization parameters. r_{max} and h_{max} are the maximum width and height of the crowns in the dataset, and are 9.1m and 43.5m, respectively. In the experiments, we tested the EQ_1, EQ_2, and EQ_3 quantization strategies using both the TSI and the TSD strategies. Finer divisions are avoided as less meaningful features representing smaller sections of the crown objects are generated. The optimal division parameters are estimated by performing a sensitivity analysis based on the species classification accuracy obtained on the independent set of 80 trees.

To assess the effectiveness of the proposed approach, we compare the method with a state-of-the-art (SoA) reference method which uses both internal and external crown geometric features to perform species classification [167]. The technique uses the point-proximity in the Euclidean space to identify point cloud segments that represent individual branches in the crown by employing a region growing technique. The growth stopping distance is d_s is set to be 0.25m, and is selected as the average of proximal-point-pair distance in the maximum density neighborhood (1m radius circle) of the crown. The six internal crown geometric features derived from individual clusters are used to derive the average internal crown characteristics. The seed point for region growing are obtained using a 3D convex hull with the shrinkage factor $\alpha = 0.5$ as in Harikumar et. al. [167]. Six external geometric features are also derived from parameters of regression fitted cone, and the 3D convex hull. Both the internal and external geometric features are provided as input to a C-SVM classifier to achieve classification. For both the proposed and the SoA method, the multiclass situation was handled using the one-versus-one classification strategy. The training and testing data corresponded to 60% and 40% of the total data. The test was carried out using the leave-one-out strategy in 5 fold cross-validation.

Table 6.1 shows the classification accuracy obtained for the different quantization strategies. Considering that $\delta\alpha$ in (6.1) and (6.2) are complementary to one another due to the constrained space in the A dimension i.e., $A \in [0, 2\pi]$, we considered $\delta\alpha$ as a TSI dimension throughout all experiments. However, there is no such relation for δr and δh and thus all the possible TSI-TSD combinations are tested. Table 6.1 shows the optimal quantization parameters derived from sensitivity analysis for the different quantization strategies. The maximum overall accuracy of 98.7% is obtained corresponding to the EQ_2 quantization with Max norm, where δh and $\delta\alpha$ are derived in a tree independent fashion, and δR derived in the tree dependent way. The high accuracy is mainly due to the inclusion of the relative height information of the trees in defining the cylindrical space dimensions, and hence including it in the feature vector. The importance of height information in the feature generation is also evident from the reduced performance for all the quantization strategies using the height based normalization which ignores the height

information. Table 6.2 shows the Producer Accuracy (PA), User Accuracy (UA), FScore (FS) and Overall Accuracy (OA), of the best-case scenario observed in 10 runs for the proposed method (PM) and the state-of-the-art (SoA) method.

Table 6.1: Optimal quantization parameters derived from sensitivity analysis for the different quantization strategies. $\delta\alpha$ is tree independent for all the strategies, while δR and δH can be selected to be tree independent/dependent.

Quantization Strategy			**Height Norm**				**Max Norm**			
	TSI	**TSD**	R_N	A_N	H_N	**Accuracy(%)**	R_N	A_N	H_N	**Accuracy(%)**
EQ_1	$\delta\alpha$	δh	-	25	90	56.2	-	40	150	56.2
	$\delta\alpha$ δh	-	-	5	150	61.2	-	15	110	56.2
EQ_2	$\delta\alpha$	δr,δh	2	-	90	96.2	3	-	70	97.5
	δr,$\delta\alpha$	δh	4	-	70	97.5	2	-	70	97.5
	δh,$\delta\alpha$	δr	2	-	60	95.0	3	-	60	**98.7**
	$\delta\alpha$,δr,δh	-	5	-	120	96.2	4	-	150	97.5
EQ_3	-	δr,δh	8	40	70	61.2	8	20	70	70.0
	δr,$\delta\alpha$	δh	5	20	60	66.2	6	25	70	66.5
	δh,$\delta\alpha$	δr	6	25	80	61.2	4	20	90	70.2
	$\delta\alpha$,δr,δh	-	4	20	70	60.0	5	35	80	65.0

Table 6.2: Producer Accuracy (PA%), User Accuracy(UA%), Fscore (FS%) and Overall Accuracy (OA) of the best case observed in 10 runs for: (a) the Proposed Method (PM), (b) the State-of-the-art Method (SoA).

Tree Species	**PM**			**SoA**		
	PA%	UA %	FS%	PA%	UA%	FS%
Norway Spruce	95.2	100.0	1.00	90.0	95.0	0.90
European Larch	100.0	100.2	1.00	95.0	86.3	0.95
Swiss Pine	100.0	100.0	1.00	85.0	94.4	1.00
Silver Fir	100.0	95.0	0.97	100.0	100.0	0.90
OA%		98.7			93.7	

In general, the proposed method addresses the problem of deriving effective crown geometric features for tree species classification. Here the optimal features are automatically derived from data rather than relying on a species, area, and forest-specific method/-model. This proposed data-centric way of deriving geometric features facilitates accurate

species classification for any set of species, area, and forest type.

6.4 Conclusion

In this chapter, a data-driven approach to tree species classification for high resolution multireturn ALS data is proposed. The individual tree crown span is approximated using a cylindrical parametric model. The space enclosed by the cylinder is quantized into finer Elementary Quantization Volumes (EQVs) to perform a detailed structural analysis of the crown. Three quantization strategies including the angular EQ_1, the radial EQ_2, and the radial-angular EQ_3 have been compared. A feature vector is obtained by progressively stacking the an attribute derived from the point-data enclosed by the individual EQVs. For each quantization strategy the feature vector was obtained by using a tree independent and tree dependent way. The variation in classification performance for two different feature vector normalization methods, including the global and height section norm, is also evaluated. The result obtained on a set of 200 trees belonging to four different conifer species proves that the EQ_2 quantization strategy with global normalization of the feature vector is optimal for classification of the considered tree species. Here an improvement of 5% in the classification accuracy is achieved with respect to the SoA method.

Chapter 7

Crown Geometric Modeling based Tree Species Classification in Multiscan TLS data

Terrestrial Laser Scanning (TLS) remote sensing systems acquire a huge number of point sample that contain very accurate and detailed three dimensional (3D) information of tree structures, and thus of individual tree species. The proposed method leverages on the fine internal and external crown structural information in TLS data to achieve species classification. We remove noise and stem points in TLS data using a novel voxel neighbourhood density-based technique. Internal and external crown geometric features derived from the branch level, and the crown level, respectively, are provided to a non-linear Support Vector Machines (SVM) to achieve species classification, and evaluate feature relevance. All experiments were conducted on a set of 75 manually delineated trees belonging to spruce, pine, and birch species.

7.1 Introduction

An accurate individual tree level species information is indispensable for an accurate and comprehensively mapping of forest properties [211]. Errors in species classification can result in erroneous conclusion on forest ecological studies [1], actuate wrong management decisions on wood procurement, and bias forest conservation policies. Terrestrial Laser

Part of the chapter appears in:

1. Harikumar, A., Xinlian, L. and Bovolo, F. ' An approach to tree species classification using voxel neighborhood density based subsampling of multiscan terrestrial LiDAR data.' , Geoscience and Remote Sensing Symposium (IGARSS), IEEE, 2018 Jul, Valencia, Spain.

Scanners (TLS) capture dense point cloud containing fine details of tree-structures including stem, crown, and leaf from a ground perspective, often making TLS a reliable means to reference data collection at the individual tree level [212]. TLS data are successfully used to derive accurate estimates of tree parameters including diameter at breast height (DBH), [213], leaf area density [214], vertical crown profile [215], tree growth [216], and biomass [217]. In particular, high density TLS data contains structural details of branches which are the building blocks of tree crown [35; 34]. However there has been no or minimal efforts towards the development of methods that can harness the potential of branch level structural differences to achieve species classification (see section 3.2). Also the difference in TLS data-acquisition perspective over ALS has consequences in the resulting point distribution modes, hence limiting the applicability of ALS-data-based methods (at least in their original form) in extracting structural information from TLS data [25]. Thus, there is a need to develop novel TLS data based methods that can accurately and efficiently model the internal crown geometry, for species classification.

Thus, in this chapter, we propose a novel technique that accurately models both the internal and external crown characteristics from multiscan TLS data, even at reduced point densities. Six novel branch geometric features derived from geometric-shape-fitting on the branch points are used to define the internal crown characteristics. The external crown geometry is characterized using a set of six state-of-the-art features that are derived from the entire tree point cloud. The rest of the chapter is organized as follows. Section 7.2 describes the proposed method. The experiments and results are reported in section 7.3. Section 7.4 concludes the chapter.

7.2 Proposed Tree Species Classification Method

The chapter proposes an approach to tree species classification using both internal and external crown structural information derived from very high density multiscan TLS data of an individual tree. The proposed method assumes that: a) branches are basic building blocks of individual crowns; and every species has a unique (sub)branch geometric characteristics (Fig. 7.4); b) they have a leaved section and a non-leaved wooden branch section; c) branches are dense towards their inner section as density decreases towards their boundaries; thus the overall branch geometry can be defined using points in the inner section.

Data Subsampling

Input TLS point cloud is subsampled in order to: a) remove isolated and noisy points; b) remove the points corresponding to the stem and the non-leaved branch sections; c) reduce

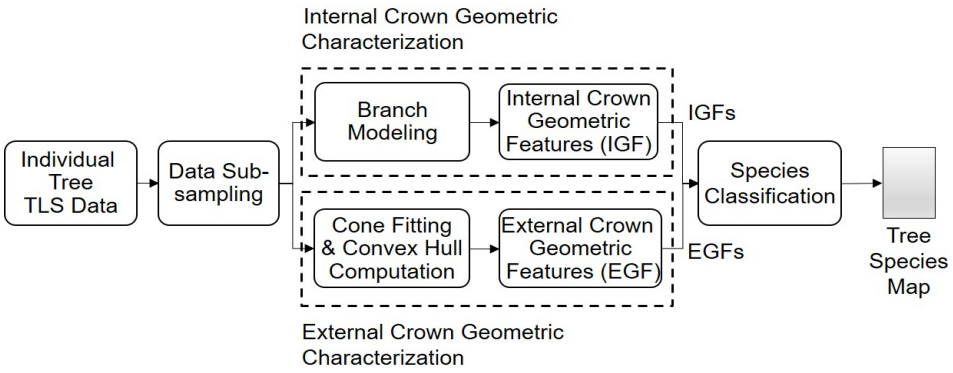

Figure 7.1: Block scheme of the proposed crown geometry based species classification approach.

the overall number of points to mitigate computational overhead. Subsampling is achieved by voxelizing the entire 3D Euclidean space spanned by the point cloud, and considering only the data points within voxels which have six immediate non-empty voxels-neighbours in their first order neighborhood. A voxel cell is referred to as non-empty when there is at least one data point within it or on its boundaries.

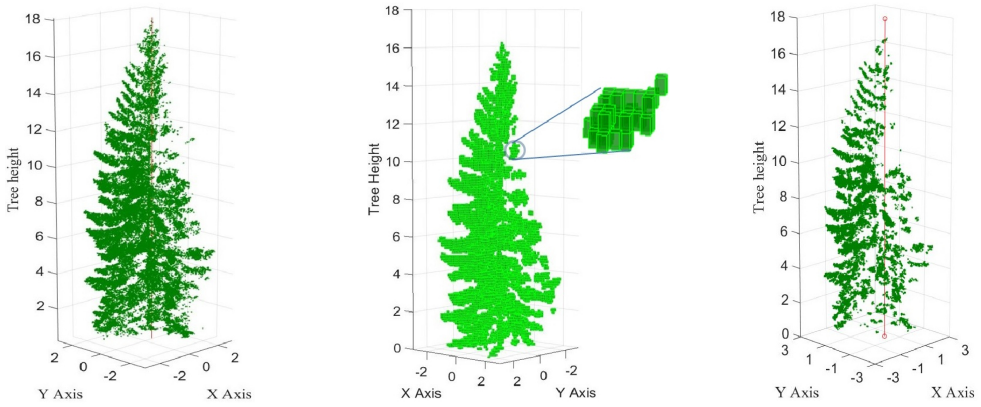

(a) (b) (c)

Figure 7.2: a) Original point cloud, b) Voxelization, c) Subsampled point cloud, for an example Spruce tree.

7.2.1 Internal Crown Geometric Characterization

The subsampled TLS point cloud is constituted of $P = \{p_1, p_2 \ldots, p_N\}$ LiDAR points where $p_n \in P$ is the spatial position of each point. Here, p_n is fully described in a 3D Euclidean feature space by its x_n, y_n and z_n Cartesian coordinates. B is the total number of branches in the crown. Each branch can be modeled as a cluster of points (referred to as branch cluster) $c_b = \{p_n; n \in I_b\}$, where I_b is the index set of all the LiDAR points

belonging to c_b.

a) *Branch Modeling:* Individual branch clusters are obtained by performing region growing, seeding from the (sub)branch tips identified using a convex-hull based technique [167]. The convex hull vertices are the (sub)branch tips, and $\alpha \in [0, 1]$ controls the compactness of the hull, with 1 and 0 being most and least compact, respectively. The region growing controlled by the growth stop parameter t is performed starting from individual branch tips to identify branch clusters in P. It is worth recollecting here that a branch cluster represents the branch geometry approximately. We model a (sub)branch b represented by cluster c_b using the ellipsoid. The ellipsoid has enough degrees of freedom to model the strong differences in the geometry of branches between coniferous and deciduous trees (Fig. 7.3). Further, it satisfies the fundamental assumptions that, the branches of most tree species are: a) tapered towards the exterior crown; b) leafless or with less leaves toward the interior of the crown/stem. The general equation of an ellipsoid is given in (7.1).

$$\begin{aligned} Ax^2 + By^2 + Cz^2 + 2Dxy + 2Exz + 2Fyz + 2Gx \\ +2Hy + 2Iz = 1 \end{aligned} \tag{7.1}$$

The parameter vector $\vec{v_b} = [A\ B\ C\ D\ E\ F\ G\ H]^T$ of the ellipsoid can be obtained from least square fitting, i.e., $(\Omega^T\Omega)^{-1}\Omega^T l$. Here Ω is the design matrix [218] obtained using the branch cluster, and l is a unit vector.

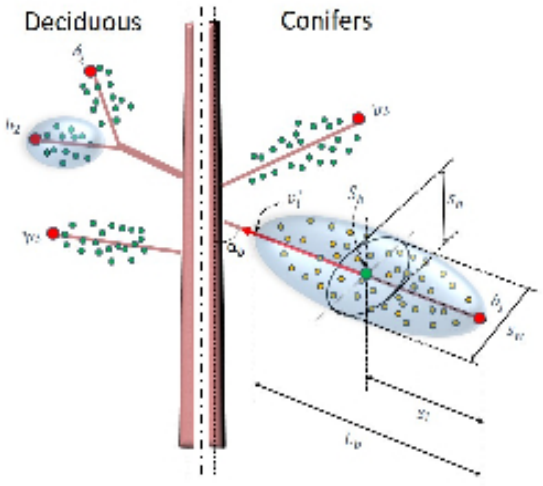

Figure 7.3: Proposed branch model. The Green and the Red points represent the LiDAR points and branch tips, respectively.

b) *Internal Crown Geometric Features (IGFs):* We use nine parameters of the regression fitted ellipse to extract six geometric properties of a branch. The parameters

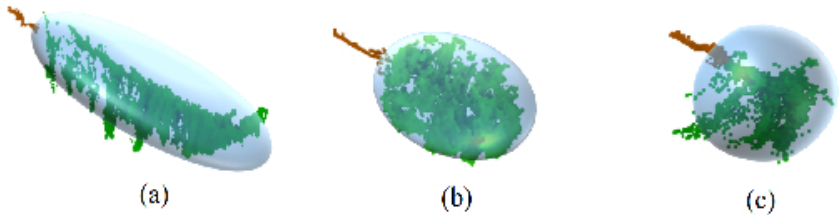

Figure 7.4: Least square fitted ellipse obtained for branches of Spruce (conifer), Pine (conifer), and Birch (deciduous),

include, the three coordinates of branch center $S^b = [s_x^b s_y^b s_z^b]$, the three semi-axis dimensions (s_l, s_w, s_h), and the three semi-axis directions (v_l, v_b, v_h). On the one hand, the angle made by v_l with the horizontal plane is the branch slope α_b, while on the other hand twice its dimension (i.e.,$2s_l$) is the branch length l_b. The sum of ratio of semi-axis dimensions along the horizontal and vertical branch planes k_b is a measure of branch compactness along v_l. A k_b closer to 0 corresponds to a compact branch along v_l, and larger values occur for branches with greater spread along v_l. The spread of the branch along the v_b is the branch width. The symmetry of the branch p_b along the v_l is measured as the ratio of semi-axis dimensions along v_b and v_h. Branches that are highly symmetric along v_l produce values closer to 1. The number of points corresponding to a branch cluster quantify the density of the branch d_b. The median value for each geometric feature is taken as the IGFs for a tree. The IGFs are described in Table 7.1, where $M(.)$ is the median operator. It is worth noting that the B_l and B_k are divided by the tree height H_T, and B_n is divided by N, to achieve feature value normalization. Fig. 7.4 shows examples of the least square fitted ellipsoids for example branch clusters (i.e., branches) with different geometric shapes.

7.2.2 External Crown Geometric Characterization

The external crown geometry is captured using six state-of-the-art EGFs derived from parameters of: a) regression fitted cone, b) convex hull, on the tree point cloud. The EGFs used include: 1) Convex hull volume to the number of points N within the crown (T_v); 2) Difference between the volume of the convex hull and the fitted cones (T_d); 3) Root mean square error associated with the regression cone fitting (T_ϵ); 4) Standard deviation of orthogonal distances from each data point the convex hull (T); 5) Ratio of the crown height H_C and the tree height H_T; and 6) Average proximity of data points to the nearest convex hull facet (T_l). Table 7.2 shows the EGFs.

Table 7.1: Proposed internal crown geometric features

Feature Id	Description	Equation
B_α	Overall branch slope	$M(\alpha_b), b \in [1, B]$
B_l	Overall branch length	$M(\frac{l_b}{H_T}) = M(\frac{2s_l}{H_T})$, $b \in [1, B]$
B_k	Overall branch compactness	$M(\frac{k_b}{H_T}) = M(\frac{s_b+s_h}{s_l})$, $b \in [1, B]$
B_w	Overall branch width	$M(\frac{w_b}{H_T}) = M(\frac{S_b^b}{H_T})$, $b \in [1, B]$
B_s	Overall branch symmetry	$M(p_b) = M(\frac{S_b^b}{S_h^b})$, $b \in [1, B]$
B_n	Overall branch density	$M(\frac{d_b}{N_b})$, $b \in [1, B]$

7.2.3 Species Classification

The performance of the classification is evaluated by providing the twelve geometric features (i.e., the six IGFs and the six EGFs) to a Support Vector Machines (SVM) classifier. The feature weights $W = \{w_i, i \in [1, F]\}$ are associated with the optimal SVM hyperplane are the feature relative relevance. Here, w_i is the feature weight of the i^{th} feature, and F is the number of features.

7.3 Experiments and Results

7.3.1 Study Area and Dataset

The high density multiscan TLS data used in the experiments is of a boreal forest in Evo located at the south of Finland, with geographic center point at $61^0 19'$ N and $25^0 11'$ E. The major species include both conifers and deciduous trees, i.e., the Scots Pine (SP), the Norway Spruce (NS) and the Silver Birches (SB). The data was acquired in July

Table 7.2: External crown geometric features

Feature Id	Description	Equation
T_v	Volume of the convex hull by the total number of points.	$\frac{V_{hull}}{N}$
T_d	Volumes difference between the cone and the covex hull to the convex hull volume.	$\frac{V_{hull}-V_{cone}}{V_{hull}}$
T_ϵ	Regression cone fit error.	$\frac{RMSE_{Cone}}{N}$
T_l	Average of distance d_n of each LiDAR point to the closest facet of convex hull	$\frac{\sum_{n=1}^{N} d_n}{N}$
T_σ	Standard deviation of orthogonal distances from each point to the convex hull.	$\sqrt{\frac{\sum_{n=1}^{N}(p_n-T_l)^2}{H_T}}$
T_h	Crown height divide by Tree height	$\frac{H_C}{H_T}$

2014 using Leica HDS6100 with a distance measurement accuracy and point spacing of ±2mm and 15.7mm, respectively, at 25 meters. The beam diameter at exit is 3mm, with a divergence as low as 2mrad. A total of 75 manually delineated trees, with 25 trees each belonging to SP, NS and SB, are used to evaluate the species classification performance.

7.3.2 Experimental Result and Discussion

The voxel size for data pruning was set to 10cm based on the point density of the TLS data. The branch tips are identified using the parameter α of the convex hull that was optimally set to 0.5 by testing on a large set of trees. The α tuning criteria used here is the minimization of the omission and commission errors associated with the branch tip detection. The threshold distance t for the region growing was taken as the mini-

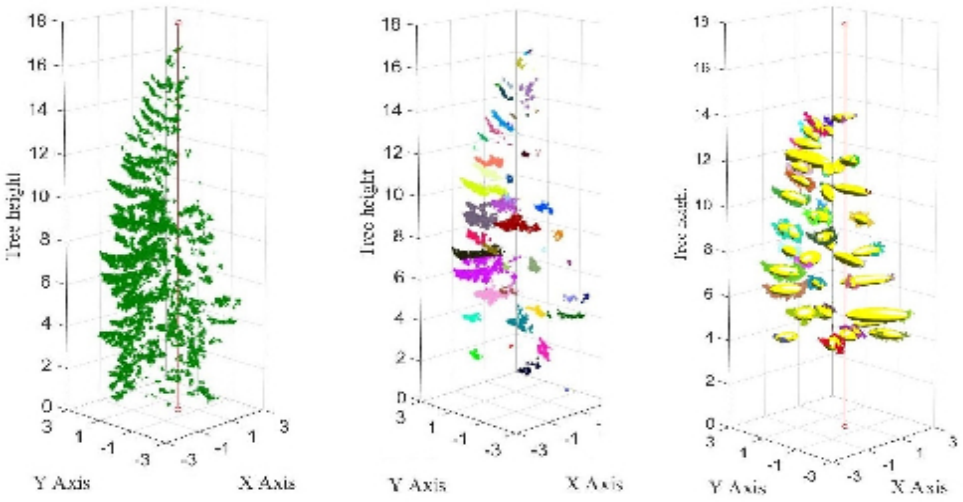

Figure 7.5: The pruned point cloud, the detected branch clusters, and the regression fit ellipsoids (NS tree).

mum distance between two points within the voxel with the lowest point density in the subsampled data.

The classification was done using a non linear SVM (with RBF kernel) using 60% and 40% of the data for training and testing, respectively. The C and γ of the RBF kernel were optimally selected as 2^6 and 0.01, respectively. We compare the classification performance of the proposed method with a state-of-the-art technique which models the internal crown characteristics using a Principal Component Analysis based branch modeling technique [167]. The confusion matrix for the best case scenarios (in 25 trials) for the proposed and state-of-the-art species classification techniques are provided in Table 7.3. The overall accuracy (OA) obtained for the proposed method and the state-of-the-art method is 80.0% and 73.3%, respectively. Here, PA and UA corresponds to the user accuracy and the producer accuracy, respectively. Fig. 7.6 shows the relevance of the six IGFs and the six EGFs. The w values obtained from SVM shows that the IGFs are more relevant than the EGFs in species classification. Biologically, different tree species have unique branch geometic shapes [32; 33]. However, accurately modeling the branches to model the difference is challenging. The higher relevance of IGFs over EGFs proves the ability of the proposed features to accurately model the difference in overall branch shape for different species. Although, the overall branch slope B_α is a good characteristic for classifying the considered spices, the large variation in branch slope across different heights makes it a feature of low importance. The overall branch length B_l largely varies in different trees due to presence of broken branches and lack of branches in some sections of tree, making it a less relevant feature in this case. However, the higher weights on the B_w and B_s is in

accordance with the fact that the branch width and symmetry of branches are different for Spruce, Pine, and Birch. However, it is worth noting that the relevance of geometric features might differ for different set of species, as key structural differences might be different for different set of species and forest types. In other words, the feature relevance depends on the species/forest type. The proposed method is a clear demonstration for the forest community, on the usability of structural information in TLS data for species classification.

Table 7.3: Confusion matrix for the best case accuracy.

Class	**Proposed method**				**State-of-the-art method**			
	Reference			**UA**	**Reference**			**UA**
	NS	**SP**	**SF**	**(%)**	**NS**	**SP**	**SF**	**(%)**
NS	9	1	0	90.0	8	2	0	80.0
SP	2	8	0	80.0	1	7	2	70.0
SF	3	0	7	70.0	2	1	7	50.0
PA (%)	64.2	88.8	100.0	**OA (%): 80.0**	72.7	70.0	77.7	**OA (%): 73.3**

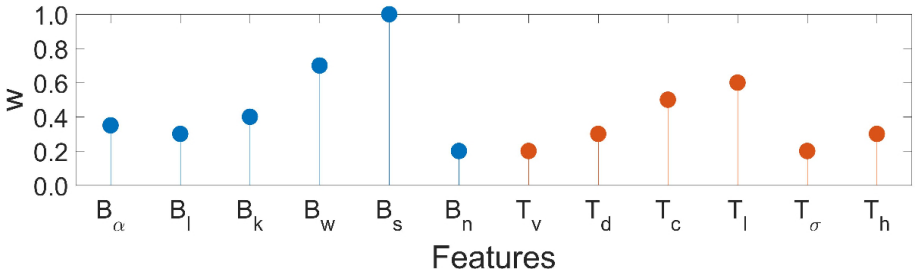

Figure 7.6: The relevance of crown geometric features

7.4 Conclusion

The chapter proposes a species classification technique using individual tree TLS data. A novel voxel neighborhood based data subsampling is performed to mitigate noise and redundancy. Six novel IGFs, and six state-of-the-art EGFS derived from the individual tree point cloud are used to perform species classification. A maximum accuracy of 80.0% is obtained in classifying Spruce, Pine, and Birch species. Future work includes the use of 3D texture information in the TLS data to improve species classification accuracy.

Chapter 8

Stem Localization and DBH Estimation in ALS data

Accurate stem location and stem Diameter at Breast Height (DBH) are critical to accurate biophysical parameter estimation at the individual tree level. High density small footprint multi-return Airborne Laser Scanning (ALS) data contain structural information of crown structures including foliage, branches and stem. Here, we identify data point sample which are likely to be reflected from the conifer stem surface using a state-of-the-art internal crown geometric modeling technique. The location of the stem is accurately estimated by analyzing horizontal divisions of the crown. The 3D conifer stem is best approximated by fitting a geometric shape on the stem surface points, and the DBH is directly estimated from the parameters of the fitted model. The experiments were conducted on a set of 60 trees belonging to three dominant European conifer species. The estimated stem location and DBH prove the method to be accurate.

8.1 Introduction

A systematic and periodic collection of accurate individual tree parameters such as the tree/crown height, the stem location, the stem Diameter at Breast Height (DBH), and the biomass on forests is highly essential to study the ecosystem, biodiversity, resources, and health of forests. By using remote sensors on airborne platforms, it is possible to collect a huge amount of forest data at the individual tree level. Remote sensing has become a highly appreciated inventory technique, due to the ability to periodically, economically,

Part of the chapter appears in:

1. Harikumar, A., Bovolo, F., and Bruzzone, L., 'An approach to conifer stem location and modeling in high density airborne LiDAR data', Proc. SPIE 10427, SPIE Conference on Image and Signal Processing for Remote Sensing XXIII, Warsaw, Poland, 11-13 September 2017.

and accurately collect individual tree level data over large forest areas. Light Detection and Ranging (LiDAR) remote sensing is one of the very few technologies that allows 3-dimensional (3D) data acquisition of tree structures. A high density multi-return ALS system acquires fine 3D structural data by combining the round-trip time of a highly directed laser beam, the orientation data from an Inertial Navigation System (INS), and the position information from the Global Positioning System (GPS). State-of-the-art ALS systems such as the Lieca ALS680i can capture up to 8 discrete returns or waveform-data against a single laser pulse, generating dense and accurate point sample (about 50 points/m^2) that contain a lot of structural information of foliage, branches and stem.

Accurate stem location is fundamental for the calibration of the individual tree level inventory data, as it is the main matching criterion between reference and Airborne Laser Scanning (ALS) data of individual trees. The stem location is the stem center at the base of the tree, and is usually measured by field campaigns. Matching techniques as in [2] can be used to link a reference stem location with an estimated one. However, this requires the stem location to be accurately estimated from the ALS data. The 2D Canopy Height Model (CHM) based techniques estimate the stem location on the assumption that the stem exists directly below the treetop which are detected based on local maxima in the CHM [59]. However often: a) conifer stem grows tilted, and b) a longer branch tip near the tree top is mistaken for the real tree top leading to poor positioning. Techniques that exploit 3D information in ALS data also exist. For example, by hierarchically clustering the LiDAR points below the crown-base height using a histogram analysis, and reconstructing the stem with a robust Random Sample Consensus (RANSAC) based estimation of the stem points, Reitberger et al., located stems with accuracies close to a meter [83]. The assumption here is that the point density is maximum near the canopy and decreases towards the ground. Lu et. al. [86] exploited the higher reflectance associated with the stem points to select them and used them as seeds in a bottom-up segmentation approach to identify the stem. However, reflectance is often not a reliable attribute for detecting the stem.

State-of-the-art methods (see section 3.3) estimate DBH in an indirect fashion by using species-specific allometric models to characterize the relationship between crown parameters and the DBH. Whatsoever, allometric models are designed based on the data of a particular forest area and type and hence often show reduced performance in different areas and types of forests. Given the large amount of structural information in ALS, there is a scope to estimate DBH in a more direct fashion. One such approach is to exploit the stem and internal crown structure (e.g. the branch direction with respect to the stem) in ALS data to estimate DBH. Thus, we propose a method that can: a) accurately estimate the position of stem even in the presence of occluding branches/foliage, and b) directly

estimate DBH from the 3D model of stem without prior knowledge of species.

The rest of the chapter is organized as follows. Section 8.2 describes the proposed methodology. The experiment performed and the the analysis of results are stated in Section 8.3. Section 8.4 concludes the chapter.

8.2 Proposed Method

The proposed method assumes that the point cloud associated with individual trees are extracted using any state-of-the-art crown delineation technique such as in [166]. For each tree, the LiDAR data points representing the stem are identified and are used to accurately estimate the stem location and the DBH. The flow chart of the proposed 3D stem detection and modeling technique is provided in Fig. 8.1.

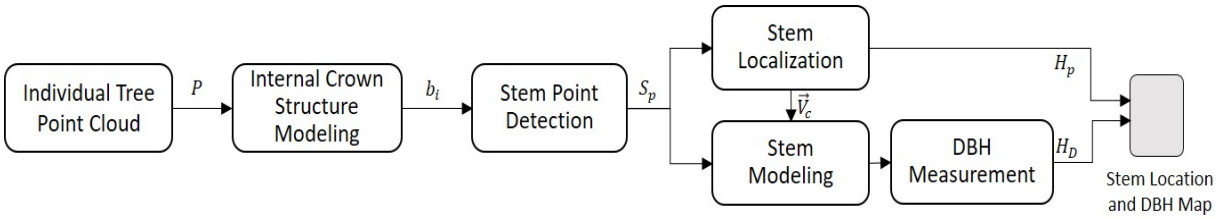

Figure 8.1: Block scheme of the proposed stem localization and modeling approach.

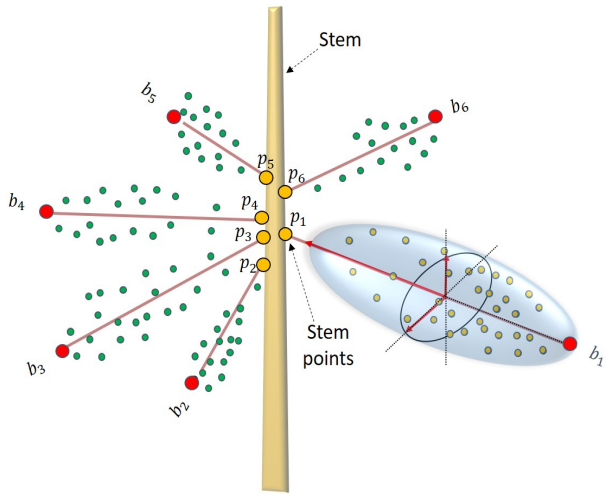

(a)

Figure 8.2: Internal crown structure model showing the branch tips (red dots) and the corresponding stem points (yellow dots).

8.2.1 Internal Crown Structure Modeling

The modeling of the internal crown relies on the following general structural characteristics of conifers: a) straight and circular (in horizontal cross-section) stem with maximum diameter at the base which decreases towards the top, and b) linear and compact branches that grow from the stem outward in directions approximately perpendicular to it. Let $P = \{p_i \in R^3, i = 1, 2, ..., N\}$ be the set of N LiDAR points in the input tree point cloud, where p_i is the 3D Cartesian coordinate set $\{x_i, y_i, z_i\}$ of the i^{th} point in the Euclidean space. Every point in P is uniquely associated to one of the B branches $b_i, i \in [1, B]$. The cloud of points r_b associated with the branch b_i is referred to as the branch cluster. Here, the B branch clusters are detected using a region growing technique recently proposed in the literature [167]. For each cluster, the growing starts from the branch tips point, proceeds towards the stem, and stops when the local point neighborhood density G_n calculated using (8.1) falls below a threshold. Any unassigned point is assigned to the nearest cluster based on the proximity in the Euclidean space.

$$G_n = \frac{Y_B}{\sum_{i=0}^{K} D_{ni}} \tag{8.1}$$

Here Y_B is the number of nearest neighbors which is considered as a constant. The individual branch tips $p_t^b, t \in [1\ B]$ (i.e., seed points) are detected using a convex hull based technique [167]. The assumption is that the boundary points of a convex hull fitted to the entire point cloud of a conifer correspond to the branch tips. Fig. 8.2 shows a representation of the proposed branch model.

8.2.2 Stem Points Detection

We refer to data points corresponding to the laser reflections from the surface of the stem (or the ones very near to it), and branch-stem junctions (i.e., the section of a branch meeting the stem) as the stem points. For every conifer branch b_i, the point in r_{b_i} that is maximally away from the respective branch tip is very likely to be a stem point. The set of stem points $S_p = \{p_i\}, i \in I_m$, where I_m is the set of indexes of the points that are farthest from the respective branch tip of the B branch clusters, closely represent the 3D stem. However, stem points that are: a) below 25% of tree height H_T, (considering the low point density in the lower section of the crown), and b) more than a threshold distance T_r away from the regression fitted line on S_c (to remove incorrectly detected stem points that are further away from the stem), are not used in stem position and DBH estimation. We choose T_r as half the maximum DBH (at 1.3 m) estimate among all the trees in the dataset, derived using the generic allometric model (8.2) [176],

$$DBH_i = f(b_0 + b_1\sqrt{h_i} + b_2\sqrt{d_i})^2 + var(\epsilon) \tag{8.2}$$

where DBH_i is the estimated DBH (in mm) of the i^{th} tree, and h_i and d_i are the tree height (in dm) and the crown diameter (in dm), respectively. As non-linear transformations were used for the dependent variables, the DBH estimates will be biased, and the effect are mitigated by bias correction [177; 176].

8.2.3 Stem Localization

As mentioned before, conifer stems often grow tilted and hence multiple stem centers need to be estimated along the tree hight profile in order to define the 3D stem location and slope. Here, we estimate a set of stem centers $S_c = \{s_i\}$, $i \in [1,\ B]$ derived from N_s equal-height section of the vertical crown profile. We consider the median of the stem points s_i in every height-section as the stem center in the respective section. A regression fitted line V_A on S_c follows the axis of the stem. The stem location is obtained as the point where the regression fitted line crosses the horizontal plane. The angle between the regression fitted line and the Z-axis is defined as the tilt of the stem, and is a addition detail derivable of the proposed approach.

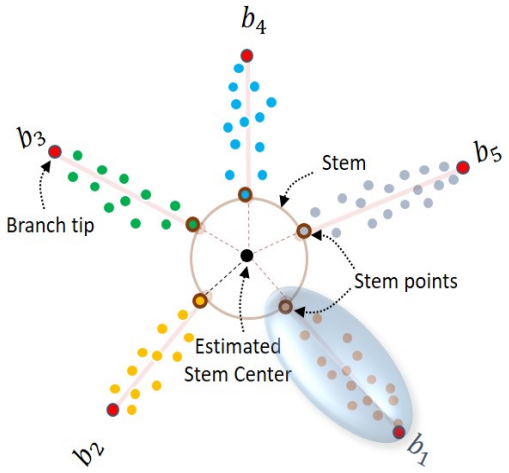

Figure 8.3: Branch clusters corresponding to the stem points in a height section are shown in unique colors. The Black dot at the center is the estimated stem location within the section.

8.2.4 Stem Modeling

The stem points are also representative for the 3D stem. Thus, we model the stem using a 3D cone that optimally fits all the stem points on its surface. The conical model is

chosen as it is one of the simplest geometric shape that approximates the stem. The cone is specified by eight parameters: the Euclidean position parameters of a point $p_m = [x_m\ y_m\ z_m]$ on the vertex of the cone, the three axis direction vector $\vec{V_c} = [u\ v\ w]$ pointing along the direction of decreasing cone radius, and the cone apex angle α. Optimal cone parameters can be found by minimizing D, which is the sum of all distances of each b stem points to the cone [219].

$$D = \sum_{i=1}^{b} e_i\ cos(\alpha/2) + f_i\ sin(\alpha/2) - t \tag{8.3}$$

Subjected to the constraints:

$$z_m = s_0 - ux_m - vy_m \tag{8.4}$$

$$w = 1 \tag{8.5}$$

where, e_i is the distance of the point p_i from the line along $\vec{V_c}$, f_i is the distance of the point p_i from the plane specified by p_0 and $\vec{V_c}$, and the constant t is the distance from the point p_m perpendicular to the nearest local cone surface. The constraint (8.4) forces the best fit cone to contain the circle centered at the point at height $Z_m/2$ in the cone axis, with radius equal to the mean distance of the points to the axis. In other words, (8.4) forces the cone axis to be closely aligned with the centroid of the point cloud. Here the $s_0 = \overline{z} - \overline{r}\ tan(\alpha/2)$, where $\overline{z}$ is the mean of z values of the LiDAR points, and $\overline{r}$ is the mean of $R \in \{r_i,\ i = [0\ N]\}$, where $r_i = \sqrt{x_i^2 + y_i^2}$. The constraint (8.5) ensures that the axis of the cone is proximal to the positive z axis. The optimal cone parameters are obtained using a Gauss-Newton algorithm [219].

8.2.5 DBH Estimation

The fitted cone with base radius r is an approximation of the 3D conifer stem. The point at the cone apex p_m together with the stem points determine the direction vector $\vec{V_c}$ of the fitted cone. Fig. 8.4a and 8.4b shows the fitted cones for a straight and a titled stem, respectively. For all cases, the diameter at breast height S_{DBH} is calculated at a distance η from the base of the cone using (8.6).

$$S_{DBH} = 2r\left(\frac{z_m - \eta}{z_m}\right) \tag{8.6}$$

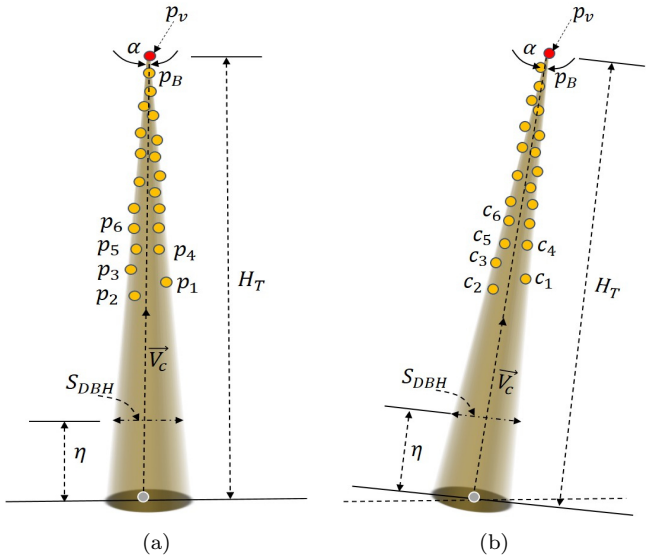

Figure 8.4: Cone fitted on the stem points for (a) straight and (b) tilted stem. The cone apex and stem points are shown as red and yellow dots, respectively.

8.3 Experiments and Results

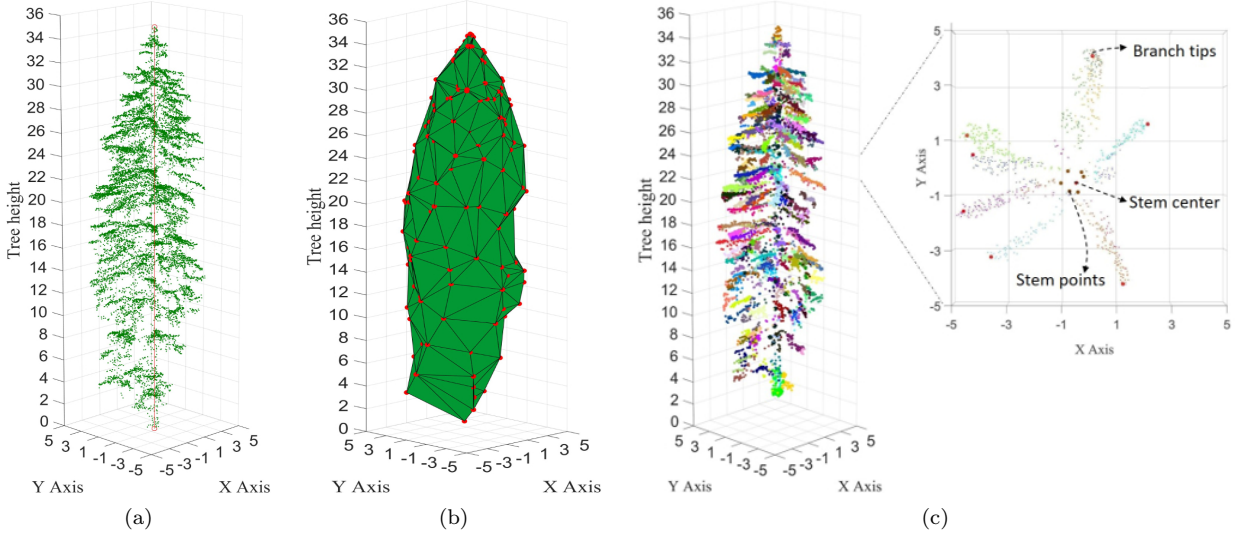

Figure 8.5: (a) The LiDAR point cloud of conifer, (b) The branch tips detected (red dots) using 3D convex hull fit. (c) Stem points (brown dots) in a sample height-section (brown dots).

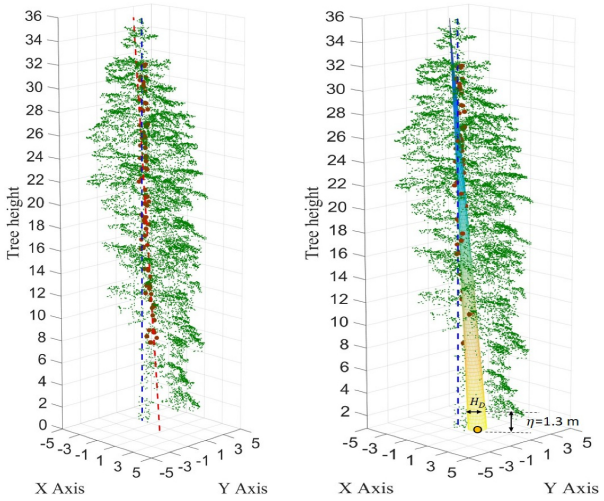

Figure 8.6: The stem axis obtained using (a) the proposed (red dotted line) and the state of the art method (blue dotted line). The stem model in (b) is used to obtain the DBH.

8.3.1 Study Area and Dataset

The study area is a mountanious forest terrain (with altitude varying from 900 to 2000 m) in the municipality of Pellizzano located north of the city of Trento in Italy. The forest in the area is dominated by conifers and include species such as Norway Spruce (Picea Abies), the European Larch (Larix Decidua), and the Swiss Pine (Pinus Cembra). The high density ALS data of the forest were acquired using a Riegl LMSQ680i sensor between 7^{th} and 9^{th} September 2012. The instrument was operated at a scanning frequency of 400 KHz from an airborne platform flown at an altitude of 660 m with a speed of 100 Km/Hr. This allowed acquisition of 10 - 50 points per meter squared in a single scan. The laser beam width of less than 0.5 mrad restricted the maximum laser footprint span to approximately 0.3 m. The flight was repeated several times to obtain very high density cloud of 50 to 200 points/m^2. A set of 60 trees belonging to the three conifer species, with average point density of more than 25 points per meter cube, and for which the stem location and Diameter at Breast Height (DBH) were recorded from field visits, were manually segmented and used in our experiments as ground truth data. The trees are divided into low density ($\leq$ 20 point/m^2) and high density ($>$ 20 point/m^2) datasets based on the maximum point density. These datasets used to test the robustness of the proposed method to variation in LiDAR point density which affects the number of available stem-points.

8.3.2 Experimental Result and Discussion

The $\alpha_{hull} \in [0, 1]$ parameter of the convex hull was optimally selected to be 0.5, to minimize the omission and commission errors associated with branch tip detection. The region growing threshold distance τ was set as 0.2 for all trees and was decided based on the LiDAR data point density, and Y_B was set to 5. Figure 8.5 shows the branch tips, the branch clusters, and the stem points, obtained for an example Norway Spruce. N_s is selected to be 10 in order to incorporate stem points from all around the stem (as, at any height, it is rare to have branches growing in all directions), which in turn improves stem point estimation.

The stem location estimated from the proposed method is compared with that obtained from the CHM Local maxima based method [59] which assumes the stem location H_p to be directly below the highest point in the tree segment (Fig. 8.6). The CHM resolution and variance of Gaussian smoothening filter were selected to be 0.1 and 1, respectively. The criteria for the resolution and variance selection is to minimize false tree top detection. The error in the stem location estimates were quantified using the Root Mean Squared Error (RMSE) on a high point density and a low point density dataset and is shown in Table 8.1 for both the proposed and state-of-the-art methods. The proposed method, by relying on the direction of branches, better approximates the stem axis, and hence accurately determines the stem position. This is evident from the fact that the RMSE error in stem location is lower than the one of the state-of-the-art method for both high-density (i.e., 1.10 vs. 1.52) and low-density (i.e., 1.39 vs 1.56) data sets, respectively). The proposed method improved RMSE error of high density dataset of 0.29m w.r.t. the low density one. In addition, RMSE behaviors have been observed as a function of the stem tilt. As expected the proposed method is more robust to tilt variations as RMSE increased at a slower rate (i.e., 0.11) w.r.t. the one of SoA method (i.e., 0.18).

To model the stem, a cone is fitted on the stem points. The initial cone parameters $\vec{V_c}$ and P_c are set as the direction vector of the regression fitted line, and the point that is at a distance H_T from origin (towards positive z axis) in the direction of the regression fitted line. All stem points at a threshold distance (i.e., T_r) of more than 0.6m from the stem are noisy points and hence are not considered for modeling. The value was set based on the maximum radius of the stems in the dataset, derived using the generic model (8.2). The DBH of a tree S_{DBH} is directly estimated by using the base radius z_m of the fitted cone using (8.6). The value of η is set to 0.48 m, which is the maximum estimated tree radius in the considered dataset (Fig. 8.6).

The proposed method shows maximum performance in the case of the high density dataset. and error increases with decreasing point density, i.e., MSE in DBH estimation is 3.80cm for the high density, whereas the MSE error almost doubled for the low density

dataset. This is due to the larger number of stem surface points (scanned by the laser scanner by increasing scan frequency or decreasing flying height). Also, the estimation results show that the proposed method overestimates the real stem DBH. This is due to: a) the reduced vertical resolution accuracy of the LiDAR point which in our case is 2cm, and b) the inclusion of points belonging to the branch stem junction into the stem points. We compared the accuracy of the proposed method with a state-of-the-art technique which uses both tree and crown level parameters to estimate the DBH [36]. The features include tree height, crown height, crown area (calculated from the CHM), and crown volume (calculated using the 3D convex hull with α_{hull} as the hull parameter). Table 8.2 shows the Mean Absolute Error (MAE), the Mean Squared Error (MSE), and the Coefficient of estimation (R^2), associated with DBH estimates obtained using the proposed and the state-of-the-art estimation methods, for the low density and the high density datasets.

Although the proposed method shows slightly lower performance than the SoA method, the fact that the DBH estimation is done without the knowledge of the tree species is a huge advantage in operational forest inventorying. Also, unlike indirect allometric equation based DBH estimation methods, the proposed method provides an added-value to forest inventory at the single tree level by allowing a more direct DBH estimation independent of species and forest type. The proposed method can improve the accuracy of forest inventorying by providing accurate stem location and 3D tilt estimates.

Table 8.1: Stem localization errors obtained for the proposed and the state-of-the-art method for high density and low density datasets.

Method	**High Density (m)**	**Low Density (m)**
	RMSE	**RMSE**
Proposed	1.1	1.3
SoA	1.5	1.5

Table 8.2: DBH estimation errors obtained for the proposed and the state-of-the-art method for high density and low density datasets

Method	**High Density (cm)**			**Low Density (cm)**		
	MSE	**MAE**	$\mathbf{R^2}$	**MSE**	**MAE**	$\mathbf{R^2}$
Proposed	4.3	0.3	0.8	7.3	0.4	0.6
SoA	3.2	0.2	0.8	5.9	0.3	0.8

8.4 Conclusion

A novel high density airborne LiDAR data based stem localization and modeling technique is proposed. The approach uses a state-of-the-art LiDAR data based branch modeling technique to identify conifer branch point-clusters. Stem points are identified as the set of points farthest from the branch tip points. A cone, whose parameters are optimally derived using 3D stem point locations, is used to model the stem. The stem location, and DBH estimation obtained by the proposed technique are found to provide smaller errors, compared to the respective state-of-the-art reference method. Future works aims at using other attributes of the points such as the scan angle, and intensity of laser return for improving stem point detection accuracy. Also the performance of the method on other forest types such as boreal and temperate needs to be evaluated.

Conclusions and Future Developments

The thesis introduces individual tree level methods to automatic extraction of species information and estimation of biophysical parameters by exploiting the 3D structural information in high density LiDAR data. The proposed methods are particularly relevant in the context of precision forestry applications which demand accurate information at the individual tree level. The focus was given on extracting forest information from high density data collected from aerial and terrestrial platforms. The thesis contains five novel contributions that improved the performance of forest information extraction over the state of the art.

Accurate tree crown detection and 3D delineation are critical to both accurate classification of tree species and estimation of biophysical parameters. Thus, as the first contribution of the thesis, we proposed a method to accurately detect and 3D delineate trees in multi-layered forests by using small footprint high density multi-return airborne LiDAR data. The method uses both 2D and 3D features representing the crown structural information, derived from the high density LiDAR data to achieve accurate detection and delineation. The results prove the usefulness of modeling the crown structural characteristics to achieve accurate crown detection and 3D delineation. The credit to the improved performance goes to the novel projection technique that performs an action equivalent to opening the crown segments along the stem of the dominant tree in the segment, which allows an effective representation of the crown profile data. Hence, the method shows improved performance over the state of the art in detecting and delineating subdominant crowns.

The second, third and fourth contributions of the thesis are directed to addressing the challenges in accurate tree species classification. In particular, the focus was on classifying trees belonging to the same taxonomic class, and thus showing similar crown characteristics e.g., most species of conifers have an approximately conical crown. Thus in all the contributions, a fine level characterization of the tree crown is proposed. The second and third contributions are species classification techniques in high density ALS

data. The former uses a set of internal (i.e., branch level) and external crown features to achieve species classification, while the latter uses species independent features that are obtained in a data-driven fashion. Considering the huge amount of structural information in TLS data, the fourth contribution is a method that uses a shape fitting technique for internal and external crown characterization. The results obtained for all the methods prove them to have improved performance when compared to the state-of-the-art ones.

The fifth and last contribution of the thesis is an accurate stem localization and DBH estimation technique for high density ALS data. Here, the stem localization is performed by modeling individual branches, and obtaining inner most points that are very likely to represent the stem, from individual branch point cloud clusters. The results confirm that the direction of branch growth can be exploited to obtain accurate stem location. Unlike the state-of-the-art methods which indirectly estimate the DBH using species specific allometric models, the proposed method directly estimate the DBH from a 3D model derived from stem points. Although the performance of the proposed method is slightly lower than the state-of-the-art one, the ability to accurately obtain DBH without species knowledge is a huge advantage in operational forest inventorying.

Although all the proposed methods provide improved results over the state of the art, there are possibilities for further improvement which need to be considered in future developments. The methods proposed in the thesis are restricted to the use of structural information in high density LiDAR data. However, other attributes such as the normalized intensity of return, scan angle, and return number also contain information of species and can be considered to derive additional information and improve crown detection and delineation, species classification, and biophysical parameter estimation. Continuous wave LiDAR data contain fine vertical profile details of the crown, that can improve performance of the proposed methods. Similarly, the use of spectral information in multispectral LiDAR data can also improve the accuracy of the proposed methods. In particular, the species classification performance can be considerably improved as the spectral characteristics of different species of trees are unique. Also, testing with different forest types and point densities will enable us to evaluate the robustness of the proposed methods. Accurate estimation of change in forest parameters from multi-temporal LiDAR data is another interesting area be studied.

List of Publications

International Journal Publications

1. Harikumar, A., Bovolo, F., and Bruzzone, L., **'A local projection based approach to individual tree detection and 3D crown delineation in multistoried coniferous forests using high density airborne LiDAR data'**, IEEE Transactions on Geoscience and Remote Sensing, Vol. 57, No. 2, pp. 1168 - 1182, Feb 2019.

2. Harikumar, A., Bovolo, F., and Bruzzone, L., **'An internal crown geometric model for conifer species classification with high density LiDAR data'**, IEEE Transactions on Geoscience and Remote Sensing, Vol. 55, No. 5, pp. 2924 2940, Feb 2017.

3. Harikumar, A., Kumar, A., Stein, A., Raju, P.L.N. and Krishna Murthy, Y.V.N, 2015. **' An effective hybrid approach to remote sensing image classification'** , International Journal of Remote Sensing' , Vol 36, No. 11, pp.2767-2785, Jun 2015

International Journal Publications (in review, submitted or in preparation):

1. Harikumar, A., Bovolo, F., and Bruzzone, L., **'Conifer stem localization and DBH estimation by stem geometric modeling in high density airborne laser scanning data'**, IEEE Geoscience and Remote Sensing Letters (under revision).

2. Harikumar, A., Xinlian, L., Bovolo, F., Hyypp, J. and Bruzzone, L., **' Tree species classification in Nordic forests using geometric information in multiscan terrestrial LiDAR data'** , IEEE Transactions on Geoscience and Remote Sensing, (in preparation)

Conferences

1. Harikumar, A., Bovolo, F., and Liang, X. **'An effective approach to 3D stem modeling and branch-knot localization in multiscan TLS data'**, IEEE 2018 Int. Geoscience and Remote Sensing Symposium, (IGARSS '19), Yokohama, Japan, 28 July - 02 August 2019 (accepted for oral presentation).

2. Harikumar, A., Paris, C., Bovolo, F., and Bruzzone, L., **'A novel data-driven approach to tree species classification using high density multireturn airborne lidar data.'**, SPIE 2018, SPIE Conference on Image and Signal Processing for Remote Sensing XXIV, Berlin, Germany, 10-14 September 2018 (oral presentation)..

3. Harikumar, A., Liang, X. and Bovolo, F. **'An approach to tree species classification using voxel neighborhood density based subsampling of multiscan terrestrial LiDAR data'**, IEEE 2018 Int. Geoscience and Remote Sensing Symposium, (IGARSS '18), Valencia, Spain, 22-27 July 2018 (poster presentation).

4. Harikumar, A., Bovolo, F., and Bruzzone, L., **'An approach to conifer stem location and modeling in high density airborne LiDAR data'**, Proc. SPIE 10427, SPIE Conference on Image and Signal Processing for Remote Sensing XXIII, Warsaw, Poland, 11-13 September 2017 (oral presentation).

5. Harikumar A., Bovolo F., Bruzzone L., **'Subdominant Tree Detection in Multilayered forests by a local projection of airborne LiDAR data'**, Int. Geoscience and Remote Sensing Symposium, (IGARSS '17), Texas, USA, 23-28 July 2017 (Oral presentation).

6. Harikumar, A., Bovolo, F. and Bruzzone, L., **'A novel approach to internal crown characterization for coniferous tree species classification'**, SPIE 2016, SPIE Conference on Image and Signal Processing for Remote Sensing XXII, Eidenburg, United Kingdom, 26-29 September 2016 (oral presentation).

7. Harikumar A., Bovolo F., Bruzzone L. **'An approach to conifer species classification based on crown structure modeling in high density airborne LiDAR data'**, IEEE 2016 Int. Geoscience and Remote Sensing Symposium, (IGARSS '16), Beijing, China, 10-15 July 2016 (oral presentation).

Bibliography

[1] R. Fleming, N. Brown, J. Jenik, P. Kahumbu, and J. Plesnik, "Emerging perspectives on forest biodiversity," *UNEP Year Book*, pp. 47–59, 2011.

[2] R. K. Dixon, A. Solomon, S. Brown, R. Houghton, M. Trexier, and J. Wisniewski, "Carbon pools and flux of global forest ecosystems," *Science*, vol. 263, no. 5144, pp. 185–190, 1994.

[3] H. K. Gibbs, S. Brown, J. O. Niles, and J. A. Foley, "Monitoring and estimating tropical forest carbon stocks: making redd a reality," *Environmental Research Letters*, vol. 2, no. 4, p. 045023, 2007.

[4] T. W. Crowther, H. B. Glick, K. R. Covey, C. Bettigole, D. S. Maynard, S. M. Thomas, J. R. Smith, G. Hintler, M. C. Duguid, G. Amatulli, *et al.*, "Mapping tree density at a global scale," *Nature*, vol. 525, no. 7568, p. 201, 2015.

[5] S. Magnussen and D. Reed, "Modeling for estimation and monitoring," *Knowledge reference for national forest assessments*, vol. 111, 2004.

[6] L. Duncanson, R. Dubayah, B. Cook, J. Rosette, and G. Parker, "The importance of spatial detail: Assessing the utility of individual crown information and scaling approaches for lidar-based biomass density estimation," *Remote Sens. Environ.*, vol. 168, pp. 102–112, 2015.

[7] M. Holopainen, M. Vastaranta, V. Kankare, M. Räty, M. Vaaja, X. Liang, X. Yu, J. Hyyppä, H. Hyyppä, R. Viitala, *et al.*, "Biomass estimation of individual trees using stem and crown diameter tls measurements," *ISPRS-International Archives of the Photogrammetry, Remote Sensing and Spatial Information Sciences*, vol. 3812, pp. 91–95, 2011.

[8] Z. Cheng, J. Gamarra, and L. Birigazzi, "Inventory of allometric equations for estimation tree biomass-a database for china. rome, italy: Unredd programme," 2014.

[9] H. Huang, P. Gong, X. Cheng, N. Clinton, and Z. Li, "Improving measurement of forest structural parameters by co-registering of high resolution aerial imagery and low density lidar data," *Sensors*, vol. 9, no. 3, pp. 1541–1558, 2009.

[10] S. Tao, Q. Guo, L. Li, B. Xue, M. Kelly, W. Li, G. Xu, and Y. Su, "Airborne lidar-derived volume metrics for aboveground biomass estimation: A comparative assessment for conifer stands," *Agricultural and forest meteorology*, vol. 198, pp. 24–32, 2014.

[11] P. Packalen, J. Vauhkonen, E. Kallio, J. Peuhkurinen, J. Pitkänen, I. Pippuri, J. Strunk, and M. Maltamo, "Predicting the spatial pattern of trees by airborne laser scanning," *International journal of remote sensing*, vol. 34, no. 14, pp. 5154–5165, 2013.

[12] F. Morsdorf, E. Meier, B. Kötz, K. I. Itten, M. Dobbertin, and B. Allgöwer, "Lidar-based geometric reconstruction of boreal type forest stands at single tree level for forest and wildland fire management," *Remote Sens. Environ.*, vol. 92, no. 3, pp. 353–362, 2004.

[13] T. Swetnam, A. M. Lynch, D. A. Falk, S. R. Yool, and D. P. Guertin, "Discriminating disturbance from natural variation with lidar in semi ‐ arid forests in the southwestern usa," *Ecosphere*, vol. 6, pp. 1–13, 2015.

[14] Á. Casas, M. García, R. B. Siegel, A. Koltunov, C. Ramírez, and S. Ustin, "Burned forest characterization at single-tree level with airborne laser scanning for assessing wildlife habitat," *Remote Sensing of Environment*, vol. 175, pp. 231–241, 2016.

[15] M. Holopainen, M. Vastaranta, and J. Hyyppä, "Outlook for the next generation' s precision forestry in finland," *Forests*, vol. 5, no. 7, pp. 1682–1694, 2014.

[16] M. Maltamo, K. Mustonen, J. Hyyppä, J. Pitkänen, and X. Yu, "The accuracy of estimating individual tree variables with airborne laser scanning in a boreal nature reserve," *Can. J. For. Res.*, vol. 34, no. 9, pp. 1791–1801, 2004.

[17] J. Hyyppa, O. Kelle, M. Lehikoinen, and M. Inkinen, "A segmentation-based method to retrieve stem volume estimates from 3-d tree height models produced by laser scanners," *IEEE Trans. Geosci. Remote Sens.*, vol. 39, no. 5, pp. 969–975, 2001.

[18] C. Paris, D. Valduga, and L. Bruzzone, "A hierarchical approach to three-dimensional segmentation of lidar data at single-tree level in a multilayered forest," *IEEE Trans. Geosci. Remote Sens.*, vol. 54, no. 7, pp. 4190–4203, 2016.

[19] P. Potapov, M. C. Hansen, S. V. Stehman, T. R. Loveland, and K. Pittman, "Combining modis and landsat imagery to estimate and map boreal forest cover loss," *Remote Sensing of Environment*, vol. 112, no. 9, pp. 3708–3719, 2008.

[20] A. C. Morel, S. S. Saatchi, Y. Malhi, N. J. Berry, L. Banin, D. Burslem, R. Nilus, and R. C. Ong, "Estimating aboveground biomass in forest and oil palm plantation in sabah, malaysian borneo using alos palsar data," *Forest Ecology and Management*, vol. 262, no. 9, pp. 1786–1798, 2011.

[21] D. Pflugmacher, W. B. Cohen, R. E. Kennedy, and Z. Yang, "Using landsat-derived disturbance and recovery history and lidar to map forest biomass dynamics," *Remote Sensing of Environment*, vol. 151, pp. 124–137, 2014.

[22] P. Hyde, R. Dubayah, W. Walker, J. B. Blair, M. Hofton, and C. Hunsaker, "Mapping forest structure for wildlife habitat analysis using multi-sensor (lidar, sar/insar, etm+, quickbird) synergy," *Remote Sens. Environ.*, vol. 102, no. 1, pp. 63–73, 2006.

[23] S. M. Jeronimo, V. R. Kane, D. J. Churchill, R. J. McGaughey, and J. F. Franklin, "Applying lidar individual tree detection to management of structurally diverse forest landscapes," *Journal of Forestry*, vol. 116, no. 4, pp. 336–346, 2018.

[24] M. Govender, K. Chetty, V. Naiken, and H. Bulcock, "A comparison of satellite hyperspectral and multispectral remote sensing imagery for improved classification and mapping of vegetation," *Water SA*, vol. 34, no. 2, pp. 147–154, 2008.

[25] Y. Lin and M. Herold, "Tree species classification based on explicit tree structure feature parameters derived from static terrestrial laser scanning data," *Agricultural and Forest meteorology*, vol. 216, pp. 105–114, 2016.

[26] M. Lang, T. Arumäe, D. Laarmann, and A. Kiviste, "Estimation of change in forest height growth," *Forestry Studies*, vol. 67, no. 1, pp. 5–16, 2017.

[27] I. Korpela, H. O. Ørka, M. Maltamo, T. Tokola, J. Hyyppä, *et al.*, "Tree species classification using airborne lidar–effects of stand and tree parameters, downsizing of training set, intensity normalization, and sensor type," *Silva Fennica*, vol. 44, no. 2, pp. 319–339, 2010.

[28] J. Peuhkurinen, L. Mehtätalo, and M. Maltamo, "Comparing individual tree detection and the area-based statistical approach for the retrieval of forest stand characteristics using airborne laser scanning in scots pine stands," *Can. J. For. Res.*, vol. 41, no. 3, pp. 583–598, 2011.

[29] D. A. Coomes, M. Dalponte, T. Jucker, G. P. Asner, L. F. Banin, D. F. Burslem, S. L. Lewis, R. Nilus, O. L. Phillips, M.-H. Phua, *et al.*, "Area-based vs tree-centric approaches to mapping forest carbon in southeast asian forests from airborne laser scanning data," *Remote sensing of environment*, vol. 194, pp. 77–88, 2017.

[30] H. Latifi, F. E. Fassnacht, J. Müller, A. Tharani, S. Dech, and M. Heurich, "Forest inventories by lidar data: A comparison of single tree segmentation and metric-based methods for inventories of a heterogeneous temperate forest," *International Journal of Applied Earth Observation and Geoinformation*, vol. 42, pp. 162–174, 2015.

[31] H. Kaartinen, J. Hyyppä, X. Yu, M. Vastaranta, H. Hyyppä, A. Kukko, M. Holopainen, C. Heipke, M. Hirschmugl, F. Morsdorf, *et al.*, "An international comparison of individual tree detection and extraction using airborne laser scanning," *Remote Sensing*, vol. 4, no. 4, pp. 950–974, 2012.

[32] J. Li, B. Hu, and T. L. Noland, "Classification of tree species based on structural features derived from high density lidar data," *Agricultural and forest meteorology*, vol. 171, pp. 104–114, 2013.

[33] K. Wang, T. Wang, and X. Liu, "A review: Individual tree species classification using integrated airborne lidar and optical imagery with a focus on the urban environment," *Forests*, vol. 10, no. 1, p. 1, 2019.

[34] W. Newman, D. Turcotte, and A. Gabrielov, "Fractal trees with side branching," *Fractals*, vol. 5, no. 04, pp. 603–614, 1997.

[35] P. Thomas, *Trees: their natural history*. Cambridge University Press, 2014.

[36] W. Yao, P. Krzystek, and M. Heurich, "Tree species classification and estimation of stem volume and dbh based on single tree extraction by exploiting airborne full-waveform lidar data," *Remote Sens. Environ.*, vol. 123, pp. 368–380, 2012.

[37] S. Kim, R. J. McGaughey, H.-E. Andersen, and G. Schreuder, "Tree species differentiation using intensity data derived from leaf-on and leaf-off airborne laser scanner data," *Remote Sensing of Environment*, vol. 113, no. 8, pp. 1575–1586, 2009.

[38] T. Lillesand, R. W. Kiefer, and J. Chipman, *Remote sensing and image interpretation*. John Wiley & Sons, 2014.

[39] G. K. Devi, B. Ganasri, and G. Dwarakish, "Applications of remote sensing in satellite oceanography: A review," *Aquatic Procedia*, vol. 4, pp. 579–584, 2015.

[40] J. Yang, P. Gong, R. Fu, M. Zhang, J. Chen, S. Liang, B. Xu, J. Shi, and R. Dickinson, "The role of satellite remote sensing in climate change studies," *Nature climate change*, vol. 3, no. 10, p. 875, 2013.

[41] J. T. Kerr and M. Ostrovsky, "From space to species: ecological applications for remote sensing," *Trends in ecology & evolution*, vol. 18, no. 6, pp. 299–305, 2003.

[42] Q. Yu, P. Gong, N. Clinton, G. Biging, M. Kelly, and D. Schirokauer, "Object-based detailed vegetation classification with airborne high spatial resolution remote sensing imagery," *Photogrammetric Engineering & Remote Sensing*, vol. 72, no. 7, pp. 799–811, 2006.

[43] P. Watt and D. Donoghue, "Measuring forest structure with terrestrial laser scanning," *International Journal of Remote Sensing*, vol. 26, no. 7, pp. 1437–1446, 2005.

[44] J. Shan and C. K. Toth, *Topographic laser ranging and scanning: principles and processing*. CRC press, 2018.

[45] E. P. Baltsavias, "Airborne laser scanning: basic relations and formulas," *ISPRS Journal of photogrammetry and remote sensing*, vol. 54, no. 2, pp. 199–214, 1999.

[46] A. Aldred, G. Bonnor, *et al.*, *Application of airborne lasers to forest surveys*, vol. 51. 1985.

[47] W. Krabill, J. Collins, R. Swift, and M. Butler, "Airborne laser topographic mapping results from initial joint nasa/us army corps of engineers experiment," 1980.

[48] R. Nelson, W. Krabill, and G. MacLean, "Determining forest canopy characteristics using airborne laser data," *Remote Sens. Environ.*, vol. 15, no. 3, pp. 201–212, 1984.

[49] R. Nelson, R. Swift, and W. Krabill, "Using airborne lasers to estimate forest canopy and stand characteristics," *Journal of Forestry*, vol. 86, no. 10, pp. 31–38, 1988.

[50] W. Krabill, J. Collins, L. Link, R. Swift, and M. Butler, "Airborne laser topographic mapping results," *Photogrammetric Engineering and Remote Sensing*, vol. 50, no. 6, pp. 685–694, 1984.

[51] H. Zwally, B. Schutz, W. Abdalati, J. Abshire, C. Bentley, A. Brenner, J. Bufton, J. Dezio, D. Hancock, D. Harding, *et al.*, "Icesat's laser measurements of polar ice, atmosphere, ocean, and land," *Journal of Geodynamics*, vol. 34, no. 3-4, pp. 405–445, 2002.

[52] A. Baccini, N. Laporte, S. Goetz, M. Sun, and H. Dong, "A first map of tropical africa' s above-ground biomass derived from satellite imagery," *Environmental Research Letters*, vol. 3, no. 4, p. 045011, 2008.

[53] J. Boudreau, R. F. Nelson, H. A. Margolis, A. Beaudoin, L. Guindon, and D. S. Kimes, "Regional aboveground forest biomass using airborne and spaceborne lidar in québec," *Remote Sensing of Environment*, vol. 112, no. 10, pp. 3876–3890, 2008.

[54] F. Morsdorf, O. Frey, E. Meier, K. I. Itten, and B. Allgöwer, "Assessment of the influence of flying altitude and scan angle on biophysical vegetation products derived from airborne laser scanning," *International Journal of Remote Sensing*, vol. 29, no. 5, pp. 1387–1406, 2008.

[55] E. Puttonen, T. Hakala, O. Nevalainen, S. Kaasalainen, A. Krooks, M. Karjalainen, and K. Anttila, "Artificial target detection with a hyperspectral lidar over 26-h measurement," *Optical Engineering*, vol. 54, no. 1, p. 013105, 2015.

[56] X. Yu, J. Hyyppä, M. Holopainen, and M. Vastaranta, "Comparison of area-based and individual tree-based methods for predicting plot-level forest attributes," *Remote Sensing*, vol. 2, no. 6, pp. 1481–1495, 2010.

[57] T. Eid, T. Gobakken, and E. Næsset, "Comparing stand inventories for large areas based on photo-interpretation and laser scanning by means of cost-plus-loss analyses," *Scandinavian Journal of Forest Research*, vol. 19, no. 6, pp. 512–523, 2004.

[58] J. Hyyppa, "Detecting and estimating attributes for single trees using laser scanner," *Photogramm J Finland*, vol. 16, pp. 27–42, 1999.

[59] A. Persson, J. Holmgren, and U. Söderman, "Detecting and measuring individual trees using an airborne laser scanner," *Photogramm. Eng. Remote Sens.*, vol. 68, no. 9, pp. 925–932, 2002.

[60] M. Wulder, K. O. Niemann, and D. G. Goodenough, "Local maximum filtering for the extraction of tree locations and basal area from high spatial resolution imagery," *Remote Sens. Environ.*, vol. 73, no. 1, pp. 103–114, 2000.

[61] A. Kato, L. M. Moskal, P. Schiess, M. E. Swanson, D. Calhoun, and W. Stuetzle, "Capturing tree crown formation through implicit surface reconstruction using airborne lidar data," *Remote Sens. Environ.*, vol. 113, no. 6, pp. 1148–1162, 2009.

[62] T. Brandtberg, T. A. Warner, R. E. Landenberger, and J. B. McGraw, "Detection and analysis of individual leaf-off tree crowns in small footprint, high sampling density lidar data from the eastern deciduous forest in north america," *Remote Sens. Environ.*, vol. 85, no. 3, pp. 290–303, 2003.

[63] A. Khosravipour, A. K. Skidmore, and M. Isenburg, "Generating spike-free digital surface models using lidar raw point clouds: A new approach for forestry applications," *Int. J. Appl. Earth Obs. Geoinf.*, vol. 52, pp. 104–114, 2016.

[64] B.-M. Straub and C. Heipke, "Concepts for internal and external evaluation of automatically delineated tree tops," *Int. Arch. Photogramm. Remote Sens.*, vol. 26, no. 8/W2, pp. 62–65, 2004.

[65] H. Weinacker, B. Koch, U. Heyder, and R. Weinacker, "Development of filtering, segmentation and modelling modules for lidar and multispectral data as a fundament of an automatic forest inventory system," *Int. Arch. Photogramm. Remote Sens. Spat. Inf. Sci..*, vol. 36, no. Part 8, p. W2, 2004.

[66] S. C. Popescu and R. H. Wynne, "Seeing the trees in the forest," *Photogrammetric Engineering & Remote Sensing*, vol. 70, no. 5, pp. 589–604, 2004.

[67] D. Tiede and C. Hoffmann, "Process oriented object-based algorithms for single tree detection using laser scanning," in *Workshop on 3D Remote Sensing in Forest*, pp. 14–15, 2006.

[68] J. P. Ardila, W. Bijker, V. A. Tolpekin, and A. Stein, "Context-sensitive extraction of tree crown objects in urban areas using vhr satellite images," *Int. J. Appl. Earth Obs. Geoinf.*, vol. 15, pp. 57–69, 2012.

[69] F. Morsdorf, E. Meier, B. Allgöwer, and D. Nüesch, "Clustering in airborne laser scanning raw data for segmentation of single trees," *Int. Arch. Photogramm. Remote Sens. Spat. Inf. Sci.*, vol. 34, no. part 3, p. W13, 2003.

[70] H. Lee, K. C. Slatton, B. Roth, and W. Cropper Jr, "Adaptive clustering of airborne lidar data to segment individual tree crowns in managed pine forests," *Int. J. Remote Sens.*, vol. 31, no. 1, pp. 117–139, 2010.

[71] P. Tittmann, S. Shafii, B. Hartsough, and B. Hamann, "Tree detection and delineation from lidar point clouds using ransac," *Proceedings of SilviLaser*, pp. 1–23, 2011.

[72] W. Li, Q. Guo, M. K. Jakubowski, and M. Kelly, "A new method for segmenting individual trees from the lidar point cloud," *Photogramm. Eng. Remote Sens.*, vol. 78, no. 1, pp. 75–84, 2012.

[73] L. Duncanson, B. Cook, G. Hurtt, and R. Dubayah, "An efficient, multi-layered crown delineation algorithm for mapping individual tree structure across multiple ecosystems," *Remote Sens. Environ.*, vol. 154, pp. 378–386, 2014.

[74] H. Hamraz, M. A. Contreras, and J. Zhang, "Forest understory trees can be segmented accurately within sufficiently dense airborne laser scanning point clouds," *Sci. Rep.*, vol. 7, no. 1, p. 6770, 2017.

[75] E. Ayrey, S. Fraver, J. A. Kershaw Jr, L. S. Kenefic, D. Hayes, A. R. Weiskittel, and B. E. Roth, "Layer stacking: a novel algorithm for individual forest tree segmentation from lidar point clouds," *Can. J. For. Res.*, vol. 43, no. 1, pp. 16–27, 2017.

[76] Y. Wang, H. Weinacker, and B. Koch, "Development of a procedure for vertical structure analysis and 3d-single tree extraction within forests based on lidar point cloud," *Int. Arch. Photogramm. Remote Sens. Spat. Inf. Sci.*, vol. 36, no. Part 3, p. W52, 2007.

[77] D. Mongus and B. Žalik, "An efficient approach to 3d single tree-crown delineation in lidar data," *ISPRS J. Photogramm. Remote Sens.*, vol. 108, pp. 219–233, 2015.

[78] J. Vauhkonen, L. Ene, S. Gupta, J. Heinzel, J. Holmgren, J. Pitkänen, S. Solberg, Y. Wang, H. Weinacker, K. M. Hauglin, *et al.*, "Comparative testing of single-tree detection algorithms under different types of forest," *Forestry*, vol. 85, no. 1, pp. 27–40, 2012.

[79] K. L. O'hara, H. Hasenauer, and G. Kindermann, "Sustainability in multi-aged stands: an analysis of long-term plenter systems," *Forestry*, vol. 80, no. 2, pp. 163–181, 2007.

[80] N. L. Lexerød and T. Eid, "An evaluation of different diameter diversity indices based on criteria related to forest management planning," *Forest Ecology and Management*, vol. 222, no. 1-3, pp. 17–28, 2006.

[81] C. McElhinny, P. Gibbons, C. Brack, and J. Bauhus, "Forest and woodland stand structural complexity: its definition and measurement," *Forest Ecology and Management*, vol. 218, no. 1-3, pp. 1–24, 2005.

[82] K. Kandare, H. O. Ørka, J. C.-W. Chan, and M. Dalponte, "Effects of forest structure and airborne laser scanning point cloud density on 3d delineation of individual tree crowns," *European Journal of Remote Sensing*, vol. 49, no. 1, pp. 337–359, 2016.

[83] J. Reitberger, C. Schnörr, P. Krzystek, and U. Stilla, "3d segmentation of single trees exploiting full waveform lidar data," *ISPRS J. Photogramm. Remote Sens.*, vol. 64, no. 6, pp. 561–574, 2009.

[84] Y. Wang, H. Weinacker, B. Koch, and K. Sterenczak, "Lidar point cloud based fully automatic 3d single tree modelling in forest and evaluations of the procedure," *Int. Arch. Photogramm. Remote Sens. Spat. Inf. Sci.*, vol. 37, no. PART B6B, pp. 45–51, 2008.

[85] C. Véga, A. Hamrouni, S. El Mokhtari, J. Morel, J. Bock, J.-P. Renaud, M. Bouvier, and S. Durrieu, "Ptrees: A point-based approach to forest tree extraction from lidar data," *Int. J. Appl. Earth Obs. Geoinf.*, vol. 33, pp. 98–108, 2014.

[86] X. Lu, Q. Guo, W. Li, and J. Flanagan, "A bottom-up approach to segment individual deciduous trees using leaf-off lidar point cloud data," *ISPRS J. Photogramm. Remote Sens.*, vol. 94, pp. 1–12, 2014.

[87] C. D. Jones, A. B. Smith, and E. F. Roberts in *Proceedings Title*, vol. II, pp. 803–806, IEEE, 2003.

[88] E. Lindberg, L. Eysn, M. Hollaus, J. Holmgren, and N. Pfeifer, "Delineation of tree crowns and tree species classification from full-waveform airborne laser scanning data using 3-d ellipsoidal clustering," *IEEE J. Sel. Top. Appl. Earth Obs. Remote Sens.*, vol. 7, no. 7, pp. 3174–3181, 2014.

[89] M. Maltamo, T. Tokola, and M. Lehikoinen, "Estimating stand characteristics by combining single tree pattern recognition of digital video imagery and a theoretical diameter distribution model," *Forest Science*, vol. 49, no. 1, pp. 98–109, 2003.

[90] L. Mehtätalo, "Eliminating the effect of overlapping crowns from aerial inventory estimates," *Can. J. For. Res.*, vol. 36, no. 7, pp. 1649–1660, 2006.

[91] K. Kansanen, J. Vauhkonen, T. Lähivaara, and L. Mehtätalo, "Stand density estimators based on individual tree detection and stochastic geometry," *Can. J. For. Res.*, vol. 46, no. 11, pp. 1359–1366, 2016.

[92] J. Vauhkonen and L. Mehtätalo, "Matching remotely sensed and field-measured tree size distributions," *Can. J. For. Res.*, vol. 45, no. 3, pp. 353–363, 2014.

[93] T. Lahivaara, A. Seppanen, J. P. Kaipio, J. Vauhkonen, L. Korhonen, T. Tokola, and M. Maltamo, "Bayesian approach to tree detection based on airborne laser scanning data," *IEEE Trans. Geosci. Remote Sens.*, vol. 52, no. 5, pp. 2690–2699, 2014.

[94] X. Liang, J. Hyyppä, V. Kankare, M. Holopainen, *et al.*, "Stem curve measurement using terrestrial laser scanning," in *Proceedings of 11th International Conference on LiDAR Applications for Assessing Forest Ecosystems*, pp. 1–6, 2011.

[95] M. W. McDaniel, T. Nishihata, C. A. Brooks, P. Salesses, and K. Iagnemma, "Terrain classification and identification of tree stems using ground-based lidar," *Journal of Field Robotics*, vol. 29, no. 6, pp. 891–910, 2012.

[96] J.-F. Lalonde, N. Vandapel, D. F. Huber, and M. Hebert, "Natural terrain classification using three-dimensional ladar data for ground robot mobility," *Journal of field robotics*, vol. 23, no. 10, pp. 839–861, 2006.

[97] B. Gorte and N. Pfeifer, "Structuring laser-scanned trees using 3d mathematical morphology," *International Archives of Photogrammetry and Remote Sensing*, vol. 35, no. B5, pp. 929–933, 2004.

[98] B. Gorte and D. Winterhalder, "Reconstruction of laser-scanned trees using filter operations in the 3d raster domain," *International Archives of Photogrammetry, Remote Sensing and Spatial Information Sciences*, vol. 36, no. Part 8, p. W2, 2004.

[99] B. Yang, W. Dai, Z. Dong, and Y. Liu, "Automatic forest mapping at individual tree levels from terrestrial laser scanning point clouds with a hierarchical minimum cut method," *Remote Sensing*, vol. 8, no. 5, p. 372, 2016.

[100] A. Bienert, S. Scheller, E. Keane, G. Mullooly, and F. Mohan, "Application of terrestrial laser scanners for the determination of forest inventory parameters," *International Archives of Photogrammetry, Remote Sensing and Spatial Information Sciences*, vol. 36, no. 5, 2006.

[101] M. Vastaranta, T. Melkas, M. Holopainen, H. Kaartinen, J. Hyyppä, and H. Hyyppä, "Laser-based field measurements in tree-level forest data acquisition," *Photogramm. J. Finl*, vol. 21, pp. 51–61, 2009.

[102] M. Torma, "Estimation of tree species proportions of forest stands using laser scanning," *Int. Arch. Photogramm. Remote Sens.*, vol. 33, no. B7/4; PART 7, pp. 1524–1531, Jul. 2000.

[103] T. Moffiet, K. Mengersen, C. Witte, R. King, and R. Denham, "Airborne laser scanning: Exploratory data analysis indicates potential variables for classification of individual trees or forest stands according to species," *ISPRS Journal of Photogrammetry and Remote Sensing*, vol. 59, no. 5, pp. 289–309, 2005.

[104] U. Pyysalo and H. Hyyppa, "Reconstructing tree crowns from laser scanner data for feature extraction," *International Archives Of Photogrammetry Remote Sensing And Spatial Information Sciences*, vol. 34, no. 3/B, pp. 218–221, Sep. 2002.

[105] X. Liang, J. Hyyppä, and L. Matikainen, "Deciduous-coniferous tree classification using difference between first and last pulse laser signatures," *International Archives of Photogrammetry, Remote Sensing and Spatial Information Sciences*, vol. 36, no. 3/W52, Sep. 2007.

[106] J. Holmgren and Å. Persson, "Identifying species of individual trees using airborne laser scanner," *Remote Sens. Environ.*, vol. 90, no. 4, pp. 415–423, Apr. 2004.

[107] H. O. Ørka, E. Næsset, and O. M. Bollandsås, "Classifying species of individual trees by intensity and structure features derived from airborne laser scanner data," *Remote Sens. Environ.*, vol. 113, no. 6, pp. 1163–1174, Jun. 2009.

[108] J. Reitberger, P. Krzystek, and U. Stilla, "Analysis of full waveform lidar data for the classification of deciduous and coniferous trees," *International journal of remote sensing*, vol. 29, no. 5, pp. 1407–1431, 2008.

[109] L. Cao, N. C. Coops, J. L. Innes, J. Dai, H. Ruan, and G. She, "Tree species classification in subtropical forests using small-footprint full-waveform lidar data," *International journal of applied earth observation and geoinformation*, vol. 49, pp. 39–51, 2016.

[110] M. Hollaus, W. Wagner, K. Schadauer, B. Maier, and K. Gabler, "Growing stock estimation for alpine forests in austria: a robust lidar-based approach," *Canadian Journal of Forest Research*, vol. 39, no. 7, pp. 1387–1400, 2009.

[111] B. Höfle, M. Hollaus, H. Lehner, N. Pfeifer, W. Wagner, *et al.*, "Area-based parameterization of forest structure using full-waveform airborne laser scanning data," *Proceedings of SilviLaser*, vol. 2008, p. 8th, 2008.

[112] X. Yu, P. Litkey, J. Hyyppä, M. Holopainen, and M. Vastaranta, "Assessment of low density full-waveform airborne laser scanning for individual tree detection and tree species classification," *Forests*, vol. 5, no. 5, pp. 1011–1031, 2014.

[113] T. G. Jones, N. C. Coops, and T. Sharma, "Assessing the utility of airborne hyperspectral and lidar data for species distribution mapping in the coastal pacific northwest, canada," *Remote Sensing of Environment*, vol. 114, no. 12, pp. 2841–2852, 2010.

[114] N. R. Vaughn, L. M. Moskal, and E. C. Turnblom, "Tree species detection accuracies using discrete point lidar and airborne waveform lidar," *Remote Sensing*, vol. 4, no. 2, pp. 377–403, 2012.

[115] S. Kim, *Individual tree species identification using LIDAR-derived crown structures and intensity data*. PhD thesis, University of Washington, Seattle, WA, USA, 2007.

[116] J. Vauhkonen, T. Tokola, M. Maltamo, and P. Packalén, "Effects of pulse density on predicting characteristics of individual trees of scandinavian commercial species using alpha shape metrics based on airborne laser scanning data," *Canadian Journal of Remote Sensing*, vol. 34, no. sup2, pp. S441–S459, 2008.

[117] C. Ko, G. Sohn, and T. K. Remmel, "Tree genera classification with geometric features from high-density airborne lidar," *Can. J. Remote Sens.*, vol. 39, no. sup1, pp. S73–S85, Jun. 2013.

[118] Y. Lin and J. Hyyppä, "A comprehensive but efficient framework of proposing and validating feature parameters from airborne lidar data for tree species classification," *International Journal of Applied Earth Observation and Geoinformation*, vol. 46, pp. 45–55, Apr. 2016.

[119] J.-H. Song, S.-H. Han, K. Yu, and Y.-I. Kim, "Assessing the possibility of land-cover classification using lidar intensity data," *International Archives of Photogrammetry Remote Sensing and Spatial Information Sciences*, vol. 34, no. 3/B, pp. 259–262, 2002.

[120] S. Kim, *Individual tree species identification using LIDAR-derived crown structures and intensity data*. University of Washington, 2008.

[121] J. Holmgren and Å. Persson, "Identifying species of individual trees using airborne laser scanner," *Remote Sensing of Environment*, vol. 90, no. 4, pp. 415–423, 2004.

[122] D. N. Donoghue, P. J. Watt, N. J. Cox, and J. Wilson, "Remote sensing of species mixtures in conifer plantations using lidar height and intensity data," *Remote Sensing of Environment*, vol. 110, no. 4, pp. 509–522, 2007.

[123] F. Coren and P. Sterzai, "Radiometric correction in laser scanning," *International Journal of Remote Sensing*, vol. 27, no. 15, pp. 3097–3104, 2006.

[124] S. Kim, T. Hinckley, and D. Briggs, "Classifying individual tree genera using stepwise cluster analysis based on height and intensity metrics derived from airborne laser scanner data," *Remote sensing of environment*, vol. 115, no. 12, pp. 3329–3342, 2011.

[125] Y. Lin and J. Hyyppä, "A comprehensive but efficient framework of proposing and validating feature parameters from airborne lidar data for tree species classification," *International journal of applied earth observation and geoinformation*, vol. 46, pp. 45–55, 2016.

[126] X. Yu, J. Hyyppä, P. Litkey, H. Kaartinen, M. Vastaranta, and M. Holopainen, "Single-sensor solution to tree species classification using multispectral airborne laser scanning," *Remote Sensing*, vol. 9, no. 2, p. 108, 2017.

[127] A. Othmani, L. F. L. Y. Voon, C. Stolz, and A. Piboule, "Single tree species classification from terrestrial laser scanning data for forest inventory," *Pattern Recognit. Lett.*, vol. 34, no. 16, pp. 2144–2150, 2013.

[128] N. C. Coops, T. Hilker, M. A. Wulder, B. St-Onge, G. Newnham, A. Siggins, and J. T. Trofymow, "Estimating canopy structure of douglas-fir forest stands from discrete-return lidar," *Trees*, vol. 21, no. 3, p. 295, 2007.

[129] J. Holmgren, Å. Persson, and U. Söderman, "Species identification of individual trees by combining high resolution lidar data with multi-spectral images," *Int. J. Remote Sens.*, vol. 29, no. 5, pp. 1537–1552, 2008.

[130] Å. Persson, J. Holmgren, U. Söderman, and H. Olsson, "Tree species classification of individual trees in sweden by combining high resolution laser data with high resolution near-infrared digital images," *International Archives of Photogrammetry, Remote Sensing and Spatial Information Sciences*, vol. 36, no. 8, pp. 204–207, Oct. 2004.

[131] L. Wang, W. P. Sousa, P. Gong, and G. S. Biging, "Comparison of ikonos and quickbird images for mapping mangrove species on the caribbean coast of panama," *Remote Sens. Environ.*, vol. 91, no. 3, pp. 432–440, Jun. 2004.

[132] S.-R. Kim, W.-K. Lee, D.-A. Kwak, G. S. Biging, P. Gong, J.-H. Lee, and H.-K. Cho, "Forest cover classification by optimal segmentation of high resolution satellite imagery," *Sensors*, vol. 11, no. 2, pp. 1943–1958, Feb. 2011.

[133] M. Dalponte, L. Bruzzone, and D. Gianelle, "Tree species classification in the southern alps based on the fusion of very high geometrical resolution multispectral/hyperspectral images and lidar data," *Remote Sens. Environ.*, vol. 123, pp. 258–270, Aug. 2012.

[134] M. Dalponte, H. O. Ørka, L. T. Ene, T. Gobakken, and E. Næsset, "Tree crown delineation and tree species classification in boreal forests using hyperspectral and als data," *Remote Sens. Environ.*, vol. 140, pp. 306–317, Jan. 2014.

[135] R. Sugumaran and M. Voss, "Object-oriented classification of lidar-fused hyperspectral imagery for tree species identification in an urban environment," in *Urban Remote Sensing Joint Event, 2007*, pp. 1–6, IEEE, Apr. 2007.

[136] P. Hyde, R. Dubayah, W. Walker, J. B. Blair, M. Hofton, and C. Hunsaker, "Mapping forest structure for wildlife habitat analysis using multi-sensor (lidar, sar/insar, etm+, quickbird) synergy," *Remote Sens. Environ.*, vol. 102, no. 1, pp. 63–73, May. 2006.

[137] C. Zhang and F. Qiu, "Mapping individual tree species in an urban forest using airborne lidar data and hyperspectral imagery," *Photogramm. Eng. Remote Sens.*, vol. 78, no. 10, pp. 1079–1087, Oct. 2012.

[138] J. E. Means, S. A. Acker, B. J. Fitt, M. Renslow, L. Emerson, C. J. Hendrix, *et al.*, "Predicting forest stand characteristics with airborne scanning lidar," *Photogrammetric Engineering and Remote Sensing*, vol. 66, no. 11, pp. 1367–1372, 2000.

[139] K. Zhao and S. Popescu, "Hierarchical watershed segmentation of canopy height model for multi-scale forest inventory," *Proceedings of the ISPRS working group' . pp. 436â*, vol. 442, 2007.

[140] L. Korhonen, J. Vauhkonen, A. Virolainen, A. Hovi, and I. Korpela, "Estimation of tree crown volume from airborne lidar data using computational geometry," *International journal of remote sensing*, vol. 34, no. 20, pp. 7236–7248, 2013.

[141] J. Vauhkonen, "Estimating crown base height for scots pine by means of the 3d geometry of airborne laser scanning data," *International Journal of Remote Sensing*, vol. 31, no. 5, pp. 1213–1226, 2010.

[142] C. Hopkinson, L. Chasmer, C. Young-Pow, and P. Treitz, "Assessing forest metrics with a ground-based scanning lidar," *Canadian Journal of Forest Research*, vol. 34, no. 3, pp. 573–583, 2004.

[143] S. C. Popescu, "Estimating biomass of individual pine trees using airborne lidar," *Biomass and Bioenergy*, vol. 31, no. 9, pp. 646–655, 2007.

[144] D. A. Zimble, D. L. Evans, G. C. Carlson, R. C. Parker, S. C. Grado, and P. D. Gerard, "Characterizing vertical forest structure using small-footprint airborne lidar," *Remote sensing of Environment*, vol. 87, no. 2-3, pp. 171–182, 2003.

[145] M. Maltamo, P. Packalén, X. Yu, K. Eerikäinen, J. Hyyppä, and J. Pitkänen, "Identifying and quantifying structural characteristics of heterogeneous boreal forests using laser scanner data," *Forest ecology and management*, vol. 216, no. 1-3, pp. 41–50, 2005.

[146] S. Solberg, E. Næsset, and O. M. Bollandsas, "Single tree segmentation using airborne laser scanner data in a structurally heterogeneous spruce forest," *Photogrammetric Engineering & Remote Sensing*, vol. 72, no. 12, pp. 1369–1378, 2006.

[147] J. Pitkänen, M. Maltamo, J. Hyyppä, and X. Yu, "Adaptive methods for individual tree detection on airborne laser based canopy height model," *International Archives of Photogrammetry, Remote Sensing and Spatial Information Sciences*, vol. 36, no. 8, pp. 187–191, 2004.

[148] J. Hyyppä, M. Schardt, H. Haggrén, B. Koch, U. Lohr, H. Scherrer, R. Paananen, H. Luukkonen, M. Ziegler, H. Hyyppä, *et al.*, "High-scan: The first european-wide attempt to derive single-tree information from laserscanner data," *The Photogrammetric Journal of Finland*, vol. 17, no. 2, pp. 58–68, 2001.

[149] J. Holmgren, A. Barth, H. Larsson, and H. Olsson, "Prediction of stem attributes by combining airborne laser scanning and measurements from harvesters," *Silva Fenn*, vol. 46, no. 2, pp. 227–239, 2012.

[150] L. Ene, E. Næsset, and T. Gobakken, "Single tree detection in heterogeneous boreal forests using airborne laser scanning and area-based stem number estimates," *Int. J. Remote Sens.*, vol. 33, no. 16, pp. 5171–5193, 2012.

[151] T. L. Swetnam and D. A. Falk, "Application of metabolic scaling theory to reduce error in local maxima tree segmentation from aerial lidar," *Forest Ecology and Management*, vol. 323, pp. 158–167, 2014.

[152] L. Eysn, M. Hollaus, E. Lindberg, F. Berger, J.-M. Monnet, M. Dalponte, M. Kobal, M. Pellegrini, E. Lingua, D. Mongus, *et al.*, "A benchmark of lidar-based single tree detection methods using heterogeneous forest data from the alpine space," *Forests*, vol. 6, no. 5, pp. 1721–1747, 2015.

[153] Z. Zhang, A. Kazakova, L. M. Moskal, and D. M. Styers, "Object-based tree species classification in urban ecosystems using lidar and hyperspectral data," *Forests*, vol. 7, no. 6, p. 122, 2016.

[154] E. Lindberg and M. Hollaus, "Comparison of methods for estimation of stem volume, stem number and basal area from airborne laser scanning data in a hemi-boreal forest," *Remote Sensing*, vol. 4, no. 4, pp. 1004–1023, 2012.

[155] F. Pirotti, "Assessing a template matching approach for tree height and position extraction from lidar-derived canopy height models of pinus pinaster stands," *Forests*, vol. 1, no. 4, pp. 194–208, 2010.

[156] S. Gupta, H. Weinacker, and B. Koch, "Comparative analysis of clustering-based approaches for 3-d single tree detection using airborne fullwave lidar data," *Remote Sensing*, vol. 2, no. 4, pp. 968–989, 2010.

[157] M. Straatsma and H. Middelkoop, *Airborne laser scanning as a tool for lowland floodplain vegetation monitoring*, vol. 187. Springer, 2006.

[158] M. A. Rahman, B. Gorte, *et al.*, "Tree filtering for high density airborne lidar data," pp. 544–553, 2008.

[159] W. Xiao, S. Xu, S. O. Elberink, and G. Vosselman, "Individual tree crown modeling and change detection from airborne lidar data," *IEEE Journal of Selected Topics in Applied Earth Observations and Remote Sensing*, vol. 9, no. 8, pp. 3467–3477, 2016.

[160] J. N. Heinzel, H. Weinacker, and B. Koch, "Prior-knowledge-based single-tree extraction," *International journal of remote sensing*, vol. 32, no. 17, pp. 4999–5020, 2011.

[161] J. C. Jenkins, D. C. Chojnacky, L. S. Heath, and R. A. Birdsey, "National-scale biomass estimators for united states tree species," *Forest science*, vol. 49, no. 1, pp. 12–35, 2003.

[162] C. J. Gleason and J. Im, "Forest biomass estimation from airborne lidar data using machine learning approaches," *Remote Sensing of Environment*, vol. 125, pp. 80–91, 2012.

[163] J. Hyyppä, T. Mielonen, H. Hyyppä, M. Maltamo, X. Yu, E. Honkavaara, and H. Kaartinen, "Using individual tree crown approach for forest volume extraction with aerial images and laser point clouds," *The International Archives of the Photogrammetry, Remote Sensing and Spatial Information Sciences*, vol. 36, no. 3, p. W19, 2005.

[164] M. Heurich, "Automatic recognition and measurement of single trees based on data from airborne laser scanning over the richly structured natural forests of the bavarian forest national park," *Forest Ecology and Management*, vol. 255, no. 7, pp. 2416–2433, 2008.

[165] M. Dalponte, L. Bruzzone, and D. Gianelle, "A system for the estimation of single-tree stem diameter and volume using multireturn lidar data," *IEEE Trans. Geosci. Remote Sens.*, vol. 49, no. 7, pp. 2479–2490, 2011.

[166] A. Harikumar, F. Bovolo, and L. Bruzzone, "Subdominant tree detection in multi-layered forests by a local projection of airborne lidar data," in *Geoscience and Remote Sensing Symposium (IGARSS), 2017 IEEE International*, pp. 2760–2763, IEEE, 2017.

[167] A. Harikumar, F. Bovolo, and L. Bruzzone, "An internal crown geometric model for conifer species classification with high-density lidar data," *IEEE Transactions on Geoscience and Remote Sensing*, vol. 55, no. 5, pp. 2924–2940, 2017.

[168] M. Rahman and B. Gorte, "Individual tree detection based on densities of high points from high resolution airborne lidar," in *In GEOBIA, 2008 - Pixels, Objects, Intelligence: GEOgraphic Object Based Image Analysis for the 21st Century*, ISPRS, 2009.

[169] A. Bucksch, R. Lindenbergh, M. Z. A. Rahman, and M. Menenti, "Breast height diameter estimation from high-density airborne lidar data," *IEEE Geoscience and Remote Sensing Letters*, vol. 11, no. 6, pp. 1056–1060, 2014.

[170] P. Neubert and P. Protzel, "Compact watershed and preemptive slic: On improving trade-offs of superpixel segmentation algorithms," in *Pattern Recognition (ICPR), 2014 22nd International Conference on*, pp. 996–1001, IEEE, 2014.

[171] A. Harikumar, F. Bovolo, and L. Bruzzone, "A novel approach to internal crown characterization for coniferous tree species classification," in *SPIE Remote Sensing*, pp. 100040H–100040H, International Society for Optics and Photonics, 2016.

[172] C. Philips, D. Li, D. Raicu, and J. Furst, "Directional invariance of co-occurrence matrices within the liver," in *Biocomputation, Bioinformatics, and Biomedical Technologies, 2008. BIOTECHNO'08. International Conference on*, pp. 29–34, IEEE, 2008.

[173] R. M. Haralick, K. Shanmugam, *et al.*, "Textural features for image classification," *IEEE Trans. Syst. Man Cybern. Part B Cybern.*, no. 6, pp. 610–621, 1973.

[174] P. Li and X. Xiao, "An unsupervised marker image generation method for watershed segmentation of multispectral imagery," *Geosciences Journal*, vol. 8, no. 3, pp. 325–331, 2004.

[175] K. Olofsson, E. Lindberg, J. Holmgren, *et al.*, "A method for linking field-surveyed and aerial-detected single trees using cross correlation of position images and the optimization of weighted tree list graphs," *Proceedings of SilviLaser*, vol. 2008, p. 8th, 2008.

[176] J. Kalliovirta and T. Tokola, "Functions for estimating stem diameter and tree age using tree height, crown width and existing stand database information," *Silva Fennica*, vol. 39, no. 2, pp. 227–248, 2005.

[177] J. Lappi, "Metsäbiometrian menetelmiä," *Silva Carelica*, p. 182, 1993.

[178] N. Otsu, "A threshold selection method from gray-level histograms," *IEEE transactions on systems, man, and cybernetics*, vol. 9, no. 1, pp. 62–66, 1979.

[179] K. Anitha, S. Joseph, R. J. Chandran, E. Ramasamy, and S. N. Prasad, "Tree species diversity and community composition in a human-dominated tropical forest of western ghats biodiversity hotspot, india," *Ecol. Complexity*, vol. 7, no. 2, pp. 217–224, Feb. 2010.

[180] A. Gebrekirstos, R. Mitlöhner, D. Teketay, and M. Worbes, "Climate–growth relationships of the dominant tree species from semi-arid savanna woodland in ethiopia," *Trees*, vol. 22, no. 5, pp. 631–641, Apr. 2008.

[181] T. Brandtberg, "Classifying individual tree species under leaf-off and leaf-on conditions using airborne lidar," *ISPRS J. Photogramm. Remote Sens.*, vol. 61, no. 5, pp. 325–340, Jan. 2007.

[182] J. Hyyppä, O. Kelle, M. Lehikoinen, and M. Inkinen, "A segmentation-based method to retrieve stem volume estimates from 3-d tree height models produced by laser scanners," *IEEE Trans. Geosci. Remote Sens.*, vol. 39, no. 5, pp. 969–975, May. 2001.

[183] S. Kim, T. Hinckley, and D. Briggs, "Classifying individual tree genera using stepwise cluster analysis based on height and intensity metrics derived from airborne laser scanner data," *Remote Sens. Environ.*, vol. 115, no. 12, pp. 3329–3342, Dec. 2011.

[184] J. Reitberger, M. Heurich, P. Krzystek, and U. Stilla, "Single tree detection in forest areas with high-density lidar data," *International Archives of Photogrammetry, Remote Sensing and Spatial Information Sciences*, vol. 36, no. 3, pp. 139–144, Sep. 2007.

[185] S. Gupta, B. Koch, and H. Weinacker, "Tree species detection using full waveform lidar data in a complex forest," in *Technical Commission VII Symposium–100 Years of ISPRS*, pp. 249 "–254, Vienna University of Technology: Vienna, Austria, Jul. 2010.

[186] V. D. Paris, Claudia and L. Bruzzone, "A hierarchical approach to three-dimensional segmentation of lidar data at single-tree level in a multilayered forest," *IEEE Trans. Geosci. Remote Sens.*, vol. PP, no. 99, pp. 1–14, Jul. 2016.

[187] A. B. Chan, N. Vasconcelos, and G. R. G. Lanckriet, "Direct convex relaxations of sparse svm," in *Proceedings of the 24th international conference on Machine learning*, pp. 145–153, Corvalis, Oregon, Jun. 20–24, 2007.

[188] V. N. Vapnik and V. Vapnik, *Statistical learning theory*, vol. 1. Wiley New York, 1998.

[189] E. L. Taylor, T. N. Taylor, and M. Krings, *Paleobotany: the biology and evolution of fossil plants.* Academic Press, 2009.

[190] M. Roggero, "Object segmentation with region growing and principal component analysis," *International Archives of Photogrammetry Remote Sensing and Spatial Information Sciences*, vol. 34, no. 3/A, pp. 289–294, Sep. 2002.

[191] R. C. Veltkamp, "Boundaries through scattered points of unknown density," *Graphical Models and Image Processing*, vol. 57, no. 6, pp. 441–452, Nov. 1995.

[192] Z. Rahman, M, B. Gorte, and A. Bucksch, "A new method for individual tree delineation and undergrowth removal from high resolution airborne lidar," *in Proc. IARPS*, vol. 38, no. 3, pp. 283–288, Sep. 2009.

[193] Z. Rahman, M and B. Gorte, "Individual tree detection based on densities of high points of high resolution airborne lidar," in *Proceedings GEOBIA, 2008 - Pixels, Objects, Intelligence: GEOgraphic Object Based Image Analysis for the 21st Century*, pp. 350–355, University of Calgary, Calgary, Alberta, Canada, 5-8 Aug. 2008.

[194] H. S. Horn, *The adaptive geometry of trees*, vol. 3, Princeton. Princeton University Press, 1971.

[195] F. Morsdorf, E. Meier, B. Kötz, K. I. Itten, M. Dobbertin, and B. Allgöwer, "Lidar-based geometric reconstruction of boreal type forest stands at single tree level for forest and wildland fire management," *Remote Sens. Environ.*, vol. 92, no. 3, pp. 353–362, Aug. 2004.

[196] C. Alexander, "Delineating tree crowns from airborne laser scanning point cloud data using delaunay triangulation," *Int. J. Remote Sens.*, vol. 30, no. 14, pp. 3843–3848, Jul. 2009.

[197] C. Paris and L. Bruzzone, "A three-dimensional model-based approach to the estimation of the tree top height by fusing low-density lidar data and very high resolution optical images," *IEEE Trans. Geosci. Remote Sens.*, vol. 53, no. 1, pp. 467–480, Jan. 2015.

[198] M. W. McDaniel, T. Nishihata, C. A. Brooks, P. Salesses, and K. Iagnemma, "Terrain classification and identification of tree stems using ground-based lidar," *Journal of Field Robotics*, vol. 29, no. 6, pp. 891–910, Nov. 2012.

[199] C. Ko, T. K. Remmel, and G. Sohn, "Mapping tree genera using discrete lidar and geometric tree metrics," *Bosque*, vol. 33, no. 3, pp. 313–319, Jan. 2012.

[200] V. Vapnik, "The nature of statistical learning theory," pp. 138–141, Springer, 2000, New York.

[201] C.-W. Hsu and C.-J. Lin, "A comparison of methods for multiclass support vector machines," *IEEE transactions on Neural Networks*, vol. 13, no. 2, pp. 415–425, Mar. 2002.

[202] K. Zhang and D. Whitman, "Comparison of three algorithms for filtering airborne lidar data," *Photogramm. Eng. Remote Sens.*, vol. 71, no. 3, pp. 313–324, Mar. 2005.

[203] C.-W. Hsu, C.-C. Chang, C.-J. Lin, *et al.*, "A practical guide to support vector classification, tech. rep.," Taipei, Apr. 2003.

[204] M. Grant and S. Boyd, "CVX: Matlab software for disciplined convex programming, version 2.1." `http://cvxr.com/cvx`, Mar. 2014.

[205] I. Guyon, J. Weston, S. Barnhill, and V. Vapnik, "Gene selection for cancer classification using support vector machines," *Machine learning*, vol. 46, no. 1-3, pp. 389–422, 2002.

[206] C.-C. Chang and C.-J. Lin, "Libsvm: a library for support vector machines," *ACM Transactions on Intelligent Systems and Technology (TIST)*, vol. 2, no. 3, p. 27, 2011.

[207] M. Gönen and E. Alpaydın, "Multiple kernel learning algorithms," *Journal of Machine Learning Research*, vol. 12, no. Jul, pp. 2211–2268, 2011.

[208] G. Hughes, "On the mean accuracy of statistical pattern recognizers," *IEEE transactions on information theory*, vol. 14, no. 1, pp. 55–63, 1968.

[209] F. Melgani and L. Bruzzone, "Classification of hyperspectral remote sensing images with support vector machines," *IEEE Transactions on geoscience and remote sensing*, vol. 42, no. 8, pp. 1778–1790, 2004.

[210] A. Barla, F. Odone, and A. Verri, "Histogram intersection kernel for image classification," in *Proceedings 2003 International Conference on Image Processing (Cat. No.03CH37429)*, vol. 3, pp. III–513, Sept 2003.

[211] L. Naidoo, M. A. Cho, R. Mathieu, and G. Asner, "Classification of savanna tree species, in the greater kruger national park region, by integrating hyperspectral and lidar data in a random forest data mining environment," *ISPRS journal of Photogrammetry and Remote Sensing*, vol. 69, pp. 167–179, 2012.

[212] M. Hauglin, T. Gobakken, R. Astrup, L. Ene, and E. Næsset, "Estimating single-tree crown biomass of norway spruce by airborne laser scanning: a comparison of methods with and without the use of terrestrial laser scanning to obtain the ground reference data," *Forests*, vol. 5, no. 3, pp. 384–403, 2014.

[213] J. G. Henning and P. J. Radtke, "Detailed stem measurements of standing trees from ground-based scanning lidar," *Forest Science*, vol. 52, no. 1, pp. 67–80, 2006.

[214] F. Hosoi and K. Omasa, "Voxel-based 3-d modeling of individual trees for estimating leaf area density using high-resolution portable scanning lidar," *IEEE transactions on geoscience and remote sensing*, vol. 44, no. 12, pp. 3610–3618, 2006.

[215] K. Calders, J. Armston, G. Newnham, M. Herold, and N. Goodwin, "Implications of sensor configuration and topography on vertical plant profiles derived from terrestrial lidar," *Agricultural and Forest Meteorology*, vol. 194, pp. 104–117, 2014.

[216] Y. Lin, J. Hyyppä, A. Kukko, A. Jaakkola, and H. Kaartinen, "Tree height growth measurement with single-scan airborne, static terrestrial and mobile laser scanning," *Sensors*, vol. 12, no. 9, pp. 12798–12813, 2012.

[217] K. Calders, G. Newnham, A. Burt, S. Murphy, P. Raumonen, M. Herold, D. Culvenor, V. Avitabile, M. Disney, J. Armston, *et al.*, "Nondestructive estimates of above-ground biomass using terrestrial laser scanning," *Methods in Ecology and Evolution*, vol. 6, no. 2, pp. 198–208, 2015.

[218] S. Bektas, "Least squares fitting of ellipsoid using orthogonal distances," *Boletim de Ciências Geodésicas*, vol. 21, no. 2, pp. 329–339, 2015.

[219] A. FORBES, "Least-squares best-fit geometric elements," 1989.